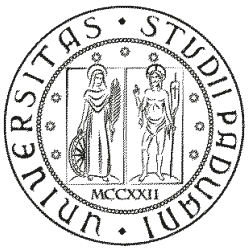

UNIVERSITÀ DEGLI STUDI DI PADOVA

Dipartimento di Fisica e Astronomia "Galileo Galilei"

Corso di Laurea magistrale in Astrophysics and Cosmology

Master Thesis

Flavour-violating signatures of non-universal axion models

Thesis Supervisor:

Dott. Luca Di Luzio

Co-Supervisor:

Prof. Stefano Rigolin

Candidate:

Beatrice Munari

Academic Year 2021/2022

Contents

Abstract

The axion provides a well-motivated extension of the Standard Model (SM) addressing the strong CP problem and yielding a dark matter candidate, with implications across particle physics, cosmology and astrophysics. It has been recently pointed out that non-universal axion models (in which the axion couples differently to different SM fermion generations) allow to suppress the axion coupling to nucleons and electrons, and relax in turn astrophysical axion bounds. A remarkable consequence of non-universal axion models are flavour-violating axion couplings, which can be tested in low-energy flavour experiments. The aim of the thesis is to study the interplay between different sources of flavour violation, involving both the axion field and the heavy radial modes, which are unavoidably present in UV complete non-universal axion models. The study of the latter sources of flavour violation, within a specific UV complete non-universal axion model, represents the original contribution of the present thesis.

Introduction

Most particle physics experiments are nowadays explained by the Standard Model (SM), the theoretical framework describing all known fundamental interactions (with the exception of gravity). However, there are several reasons (based both on theoretical arguments and experimental facts, such as the presence of the DM matter in the Universe or the small value of the QCD angle) why the SM of particle physics should extend. One of the most popular extensions of the SM is provided by the axion framework, which originally arose as a solution to the strong CP problem, namely to explain the absence of CP violation in strong interactions. Following the seminal work of R. Peccei and H. Quinn [1; 2], which proposed a spontaneously broken and anomalous $U(1)_{PQ}$ (hereafter denotes as Peccei Quinn (PQ) symmetry) global symmetry as the solution of the strong CP problem, S. Weinberg [3] and F. Wilczek [4] subsequently realized the existence of an associated (pseudo) Goldstone boson that was named "axion" like the name of a laundry soap, since it "washes out" CP violation from strong interactions. After a while it was also realized that axions do contribute to the energy density of the Universe and they might comprise the totality (or a fraction) of the cold Dark Matter (DM) [5; 6; 7].

Experimental axion searches are often interpreted in the context of a couple of benchmark axion models, which are the so-called KSVZ [8; 9] and DFSZ [10; 11] axion models. However, benchmark axion models are sometimes too restrictive and, given the active experimental axion program, it is important to consider more general axion models in order to widen the prospects for an axion discovery.

For instance, both KSVZ and DFSZ models are based on the not so strongly motivated assumption of universality of PQ charges, namely that all SM fermion generations of a given flavour (up- and down-type quarks and charged leptons) have the same PQ charge. On the other hand, relaxing the assumption of universality of PQ charges is interesting in several respects, including: *i*) the possibility of relaxing the Supernova bound on the axion mass [12], *ii*) a possible connection with the SM flavour puzzle [13] and *iii*) the experimental opportunity of discovering the axion via flavoured axion searches. In fact, one of the most striking consequences of non-universal axion models is that, after going to the mass basis, flavour-violating axion couplings to SM fermions are generated.

The goal of this thesis is to study flavour-violating signatures of non-universal axion models. In particular, we will investigate the interplay between different sources of flavour violation, arising both from flavour-violating axion couplings and the ultraviolet (UV) degrees of freedom present in UV complete non-universal axion models. The latter sources

of flavour violation have been less studied in the literature (for a work going in this direction see e.g. [14]) and they constitutes the original contribution of the present thesis, which is structured as follows.

In the first chapter, we provide the reader with an organic introduction to axion theory. We discuss the strong CP problem, as the theoretical framework from which the axion arises, and explain the structure of the QCD vacuum. We next introduce the PQ mechanism as a solution to the strong CP problem and the axion as a low-energy remnant. Axion properties, such as mass and couplings, are derived within an Effective Field Theory (EFT) framework. We finally discuss axion UV completions and, in particular, the so-called KSVZ and DFSZ benchmark axion models.

The second chapter encompasses a more phenomenological discussion about axion physics. The chapter is divided in three main sections concerning astrophysical bounds, cosmological implication and experimental searches. Although this is in principle a vast area of research, the emphasis is given here to astrophysical aspects, which are more closely connected to the non-universal axion models considered in this thesis.

In the third chapter, we introduce the general structure of non-universal axion models. After presenting some general motivations, we focus on the main theoretical consequences of these new models discussing, in particular, flavour violating sources both from infrared (IR) and UV dynamics.

In the forth chapter we analyse in greater detail a specific non-universal axion model. After specifying the full Lagrangian, we discuss the Yukawa and scalar sectors, carry out explicitly the diagonalization of fermion masses and compute the scalar spectrum. This is a preliminary step that is needed in order to integrate out the heavy scalar degrees of freedom of the UV completion and obtain in turn the flavour-violating 4-fermion operators, which constitutes the UV sources of flavour violation. Finally, we provide a comparison between different sources of flavour violation, highlighting possible correlations which depend however on a set of working assumptions.

We conclude in the fifth chapter, where we summarize the main results of the thesis and discuss a possible outlook for a future work.

Chapter 1

Axion theory

In this first chapter, we introduce the axion concept from a theoretical point of view. After briefly discussing why it is necessary to go beyond the SM, we will give a theoretical motivation for the introduction of the axion particle based on the so-called strong CP problem. In the second part, we will show how the axion solves the strong CP problem and discuss standard axion models.

1.1 The axion as a pathway beyond the Standard Model

Up to now, the SM seems to be the most accurate theory which can be used to describe particle physics. It comprises some fundamental building blocks: fermions, gauge bosons, and the Higgs boson. The first ones include three generators of quarks and leptons. The gauge bosons are $W^{\pm}$ and Z, photons, and gluons, which respectively mediate weak, electromagnetic, and strong interactions. The Higgs boson is a scalar field responsible for giving mass to all SM particles. The SM, at the level of accuracy of today experiments, has been tested down to scales of the order of 10^{-16}cm. However, the SM seems not to be the ultimate theory of particle physics. Indeed, cosmological experiments and observations suggest the presence of a large quantity of DM in the Universe and highlights a matter-antimatter asymmetry. In addition, SM is not able to describe inflation too. All of these evidences, as well as the origin of neutrino masses, remain unexplained in the SM. Moreover, the SM suffers also from other, more theoretical, issues called naturalness problems. They are related to the fact that some parameters are extremely small. These include, for instance the Higgs mass parameter $m_H \sim 10^{-17} m_{PL}$ or, as we will discuss in the next section, the QCD theta angle which is $\theta \lesssim 10^{-10}$ [15]. Finally, using SM we cannot explain the specific structure of Yukawa matrices. Hence, it should be quite clear that it is necessary to go beyond the SM in order to solve some of these issues.

A good way to extend the SM would be to find a new theory that solves at the same time several of the above mentioned problems. This is one of the reasons why the axion, a spin-zero pseudo-scalar particle predicted by PQ mechanism [1; 2], is considered to be a compelling candidate. Indeed, the non-trivial vacuum structure of Quantum Chromodynamics (QCD) leaves us with an open question, the so-called Strong CP

problem: why there is no CP violation in strong interaction, namely why is CP a good symmetry? Peccei and Quinn tried to solve the problem introducing a new $U(1)_{PQ}$ symmetry, anomalous at the quantum level which spontaneously breaks at high energy. Subsequently, Weinberg and Wilczek [3; 4] identified the pseudo Nambu-Goldstone boson, produced by the spontaneous symmetry breaking (SSB) of this new global symmetry, as the axion (in the following, the axion field will be indicated as $a(x)$). As we will discuss later, the axion acquires a mass and it couples with other particles, such as electrons, photons, pions and kaons. Both the mass and the interactions, are inversely proportional to f_a, the energy scale at which the $U(1)_{PQ}$ symmetry breaks down. Although in the original models f_a was of the order of Electroweak (EW) scale, it was later on realized that f_a needs to be much larger than the EW scale [11; 16]. This fact has crucial consequences: since the axion mass is small ($m_a \ll$ eV) and it is weakly coupled with other particles, it could play the role of DM particle. In this way the solution of a theoretical problem related to the QCD vacuum structure, could also be the right way to solve a critical cosmological issue.

Furthermore, the axion hypothesis has many other implications both in cosmology and astrophysics. Indeed, as mentioned above, since the axion is light and its couplings are particularly small, it constitutes a so-called weakly interacting slim particle (WISP) [17]. This implies important constraints regarding astrophysics and, especially, stellar cooling. In addition, even though, we will show in the next sections that the axion is lighter than at least two of the three types of neutrinos, with a mass that is $m_a \ll$ eV, it could be the major constituent of the DM of the Universe.

Up to the present day, experiments aimed at detecting the existence of these particles did not give any positive result, but it must be stressed that only a small part of the relevant parameter space has been explored so far. It is likely that in the coming years a large portion of the axion parameter space will be explored, also using new detection techniques.

1.2 The Strong CP Problem

To the arbours of the development of the theory of QCD, the $U(1)_A$ problem was considered one of the greatest difficulties to overcome: although it seemed to be a good symmetry on a theoretical level, this was not reflected at all in the real world [18]. In fact, as a consequence of the spontaneous $U(1)_A$ symmetry breaking, a pseudo Goldstone boson with a mass smaller than $\sqrt{3}m_\pi$ would be predicted [19]. Nevertheless, the heaviness of the meson η' did not seem to confirm this prediction. The solution to this problem came with the formalisation of the concept of instantons [20]. On the other hand, this new field dragged with it a new term of CP violation. Let us discuss this point in more detail. From the CPT theorem we know that the only transformation which maintains the action unaffected is a combination of all three symmetries: C, P and T. From theoretical considerations we can establish that only electromagnetism remains unchanged under an individual C, P and T transformation, and in turns under a CP one. While, in the case of strong interactions we expect a detectable CP violation, since CP is not

a symmetry of the theory. However, experimental results on the neutron Electric Dipole Moment (nEDM) show with good accuracy the absence of a CP violation (see e.g. section 1.2.3). This fact, known as strong CP problem, will be discussed in the following sections. First, we will discuss the non-trivial vacuum structure of QCD and how the strong CP problem emerges, then we will introduce the PQ solution and present some axion models.

1.2.1 Instantons and the QCD vacuum structure

In order to study properties of the QCD vacuum structure, let us introduce the QCD Lagrangian:

$$\mathcal{L}_{QCD} = \sum_q \bar{q}(i\not{D} - m_q e^{i\theta_q \gamma_5})q - \frac{1}{4}G^a_{\mu\nu}G^{a\mu\nu} + \theta\frac{g_s}{32\pi^2}G^a_{\mu\nu}\tilde{G}^{a\,\mu\nu} \ , \quad (1.1)$$

where the apex a is a colour index and G represents the field strength tensor of QCD. In particular we will use the following notation

$$G\tilde{G} = G^a_{\mu\nu}\tilde{G}^{a\,\mu\nu}, \qquad \tilde{G}^{a\,\mu\nu} = \frac{1}{2}\epsilon^{\mu\nu\rho\sigma}G^a_{\rho\sigma} \ , \quad (1.2)$$

with $\epsilon^{0123} = -1$ and

$$G^a_{\mu\nu} = \partial_\mu A^a_\nu - \partial_\nu A^a_\mu + i g_s f^{abc} A^b_\mu A^a_\nu \ . \quad (1.3)$$

We focus our attention on the last term of eq. 1.1. We will call it the *theta* term or $G\tilde{G}$ term: it is allowed by gauge invariance and renormalisability (it is a 4-dimensions operator as the second term in the Lagrangian). However, this term carries crucial properties. Firstly, it violates both P and T symmetry, consequently because of the CPT theorem, it also violates CP. To prove this in a simple way, one could demonstrate it using Electrodynamics and then generalise it including the non-Abelian term. Secondly, through a mathematical manipulation of the *theta* term, it is possible to demonstrate that it is described by a total derivative: [1]

$$G\tilde{G} = \partial_\mu[\epsilon^{\mu\nu\rho\sigma}(A_\nu G^a_{\rho\sigma} - \frac{g_s}{3}f^{abc}A^a_\nu A^b_\rho A^c_\sigma)] \ . \quad (1.4)$$

We will call the term in square brackets Chern-Simons current and indicate it with K^μ.

As a consequence, since the $G\tilde{G}$ term is a total derivative, one does not expect effects in the perturbative theory. However, it can bear some physical consequences due to the presence of QCD instantons. The QCD instantons are classical solutions of the Euclidean Equation of Motion (EOM) with a finite action S_E. These solutions which correspond to classical configurations are topological and can be found studying the Euclidean action. Considering, at this stage, only gluons, it is proportional to:

$$\int d^4x G\tilde{G} = \int d^4x \partial_\mu K^\mu = \int_{S_3} d\sigma_\mu K^\mu, \quad (1.5)$$

[1] Again, to demonstrate it one can pass through the simpler electrodynamics case and then generalise it showing that the extra pieces are zero because of the Jacoby Identity.

where the last passage corresponds to a surface integral with 3-Sphere at infinity. In order for this configuration to have a non-zero contribution, we have to impose the action is finite, namely

$$G^a_{\mu\nu}\Big|_{S_3} \xrightarrow{|x|\to\infty} 0 \ . \tag{1.6}$$

Besides the trivial solution $A^a_\mu|_{S_3} = 0$, since we are in a gauge theory, it is possible to perform a gauge transformation giving:

$$A'^a_\mu\Big|_{S_3} = (U^{-1}A_\mu U + \frac{i}{g_s}U\partial_\mu U)\Big|_{S_3} , \tag{1.7}$$

which gives (if we consider $A_\mu = 0$)

$$A'^a_\mu\Big|_{S_3} = \frac{i}{g_s}U\partial_\mu U\Big|_{S_3} \ . \tag{1.8}$$

This gauge transformation is called *pure gauge*. What we want to compute is a solution from the vacuum, mapping this $SU(2)$ gauge transformations in the S_3 Euclidean space [21]. To discuss the existence of integral solutions of eq. 1.5, it is necessary to introduce a topological quantity described by the *winding number* $\in \mathbb{Z}$. Taking a point, the winding number represents the number of times a curvilinear trajectory revolves around it counterclockwise. However, it is possible to demonstrate that this parameter has a physical description, i.e. it is strictly connected to the vacuum state. It is important to notice that it is not possible to pass from a configuration described by a given winding number into another configuration with a different winding number maintaining the action finite. To learn the connection between maths and physics, let us discuss the following equation about the action S:

$$\begin{aligned} S &= \frac{1}{4}\int d^4x G^a_{\mu\nu}G^{a\,\mu\nu} = \\ &= \frac{1}{4}\int d^4x[\pm G^a_{\mu\nu}\tilde{G}^{a\,\mu\nu} + \frac{1}{2}(G^a_{\mu\nu} \mp \tilde{G}^a_{\mu\nu})^2] \ . \end{aligned} \tag{1.9}$$

The last term of the latter equation is always equal, or larger, than zero since it is the intgral of a positive quantity. This yields the Bogomol'nyi inequality [22]. Instead, the first term in the last equality, which is what we called Chern-Simons current K^μ in eq. 1.4, requires to be studied. In particular, we can work in the temporal gauge, where $A^a_0 = 0$, so that the only non vanishing component of the Chern-Simons current is the temporal one, while $K_i = 0$ [23]. In this way, passing into the Minkowsky spacetime:

$$\begin{aligned} &\frac{g_s^2}{32\pi^2}\int d^4x G^a_{\mu\nu}\tilde{G}^{a\,\mu\nu} = \frac{g_s^2}{32\pi^2}\int d^4x \partial_0 K^0 = \\ &\frac{g_s^2}{32\pi^2}\int d^3x K^0\Big|_{t=-\infty}^{t=+\infty} = \frac{g_s^2}{32\pi^2}(m-n) \equiv \nu \ . \end{aligned} \tag{1.10}$$

Therefore, since ν is a topological invariant and the last term in eq. 1.9 is a non negative quantity as just discussed, the action will be minimal if we have a self or anti-self dual field, that is:

$$G^a_{\mu\nu} = \pm \tilde{G}^a_{\mu\nu} \, . \tag{1.11}$$

Coming back to the physical interpretation of the winding number, considering 1.10, the instantonic solution described by the passage from m to n, can be considered as a tunnelling effect from the vacuum state $|m\rangle$ to $|n\rangle$ through a gauge rotation [24]. The transition probability between a vacuum state and the other one is described by the exponential of the instanton action e^{-S_ν} where, from [25],

$$S_\nu = \frac{8\pi^2}{g_s^2}\nu \, . \tag{1.12}$$

Clearly, the higher the number, the larger the suppression and, therefore, the lower the probability of tunnelling. This is the reason why configurations characterised by a winding number larger than one are typically negligible. The explicit configuration with a $\nu = 1$ was found by Belavin et al. in [26] and yields $S_1 = \dfrac{8\pi^2}{g_s^2}$. In conclusion, the action can be rewritten with an extra factor as

$$S \to S + i\theta \frac{g_s^2}{32\pi^2} \int d^4x G^a_{\mu\nu} \tilde{G}^{a\,\mu\nu} \, . \tag{1.13}$$

The last expression explicitly shows that the non-trivial structure of the Yang-Mills vacuum demands a gauge field transformation with a non-trivial winding number. This fact requires the inclusion of the $G\tilde{G}$ term in the Lagrangian, which, in turn, has the necessary features to solve the $U(1)_A$ problem. Indeed, the complex nature of QCD explains why the $U(1)_A$ is no more a symmetry of QCD [21; 20] and gives an explanation to the heaviness of η' meson.

1.2.2 θ dependence of QCD vacuum energy

We discuss how the energy depends on θ and to achieve this point let us consider the partition function.

In the Euclidean[2] the partition function is given by the path integral of the exponential of the action[3] :

$$Z = \int \mathcal{D}A e^{-\frac{1}{4}\int d^4x GG + i\theta \frac{g_s^2}{32\pi^2}\int d^4x G\tilde{G}} \, . \tag{1.14}$$

We can approximate this path integral along one of the instanton solutions discussed before, making a saddle point approximation. Therefore, the first functional derivative contribution goes to zero because of the fact that it is a solution of EOM, and just the correction from the quadratic term in the path integral remains. Using the results computed in eq. 1.12 and considering the case of unit winding number, the partition function can be approximated as

$$Z \approx e^{-\frac{8\pi^2}{g_s^2} \pm i\theta} , \tag{1.15}$$

[2] In order to pass from the Minkowski coordinates to the Euclidean ones, it is necessary to perform the analytic continuation $t = -it_E$. Due to the presence of the $\epsilon^{\mu\nu\rho\sigma}$ tensor, the $G\tilde{G}$ term gains an i factor.

[3] Notice that in eq. 1.14 A stands for the gluons fields.

where the plus or minus sign stands for the instanton and anti-instanton contributions. Summing over them we get:

$$Z \propto 2\cos\theta e^{-\frac{8\pi^2}{g_s^2}} . \tag{1.16}$$

The above result is computed in the semi-classical approximation, considering $\hbar \to 0$ and expanding the action in this limit. To take into account also the quantum corrections, it is possible to modify the coupling constant g_s turning it into a running constant $g_s(\mu = 1/\rho)$ where ρ describes the centre of the instanton field configuration, i.e. the size of the instanton. In the light of the fact that we are computing a path integral, we should sum over all possible ρ: at the classical level, considering energy around $1/\Lambda_{QCD} \sim 150$MeV, this contribution diverges since the coupling constant becomes larger and larger. However, some instanton configurations will dominate the contribution to the path integral. To see this, let us define the expression for the coupling constant running with the energy as

$$g_s^2(\mu) = \frac{8\pi^2}{\beta_0 \log(\frac{\mu}{\Lambda_{QCD}})}, \tag{1.17}$$

where $\beta_0 = 11 - 2n_f/3$ is always positive with $n_f = 1, 2, ..., 6$ representing the active flavours. When the energy is high an exponential suppression takes place. On the contrary, if we consider a low energy (large distance) regime, both g_s and ρ become lager, and the exponential is not suppressed. These configurations are the so called *large instantons*. Formally this becomes:

$$e^{-\frac{8\pi^2}{g_s^2(1/\rho)}} = (\rho\Lambda_{QCD})^{\beta_0} . \tag{1.18}$$

In conclusion, it is crucial to notice that, since the semi-classical approximation breaks down at energy around $1/\Lambda_{QCD}$, other approaches based e.g. on Chiral Perturbation Theory (χPT) are necessary[4]. Moreover, it can be shown that at large V_4 Euclidean volume the partition function of QCD, $Z(\theta)$, is related to the QCD vacuum energy density $E(\theta)$ as $Z \approx e^{-E(\theta)V_4}$. In the following, we will exploit this relation in order to derive some general properties of the theta dependence of the QCD vacuum energy density.

Including quarks

Up to now, the discussion was made by neglecting quarks. Hence, we need to generalise the theory including the quark sector. Rewriting the mass terms in eq. 1.1 and including the Hermitian conjugate ones, we obtain:

$$\mathcal{L}_{QCD_{masses}} = \sum_q (\bar{q} i \not{D} q - m_q \bar{q}_L e^{i\theta_q} q_R - m_q \bar{q}_R e^{-i\theta_q} q_L) . \tag{1.19}$$

[4]QCD can be treated in perturbation theory at high energies, since the asymptotic freedom ensures the small coupling values. This is no longer a good approach at low energies where the Landau pole does not allow us to use perturbation theory. Hence, one needs alternative low-energy descriptions, such as chiral perturbation theory [27].

Let us perform a global chiral transformation on a single quark field $q \to e^{i\gamma_5\alpha}q$, which, in left-right components, reads:

$$\begin{cases} q_L \to e^{-i\alpha}q_L \\ q_R \to e^{i\alpha}q_R \end{cases} . \tag{1.20}$$

The mass term is not invariant under this transformation: precisely the operator $m\bar{q}q$ transforms as $m\bar{q}q \to m^{2i\alpha}\bar{q}q$. In this way, the θ_q term is rotated of an angle 2α and so it transforms as

$$\theta_q \to \theta_q + 2\alpha \, . \tag{1.21}$$

At the same time the axial current $J^5_\mu = \bar{\psi}\gamma_\mu\gamma_5\psi$ is anomalous, indeed we obtain an extra term which is also reflected by the non-invariance of the path integral measure [28]:

$$\mathcal{D}q\mathcal{D}\bar{q} \to \mathcal{D}q\mathcal{D}\bar{q}e^{-i\frac{g_s^2}{16\pi^2}\alpha\int d^4x G\tilde{G}} \, . \tag{1.22}$$

Note that, the extra term in the transformation has the same structure of the θ term in 1.1. Because of this, the θ gets a shift as well with the opposite sign:

$$\theta \to \theta - 2\alpha \, . \tag{1.23}$$

Therefore, putting together the two results, we can define a new object $\bar{\theta}$ as the only invariant quantity:

$$\bar{\theta} = \theta_q + \theta \, . \tag{1.24}$$

Being an invariant term, this is the only physical quantity. All the constraints which we will find, will be referred to this new parameter, namely it is not possible to measure separately the topological θ and the phase of the quark mass[5].

The relation in eq. 1.24 can be rewritten in the electroweak (EW) theory context. Let us consider the quark multiplet $q = (u, d, ...)$ and an axial transformation in the flavour space $q \to e^{i\gamma_5\alpha Q_a q}$, where Q_a is a $n_f \times n_f$ diagonal matrix. The Lagrangian term involving the quark masses is described by a diagonal matrix M_q which originates from the Yukawa matrix, which, in turn, transforms separately on the right and left handed terms. The implementation of the rotation above in the Lagrangian provides a shift in the mass phase $M_q \to M_q e^{2i\alpha Q_a}$, i.e.:

$$\arg\det M_q \to \arg\det M_q e^{2i\alpha Q_a} = \arg\det M_q + 2\alpha \,\mathrm{Tr}\, Q_a \, . \tag{1.25}$$

In the same way, but with the opposite sign, the theta term transforms as:

$$\theta \to \theta - 2\alpha \,\mathrm{Tr}\, Q_a \, . \tag{1.26}$$

Finally, if we consider the mass matrix as proportional to the product of the up and down Yukawa matrices, the physical value will become:

$$\bar{\theta} = \theta + \arg\det Y_u Y_d \, . \tag{1.27}$$

Let us now consider a rotation through which we reabsorb θ_q term so that $\bar{\theta} = \theta$. It is possible to define three different properties about the θ dependence of the vacuum energy, as discussed in the following.

[5]Notice that, conventionally, θ_q term is not present in the Lagrangian. This is due to a possible rotation through which θ_q phase is reabsorbed in θ term that, in turns, is not present in QCD Lagrangian.

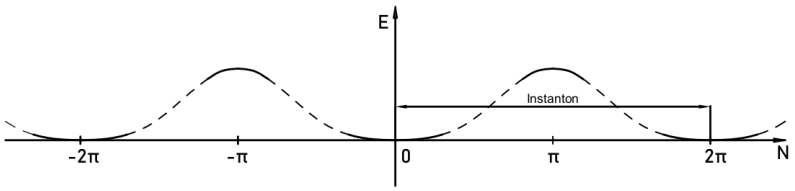

Figure 1.1: The figure represents how energy changes with respect to $N = \theta\nu$. From the diagram, the three properties described below are clear: the global minimum of the energy is located in zero, the function has a periodicity of 2π and, finally, it exhibits an even behaviour. It is crucial to point out that we do not know anything about the trend of the function between the minimums and the maximum, which is for this reason sketch with a dashed line.

1. $\theta = 0$ corresponds to a global minimum.
   The proof of this statement is proved by [29]. Briefly, exploiting the Cauchy-Schwarz inequality:

$$\begin{aligned} Z(\theta) &= \int \mathcal{D}\phi e^{-S_{\theta=0}+i\theta\frac{g_s^2}{32\pi^2}\int d^4x G\tilde{G}} \\ &\leq \int \left| \mathcal{D}\phi e^{-S_{\theta=0}+i\theta\frac{g_s^2}{32\pi^2}\int d^4x G\tilde{G}} \right| \\ &= \int \mathcal{D}\phi e^{-S_{\theta=0}} = Z(0) \end{aligned} \tag{1.28}$$

   Note that in the first passage we use the fact that the path integral measure is always positive defined, since we are working in a vector-like gauge theory like QCD [30], that is the theory which we are dealing with. Moreover, the absolute value removes the imaginary part of the exponential. Hence, recalling the relation $Z(\theta) \approx e^{-E(\theta)V_4}$, one finds $E(\theta = 0) \leq E(\theta)$.

2. $E(\theta) = E(\theta + 2\pi)$.
   This is simply due to the fact that ν is an integer number and θ is a global phase. As a consequence, the $G\tilde{G}$ integral in the exponential corresponds to $\theta\nu$ which has a 2π periodicity.

3. $E(\theta) = E(-\theta)$.
   The demonstration of this property is provided by performing a CP transformation $\phi \to \phi'$. The measure of the path integral is symmetric under it, i.e. $\mathcal{D}\phi$ remains invariant, but the *theta* term in the exponential changes sign. Hence the partition function, and then also the energy, is even.

Without having to make specific calculations, the three properties above define the positivity (including the value of the minimum), the periodicity and the even behaviour of the vacuum energy function, as suggested by the instanton approximation. As we can see in Fig. 1.1, the function could be approximated by a cosine-like function. Nevertheless, it is important to notice that we do not know at this point the exact functional dependence. We will find in the next sections, using χPT, what is the correct dependence from θ of the QCD energy density.

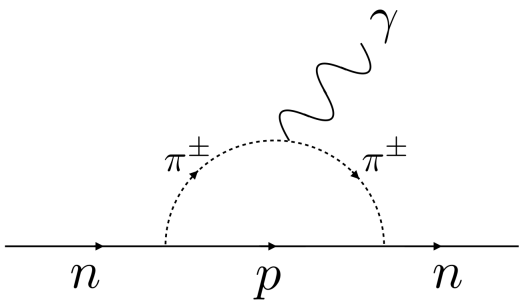

Figure 1.2: Neutron EDM Feynman diagram. It can be seen the presence of the loop and the photon emission which gives the suppression factor in the definition of the neutron dipole. Figure from [31].

1.2.3 The neutron Electric Dipole Moment

The physical quantity $\bar{\theta}$ can be tested via the measurement of the nEDM. Let us consider the non relativistic Hamiltonian:

$$\mathcal{H} = -d_n \vec{E} \cdot \hat{S} \tag{1.29}$$

The action of a time-transformation changes the sign of the last expression. Therefore, because of the validity of the CPT theorem, if $d_n \neq 0$, than CP should be violated. This is not what happen in experiments: no CP-violation in the strong sector has ever been seen. Hence, it is possible to put a constraint in the value of d_n, obtaining [15]:

$$d_n < 1.8 \cdot 10^{-26} e\,\text{cm} \quad (90\%\ \text{CL})\ . \tag{1.30}$$

Starting from the relativistic QCD theory, the nEDM is generated as the non-relativistic limit of the following Lagrangian term:

$$\mathcal{L} = -d_n \frac{i}{2} \bar{n} \sigma_{\mu\nu} \gamma_5 n F^{\mu\nu}\ . \tag{1.31}$$

Since the Lagrangian operator has dimension equal to 5, then d_n should go as the inverse of a mass. Hence, given that the only possible mass term is the neutron one, m_n, one could expect that $d_n \propto \frac{1}{m_n}$. If that were the case, it would be a problem: d_n would become too large because of the size of the neutron mass. However, it is crucial to take into account two points. Firstly, as one can see in Fig. 1.2, the process is described by a loop, then a suppression factor is expected. Secondly, we gain a possible imaginary phase[6] from the quark mass[7], so one can write: $m_q e^{i\bar{\theta}} \sim m_q(1 + i\bar{\theta})$ if $\bar{\theta}$ is sufficiently small (hypothesis which we will confirm in a while). On the whole of that, the d_n gains two suppression factors and it will become[8]:

$$d_n \sim \frac{1}{m_n} \frac{e^2}{16\pi^2} \frac{m_q}{m_n} \bar{\theta} \sim 10^{-4}\, \bar{\theta}\, e\, \text{GeV}^{-1}\ . \tag{1.32}$$

[6]The final results should be proportional to the imaginary part since the dipole operator in eq. 1.31 is purely imaginary.

[7]We are working on the opposite situation with respect to before: here the base considered reabsorbs, with a rotation, the $G\tilde{G}$ term, leaving only the quark mass term. In this way $\bar{\theta} = \theta_q$.

[8]In eq. 1.32, the last m_n in the denominator allows us to get back the correct mass dimensions

This is obviously a naive approximation which could give an idea of which factors are involved. Most accurate computations based on barion χPT, lattice QCD[9] or QCD sum-rules, give us a more restrictive constraint [32; 33; 34]:

$$d_n = 2.4 \cdot 10^{-16} \bar{\theta} e \,\text{cm} \sim 1.2 \cdot 10^{-2} \bar{\theta} e \,\text{GeV}^{-1}, \tag{1.33}$$

thus the bound on $\bar{\theta}$ is:

$$|\bar{\theta}| \lesssim 10^{-10} \,. \tag{1.34}$$

The strong CP problem is to figure out why this value is so small. As we defined in eq. 1.23, $\bar{\theta}$ has two contributes. This means that either there is a cancellation between them, but there is no physical connection between the θ and θ_q, or both of them are zero. This is not the end of the story, indeed it can be demonstrated that $\bar{\theta}$ is radiatively stable. It is necessary to consider 7-loop effects to obtain the first divergent contribution [35]. In the light of this, it is readily apparent that the solution to the strong CP problem must come from deeper considerations.

1.2.4 Non-axionic solutions

During the years many proposals have been introduced to solve the CP problem without using the axion: we will outline three of them.

- The first way to avoid the CP problem could be to consider massless quarks (at least up quark mass). One can easily check from eq. 1.27 the theory would gain a new U(1) axial symmetry, if the quarks had null mass. In this way, it would be possible to rotate away the θ-term via an axial field redefinition of the massless quark. Even though for some time this was believed to be a possible solution, recent studies from lattice QCD [36] excluded the possibility of massless up quark, giving a non-zero mass value that is $m_u^{\bar{M}S}(2\text{GeV}) = 2.32(10)\,\text{MeV}$. Moreover, even the introduction of a new massless quark would not explain the problem as there would be unwanted repercussions on the hadron's spectrum.

- Another choice is to consider that P or CP are softly broken. In particular, one could consider that P (or CP) is a symmetry in the UV theory, giving $\bar{\theta} = 0$; models like these were proposed also in Grand-Unified Theory context in [37]. However both P and CP are violated in weak theory: chiral structure needs a P symmetry violation to be explained, whereas CP violation is needed to generate the CKM phase. In this regime the $\bar{\theta}$ is non vanishing and calculable. The main problem is to define a reasonable value of $\bar{\theta}$ to describe weak interaction and, at the same time, to respect the experimental bound of $|\bar{\theta}| \sim 10^{-10}$ in the quark sector.

- The last option discussed is to consider the solution of the CP problem using the IR dynamics of QCD. From this point of view the presence of the parameter θ could come from an incorrect consideration of the topology of space time, which should therefore

[9] In the Lattice theory the spacetime continuum is replaced with a set of discrete points and the path integral in the Euclidean space becomes just an ordinary integral described by a huge number of variables.

be changed [38; 39]. However, this type of solutions often fails in the explanation of the $U(1)_A$ problem, leaving the heavy mass of η' beyond comprehension.

While some of the solutions proposed so far are experimentally excluded, others (like the softly P or CP broken solution) are difficult to be tested experimentally since the dynamics is hidden in the UV at very high-energy. In the next section, we will present instead what is arguably the most appealing solution: the Peccei-Quinn mechanism. It is able to provide an explanation of the strong CP problem and, simultaneously, it delivers a new detectable particle in the IR, the axion.

1.3 The Peccei-Quinn Mechanism

In 1977 Peccei and Quinn [1; 2] proposed a solution of the strong CP problem which assumes the presence of a new spin zero field $a(x)$, called axion field. Using a bottom-up approach in the EFT context it is possible to write the following effective Lagrangian:

$$\mathcal{L}_a = \frac{1}{2}(\partial_\mu a)^2 + L(\partial_\mu a, \psi_{SM}) + \frac{g_s^2}{32\pi^2}\frac{a}{f_a}G\tilde{G} \, . \tag{1.35}$$

The axion field posses a pseudo-shift symmetry that is $a(x) \to a(x) + \alpha f_a$, where f_a indicates a mass scale known as axion decay constant. The shift of the action under this pseudo-symmetry is:

$$\delta S = \frac{g_s^2}{32\pi^2}\alpha G\tilde{G} \, . \tag{1.36}$$

Hence, the parameter α is able to wash $\bar{\theta}$ out, if we choose it to be $\alpha = -\bar{\theta}$. However, a crucial point is in order here. The vacuum expectation value (VEV) of the axion field must be set to zero, otherwise the strong CP problem will be reintroduced. This statement is guaranteed by the Vafa-Witten theorem [29], which follows from eq. 1.28. Indeed, the same properties of θ apply as well to the background axion field, that is $\langle a \rangle = 0$ is a global minimum of the axion potential. Also in this case this is a consequence of the fact that QCD is a vector-like theory, and, in turn, this guarantees that in the path integral measure is positive definite [30]. The very same results can be found computing the minimum of the axion potential $V(a)$ within the chiral Lagrangian techniques, as we will do in the next section.

Before discussing the proprieties of the axion effective Lagrangian, some remarks are in order. The new gauge term in eq. 1.35 is no more described by a total derivative, hence one should expect effects in perturbation theory. Moreover the Lagrangian is non-renormalisable, in particular the axion-gluon operator has dimension 5. This means that f_a describes the cut off energy at which the EFT breaks down and, for this reason, a UV completion is necessary. The first axion model was build by Peccei and Quinn [1; 2] in which they included a $U(1)_{PQ}$ global chiral symmetry, extending the global symmetries of the SM. This new symmetry is spontaneously broken and anomalous under QCD. Later on Weiberg and Wilczek [4; 3], built on the original model and identified the pseudo-Goldstone boson produced by the spontaneous symmetry

breaking as the axion particle. Before coming to the discussion of explicit axion models, we will consider in the following some general properties of axion effective Lagrangians.

1.3.1 The effective axion Lagrangian

The main goal of this section is to derive the axion potential using an EFT within χPT (see e.g. [40]), since we are working at low energies, below the scale of QCD confinement $\Lambda_{QCD} \sim 200\text{MeV}$. The choice to work with χPT will be justified at the end of this section with the computation of the axion mass, which turns out to be parametrically smaller than Λ_{QCD}. The following discussion is model-independent and, for simplicity, we will take into account a 2-flavour QCD with:

$$q = \begin{pmatrix} u \\ d \end{pmatrix}, \qquad M_q = \begin{pmatrix} m_u & 0 \\ 0 & m_d \end{pmatrix}, \tag{1.37}$$

since the up and down quarks are the lightest ones with masses $m_u \simeq 2.32\text{MeV}$ and $m_d \simeq 4.71\text{MeV}$ [36]. In these terms the axion effective Lagrangian reads

$$\mathcal{L}_a^{eff} = \frac{1}{2}(\partial_\mu a)^2 - \bar{q}_L M_q q_R + \frac{\partial_\mu a}{2f_a}\bar{q}c_q^0\gamma^\mu\gamma_5 q + \frac{1}{4}g_{a\gamma}^0 aF\tilde{F} + \frac{a}{f_a}\frac{g_s^2}{32\pi^2}G\tilde{G} + \text{h.c.}\,, \tag{1.38}$$

where c_q^0 and $g_{a\gamma}^0$ describes respectively the coupling diagonal matrix between axion and quark axial current and the coupling between $F\tilde{F}$ and the axion field. The meaning and the physical derivation of these couplings will be discussed in section 1.4.

There is a preferred basis in which to perform the computation, indeed it is convenient to rotate away the $a\tilde{G}G$ through a field-dependent axial transformation of quarks field, i.e.

$$q \to e^{i\gamma_5 \frac{a}{2f_a}Q_a} q\,. \tag{1.39}$$

Applying the rotation to 1.35 two new terms are added from the non-invariance of the path-integral measure:

$$\delta\mathcal{L}_a^{eff} = -\frac{a}{f_a}\frac{g_s^2}{32\pi^2}\,\text{Tr}(Q_a)G\tilde{G} - N_c\frac{\alpha}{4\pi f_a}\,\text{Tr}(Q_a Q^2)F\tilde{F}\,. \tag{1.40}$$

In particular, requiring $\text{Tr}(Q_a) = 1$ it is possible to cancel out the gluon-axion coupling. To achieve this configuration we choose $Q_a = 1/2\ \text{diag}(1,1)$. The above transformation gives the following replacements:

$$\begin{aligned} &g_{a\gamma}^0 \to g_{a\gamma} = g_{a\gamma}^0 - (2N_c)\frac{\alpha}{2\pi f_a}\,\text{Tr}(Q_a Q^2), \\ &c_q^0 \to c_q = c_q^0 - Q_a, \\ &M_q \to M_a = e^{i\frac{a}{2f_a}Q_a} M_q e^{i\frac{a}{2f_a}Q_a}, \end{aligned} \tag{1.41}$$

where $\alpha = e^2/4\pi$ and N_c is the number colours equal to 3. The Lagrangian in 1.38 becomes:

$$\mathcal{L}_a^{eff} = \frac{1}{2}(\partial_\mu a)^2 - \bar{q}_L M_a q_R + \frac{\partial_\mu a}{2f_a}\bar{q}c_q\gamma^\mu\gamma_5 q + \frac{1}{4}g_{a\gamma}aF\tilde{F} + \text{h.c.}\,. \tag{1.42}$$

Now, it is possible to compute the chiral axion Lagrangian describing an EFT below the QCD confinement, Λ_{QCD}. To achieve this, it is sufficient to rewrite the Lagrangian using the new definition of mass given by the last term in eq. 1.41. We collect the pion fields in the Σ matrix which reads:

$$\Sigma = \exp\left(i\frac{\pi^a\sigma^a}{f_\pi}\right) = \mathbb{1}\cos\frac{\pi}{f_\pi} + i\frac{\sigma^a\pi^a}{\pi}\sin\frac{\pi}{f_\pi}, \tag{1.43}$$

where $\pi = \sqrt{\pi_0\pi_0 + 2\pi_+\pi_-}$, $f_\pi = 92.21$MeV represents the pion decay constant, σ^a stands for the Pauli matrices and the pion matrix is

$$\pi^a\sigma^a = \begin{pmatrix} \pi^0 & \sqrt{2}\pi^+ \\ \sqrt{2}\pi- & -\pi^0 \end{pmatrix}. \tag{1.44}$$

With these definitions the chiral Lagrangian reads:

$$\mathcal{L}_a^{\chi PT} = \frac{f_\pi^2}{4}\left[\mathrm{Tr}[(D^\mu\Sigma)^\dagger D_\mu\Sigma] + \mathrm{Tr}(\chi^\dagger\Sigma + \chi\Sigma^\dagger)\right] + \frac{\partial_\mu a}{f_a}\frac{1}{2}\mathrm{Tr}[c_q\sigma^a]J_\mu^a, \tag{1.45}$$

where $\chi = 2B_0M_a$, B_0 is linked to quark condensate state, and J_μ^a is the chiral axial current define, at lower order (LO), as:

$$J_\mu^a = \frac{i}{4}f_\pi^2\,\mathrm{Tr}[\sigma^a\{\Sigma, D^\mu\Sigma\}]\,. \tag{1.46}$$

The axion potential and mass

The non derivative part of equation 1.45 represents the potential of the axion field:

$$V(a,\pi^0) = -\frac{1}{2}f_\pi^2B_0\,\mathrm{Tr}[\Sigma M_a^\dagger + h.c.], \tag{1.47}$$

where M_a is defined in the last term of 1.41. Notice that we are not considering $\pi^\pm$ contributions since they cannot mix with the neutral axion field due to $U(1)_{EM}$ gauge invariance. Taking as before the conventional choice of $Q_a = 1/2\ \mathrm{diag}(1,1)$ we can rewrite the potential as:

$$\begin{aligned} V(a,\pi^0) &= -f_\pi^2B_0\,\mathrm{Re}\,\mathrm{Tr}[\Sigma M_a^\dagger] \\ &= -f_\pi^2B_0\,\mathrm{Re}\,\mathrm{Tr}\left[e^{i\frac{\pi}{f_\pi}}\begin{pmatrix} m_u & 0 \\ 0 & m_d \end{pmatrix}e^{i\frac{a}{2f_a}\mathbb{1}}\right]. \end{aligned} \tag{1.48}$$

We further decompose the exponential pion matrix into a real and imaginary component, using the relation:

$$e^{i\frac{\pi}{f_\pi}}\Big|_{\pi^\pm\to 0} = \mathbb{1}\cos\frac{\pi^0}{f_\pi} + i\sigma^3\sin\frac{\pi^0}{f_\pi}\,. \tag{1.49}$$

In particular, since we are interesting in the real part of the trace, the only surviving terms are those are quadratic in the sine or cosine. By performing the computation we get:

$$V(a,\pi^0) = -f_\pi^2B_0(m_u+m_d)\left[\cos\frac{\pi^0}{f_\pi}\cos\frac{a}{2f_a} + \frac{m_u-m_d}{m_u+m_d}\sin\frac{\pi^0}{f_\pi}\sin\frac{a}{2f_a}\right]. \tag{1.50}$$

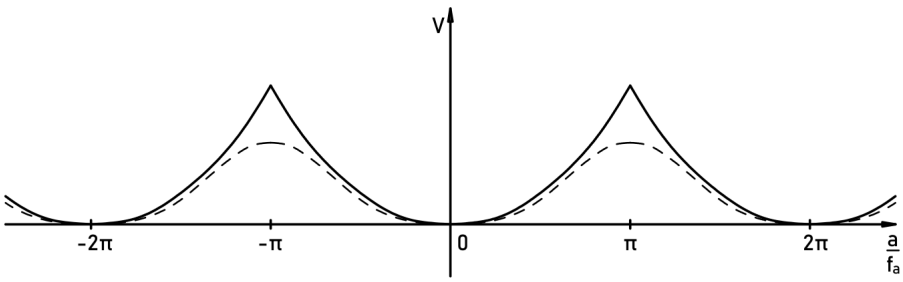

Figure 1.3: The figure compare the two ways of computing the axion potential discussed in the text: the instanton potential is indicated with the a dashed line, instead the chiral axion potential is sketch with a solided line. It is clear that at the minimum the behaviours of the different potentials coincide, whereas, around the maximum, the difference is large.

At this point it is easy to verify that the axion potential field is described by[10] [41; 42]:

$$V(a,\pi^0) = -m_\pi^2 f_\pi^2 \sqrt{1 - \frac{4m_u - m_d}{(m_u+m_d)^2}\sin^2\frac{a}{2f_a}}\cos\left(\frac{\pi^0}{f_\pi} - \phi(a)\right), \quad (1.51)$$

with

$$\tan\phi(a) = \frac{m_u - m_d}{m_u + m_d}\tan\frac{a}{2f_a}\,. \quad (1.52)$$

Since the ultimate goal is the mass computation associated with the axion field, it is now convenient to discuss the minimum of the newly calculated potential. The presence of trigonometric functions together with the minus sign in front of the square root, implies that the global minimum lies where the cosine and the sine reach the maximum and the minimum respectively. Hence, the absolute minimum is located in $\langle\pi^0\rangle = \phi(\langle a\rangle\, f_\pi)$ and $\langle a\rangle = 0$. Remembering the definition of $\phi(a)$ in eq. 1.52 we can establish that the absolute minimum is located in:

$$\begin{cases} \langle a\rangle = 0 \\ \langle\pi^0\rangle = 0 \end{cases}, \quad (1.53)$$

which implies that the strong CP problem has been solved. Note that the instanton potential defined in section 1.2.2 differs from the χPT potential just computed, as it can be seen in Fig. 1.3. Indeed, although around $a = 0$ the two potentials have the same behaviour, around the maximum, so for $a \sim f_a$, they differ from each other by a factor of order 1. This deviation is due to the fact that at confinement regime, χPT is a reliable theory, instead the instanton semi-classical approach does not work anymore because of the presence of quantum fluctuation deriving from gauge configurations which are non negligible, but they have been neglected in the semi-classical approach.

At this point, the axion mass can be computed expanding the potential in $a/f_a \ll 1$ and neglecting terms of $O(a^4)$ which will be related

[10] To achive this last expression it is convenient to use the trigonometric formula: $\frac{\cos x\cos y + \alpha\sin x\sin y}{\sqrt{\cos^2 x + \alpha^2\sin^2 y}} = \cos[y - \arctan(\alpha\tan x)]$.

to self interactions. The axion mass is:

$$m_a^2 = \frac{m_\pi^2 f_\pi^2}{f_a^2} \frac{m_u m_d}{(m_u + m_d)}, \tag{1.54}$$

which becomes, using the known values:

$$m_a^2 \sim 5.7\text{meV}\left(\frac{10^9\text{GeV}}{f_a}\right). \tag{1.55}$$

The value of the axion mass fully justifies, a posteriori, the choice of the chiral theory: if $f_a \gg 1\text{GeV}$, then we are sure that $m_a \ll \Lambda_{\chi PT}$. Astrophysical and laboratory constraints assure us that f_a is large enough, specifically $f_a \gtrsim 10^9\text{GeV}$.

To summarise, the axion is very light (sub-eV regime) and it is very weakly coupled: indeed, since f_a is large, then axion couplings $g_a \propto 1/f_a$ are suppressed. Another remarkable outcome is that the Compton wavelength of the axion, which is proportional to $1/m_a$, turns out to be macroscopic.

1.3.2 Axion couplings

We will here discuss the most important couplings which involve the axion particle since they will be important both from a phenomenological and theoretical point of view.

Axion-photon coupling

The axion particle couples to photon via a loop diagram as represented in 1.4. This coupling is particularly interesting from a phenomenological, especially astrophysical, point of view as it sets strong constraints on the axion parameter space. The expression of this coupling constant can be computed through simple steps. The quark field transformation in 1.39 as well as generating the $G\tilde{G}$ term, is anomalous even under QED being the quarks electromagnetic charged particles. The anomalous $F\tilde{F}$ term is defined as:

$$\delta S = -2N_c \frac{e^2}{32\pi^2} \frac{1}{f_a} \text{Tr}(Q_a Q_{em}^2) \frac{e^2}{32\pi^2} \int d^4x F\tilde{F}\,, \tag{1.56}$$

and we define the $g_{a\gamma}$ in the following way:

$$g_{a\gamma} = g_{a\gamma}^0 - 3\frac{e^2}{4\pi^2} \frac{1}{f_a} \text{Tr}(Q_a Q_{em}^2)\,. \tag{1.57}$$

This expression is equivalent to the first one in eq. 1.41 and $g_{a\gamma}^0$ [11] represents a model-dependent contribution. This time, the most convenient choice is to define the matrix Q_a so that the mass mixing between pions and axions is zero. This allows us to avoid calculating extra contributions to the axion-photon couplings involving mixed axion-pion propagators. Bearing in mind these considerations, the relevant matrices in flavour space are given by:

$$Q_{em} = \begin{pmatrix} 2/3 & 0 \\ 0 & -1/3 \end{pmatrix}, \quad Q_a = \begin{pmatrix} \dfrac{m_d}{m_u + m_d} & 0 \\ 0 & \dfrac{m_u}{m_u + m_d} \end{pmatrix}. \tag{1.58}$$

[11] We will derive the exact expression of $g_{a\gamma}^0$ in section 1.4.

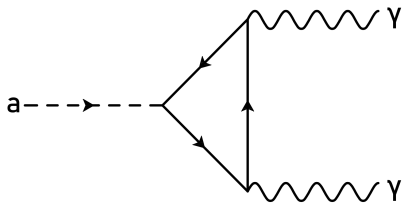

Figure 1.4: The Feynman loop diagram showing the axion-photon coupling. The value of the $g_{a\gamma}$ depends on the specific features of fermions which running in the anomalous triangle.

Computing the expression of the coupling in the chiral Lagrangian theory the final result reads:

$$g_{a\gamma} = g^0_{a\gamma} - \frac{\alpha}{2\pi f_a}\left[\frac{2}{3}\frac{4m_d + m_u}{m_u + m_d}\right] . \tag{1.59}$$

Axion-electron coupling

The interaction between axion and electron is described by the Lagrangian term

$$C_{ae}\frac{\partial_\mu a}{2f_a}\bar{e}\gamma^\mu\gamma_5 e . \tag{1.60}$$

The coupling is described by $C_{ae} = c^0_e + \delta c_e$ where c^0_e is the tree level contribution while δc_e is a radiative one. The latter is due to the presence of a photon loop and it is defined by:

$$\delta c_e = \frac{3\alpha^2}{4\pi^2}\left[\frac{E}{N}\log\left(\frac{f_a}{\mu_{IR}}\right) - \frac{2}{3}\frac{4m_d + m_u}{m_d + m_u}\log\left(\frac{\Lambda_{\chi PT}}{\mu_{IR}}\right)\right] , \tag{1.61}$$

in particular the first term is related to the running axion-electron coupling from f_a to μ_{IR} and the second one is due to the pion coupling. We indicated with $\Lambda_{\chi PT}$ the cut-off scale of the chiral symmetry (around $\sim$ 1Gev) and with μ_{IR} the energy scale of the physical process (around $\sim m_e$).

Axion-nucleon coupling

In order to describe the axion-nucleon coupling, let us take an EFT with energy $\ll \Lambda_{QCD}$, where the nucleons are non-relativistic. The derivation of the coupling expression comes out from the matching between the quark current term in the axion effective Lagrangian 1.42 and the following non-relativistic axion-nucleon Lagrangian. We will call $N = (p, n)^T$ the nucleon iso-spin doublet, v^μ the 4-velocity and S^μ the spin operator with $2\bar{p}S^\mu p = \bar{p}\gamma^\mu\gamma_5 p$. Neglecting NLO terms, considering iso-spin as an active flavour symmetry and using the axion as an external current the Lagrangian reads [40]:

$$\begin{aligned}\mathcal{L}_N &= \bar{N} v^u \partial_\mu N + 2 g_A \frac{c_u - c_d}{2} \frac{\partial_\mu a}{2 f_a} \bar{N} S^\mu \sigma^3 N + \\ &+ 2 g_0^{ug} \frac{c_u + c_d}{2} \frac{\partial_\mu a}{2 f_a} \bar{N} S^\mu N + \dots \\ &= \bar{N} v^u \partial_\mu N + 2 g_A \frac{c_u - c_d}{2} \frac{\partial_\mu a}{2 f_a} (\bar{p} S^\mu p - \bar{n} S^\mu n) + \\ &+ 2 g_0^{ud} \frac{c_u + c_d}{2} \frac{\partial_\mu a}{2 f_a} (\bar{p} S^\mu p + \bar{n} S^\mu n) + \dots \ ,\end{aligned} \tag{1.62}$$

where, considering the first step, the second term represents the iso-triplet and the last one the iso-singlet. Now we can perform the matching and taking for instance an external proton state, $\langle p| L_a^{eff} |p\rangle = \langle p| L_N |p\rangle$ we obtain:

$$\begin{aligned}&\frac{\partial_\mu a}{2 f_a} c_u \langle p| \bar{u} \gamma^\mu \gamma_5 u |p\rangle + \frac{\partial_\mu a}{2 f_a} c_d \langle p| \bar{d} \gamma^\mu \gamma_5 d |p\rangle = \\ &= \frac{\partial_\mu a}{2 f_a} g_A \frac{c_u - c_d}{2} 2 \langle p| \bar{p} S^\mu p |p\rangle + \frac{\partial_\mu a}{2 f_a} g_0^{ud} \frac{c_u + c_d}{2} 2 \langle p| \bar{p} S^\mu p |p\rangle \ .\end{aligned} \tag{1.63}$$

The first two terms in the left-hand-side could be respectively rewritten in terms of the spin operator as $S^\mu \Delta u$ and $S^\mu \Delta d$, instead those in the right-hand-side are simply proportional to S^μ. In this way the matching gives:

$$\begin{aligned}g_A &= \Delta u - \Delta d \\ g_0^{ud} &= \Delta u + \Delta d \ .\end{aligned} \tag{1.64}$$

and substituting these expressions in eq. 1.62 we get:

$$\mathcal{L}_N \supset \frac{\partial_\mu a}{2 f_a} \Big[(c_u \Delta u + c_d \Delta d)(\bar{p} \gamma^\mu \gamma_5 p) + (c_d \Delta u + c_u \Delta d)(\bar{n} \gamma^\mu \gamma_5 n) \Big] \ . \tag{1.65}$$

The coupling matrix $C_{aN} = \mathrm{diag}(C_{ap}, C_{an})$ is computed recalling that $c_q = c_q^0 - Q_a$ with Q_a defined as in eq. 1.58. Rewriting the axion-nucleon coupling as

$$\frac{\partial_\mu a}{2 f_a} \bar{N} C_{aN} \gamma^\mu \gamma_5 N \ , \tag{1.66}$$

the C_{aN} components read:

$$C_{ap} = -\left(\frac{m_d}{m_u + m_d} \Delta u + \frac{m_u}{m_u + m_d} \Delta d \right) + c_u^0 \Delta u + c_d^0 \Delta d \ , \tag{1.67}$$

$$C_{an} = -\left(\frac{m_u}{m_u + m_d} \Delta u + \frac{m_d}{m_u + m_d} \Delta d \right) + c_d^0 \Delta u + c_u^0 \Delta d \ , \tag{1.68}$$

where the low-energy QCD parameters are computed via lattice QCD techniques: $\Delta u = 0.897(27)$, $\Delta d = -0.376(27)$ and $\left.\frac{m_u(2\mathrm{GeV})}{m_d(2\mathrm{GeV})}\right|_{\overline{MS}} = 0.48(3)$ [42].

1.4 From axion EFTs to axion models

In this section, we will introduce three different axion models, which provide the standard benchmarks for axion experimental searches. Before discussing that, however, it could be useful to understand what is the origin of the effective couplings $g^0_{a\gamma}$ and c^0_q defined in eq. 1.38, since we will see that they are model-dependent quantities. The current associated to the spontaneously broken $U(1)_{PQ}$ symmetry is anomalous and hence its divergence is equal to:

$$\partial^\mu J^{PQ}_\mu = \frac{g_s^2 N}{16\pi^2} G\tilde{G} + \frac{e^2 E}{16\pi^2} F\tilde{F}, \tag{1.69}$$

where N and E represent QCD and EM anomaly coefficients. The spontaneous breaking of the PQ symmetry is characterised by the order parameter, v_a, and from the Goldstone theorem it follows that $\langle 0|J^{PQ}_\mu|a\rangle = iv_a p_\mu$. Therefore, focusing on the two terms related to the anomalies and to the axion interaction with the PQ current, the axion Lagrangian reads:

$$\mathcal{L}_a = \frac{a}{v_a}\frac{g_s^2 N}{16\pi^2} G\tilde{G} + \frac{a}{v_a}\frac{e^2 E}{16\pi^2} F\tilde{F} + \frac{\partial_\mu a}{v_a} J^{PQ}_\mu \,. \tag{1.70}$$

Comparing this with the expression 1.38, one finds:

$$f_a \equiv \frac{v_a}{2N} \tag{1.71}$$

and

$$g^0_{a\gamma} \equiv \frac{\alpha}{2\pi f_a}\frac{E}{N} \,. \tag{1.72}$$

The last term in eq. 1.70 can be rewritten using right and left component of a chiral fermion f, as $-J^{PQ}_\mu|_f = \bar{f}_L \chi_{f_L} \gamma^\mu f_L + \bar{f}_R \chi_{f_R} \gamma^\mu f_R$, where χ_f represents the PQ charge. Finally, neglecting the vector current components which vanish upon integration by parts and the application of the equation of motion, the last term becomes:

$$\frac{\partial_\mu a}{v_a} J^{PQ}_\mu = \frac{\partial_\mu a}{2f_a} \bar{f} c^0_f \gamma^\mu \gamma_5 f, \tag{1.73}$$

with

$$c^0_f \equiv \frac{\chi_L - \chi_R}{2N} \,. \tag{1.74}$$

1.4.1 WW model

The first model proposed to realise the PQ mechanism was further developed by Weinberg and Wilczek [3; 4] and it is known as WW model. Two extra doublets are introduced to implement the $U(1)_{PQ}$, whereas the SM quarks, charged under the PQ symmetry, are responsible for the QCD current anomaly. The main assumption of this model is to consider the decay constant f_a of the order of the electroweak scale ($f_a \sim 250$GeV), which yields a lifetime of the order of $\tau_a \sim 0.7$s. This model was quickly ruled out by experimental evidence involving the meson decays $K^+ \to \pi^+ a$ [43] or Quarkonia decays $J/\psi \to \gamma a$ [44].

From the WW model failure, a new class of so-called "invisible" axion models arised. In these models the PQ scale is decoupled from

the electroweak scale, thus the axion couplings can be enough suppressed to survive the experimental constraints. In the following we describe two different types of "invisible" axion models, which differ according to the type of fermions which generate the QCD anomaly of the PQ current.

1.4.2 KSVZ model

In the Kim-Shifman-Vainsthein-Zakharov (KSVZ) model [8; 9] the SM content is extended with a new vector-like fermion $Q \sim (3,1,0)$ and a SM-singlet complex scalar $\Phi \sim (1,1,0)$. On the other hand, unlike the WW model, the SM quarks and leptons are not charged under $U(1)_{PQ}$. The Lagrangian reads

$$\mathcal{L}_{KSVZ} = |\partial_\mu \Phi|^2 + \bar{Q} i \not{D} Q - (y_Q \bar{Q}_L Q_R \Phi + \text{h.c.}) - V(\Phi) \tag{1.75}$$

and it is clearly symmetric under the $U(1)_{PQ}$ transformations defined as

$$\Phi \to e^{i\alpha\Phi}, \qquad Q_L \to e^{i\alpha/2} Q_L, \qquad Q_R \to e^{-i\alpha/2} Q_R \,. \tag{1.76}$$

The mexican-hat potential is defined as

$$V(\Phi) = \lambda \left(|\Phi|^2 - \frac{v_a^2}{2} \right) \tag{1.77}$$

and it breaks the $U(1)_{PQ}$ symmetry with order parameter v_a. In particular, from the explicit expression of Φ in polar coordinate

$$\Phi = \frac{1}{\sqrt{2}} (v_a + \rho) e^{ia/v_a} \,, \tag{1.78}$$

one can easily notice that the axion field corresponds to the Goldstone mode, so it is massless at tree level. On the other hand, the radial mode ρ acquires a mass that is $m_\rho^2 = 2\lambda v_a^2$. After the SSB, because of the presence of the Yukawa interaction in 1.76, also the new fermion acquires a mass of $m_Q = y_Q v_a / \sqrt{2}$. Considering that $v_a \gg v_{EW}$, then it is possible to integrate out the heavy radial model and obtain:

$$\mathcal{L}_{KSVZ} = -m_Q \bar{Q}_L Q_R e^{ia/v_a} + \text{h.c.} \,. \tag{1.79}$$

In order to decoupled also the heavy fermion field from the axion, we perform an axion-dependent axial rotation

$$Q \to e^{-i\gamma_5 \frac{a}{2v_a}} Q \,. \tag{1.80}$$

Once this is done, also the heavy new fermion field can be integrated out. Nevertheless, the above rotation is anomalous under QCD and therefore the Lagrangian gets a new term:

$$\delta\mathcal{L}_{KSVZ} = \frac{g_s^2}{32\pi^2} \frac{a}{v_a} G\tilde{G}. \tag{1.81}$$

Comparing this with eq. 1.70, it implies $2N = 1$ and hence $f_a = v_a$. This $a\tilde{G}G$ operator is the basic ingredient required by the PQ mechanism and it represents also the only axion coupling with the SM fields. As a consequence in the $KSVZ$ model both c_f^0 and $g_{a\gamma}^0$ are zero.

It is also possible to make an alternative choice for the heavy fermion Q and consider a general representation $Q \sim (C, I, Y)$ under the SM gauge group: $SU(3)_C \times SU(2)_L \times U(1)_Y$. In this case an anomalous EM terms arises as well, implying a non-zero $g^0_{a\gamma}$ [12].

1.4.3 DFSZ model

The Dine-Fischler-Srednicki-Zhitnitsky (DFSZ) model [10; 11] presents another possible UV completion where the anomaly, as in the WW model, is due to SM quarks. However, in this case, the SM fields are extended with two Higgs doublets $H_i \sim (1, 2, -1/2)$, with $i = 1, 2$, and a complex scalar field σ which allows the decoupling between PQ and EW scale. We are particularly interested in this model since in the following chapters we will use it as a theoretical basis for our calculations. The most general potential of this model containing all the gauge invariant terms, reads:

$$V(H_1, H_2, \sigma) = \tilde{V}_{moduli}(|H_1|, |H_2|, |\sigma|, |H_1 H_2|) + \lambda H_1 H_2^\dagger \sigma^2 + \text{h.c} \ . \quad (1.82)$$

The global symmetries of the scalar kinetic terms include three $U(1)$ rephasings, one for each field introduced. These are broken by the last term in the potential down to two linearly independent $U(1)$, which can be chosen to be the SM hypercharge and the PQ symmetry:

$$U(1)_{H_1} \times U(1)_{H_2} \times U(1)_\sigma \to U(1)_Y \times U(1)_{PQ} \ . \quad (1.83)$$

Neglecting both radial and charged modes (which have no projection on the neutral axion Goldstone mode), we can parametrize the scalar fields as

$$H_i = \frac{v_i}{\sqrt{2}} e^{i a_i / v_i} \begin{pmatrix} 1 \\ 0 \end{pmatrix} + \dots \ , \qquad \sigma = \frac{v_\sigma}{\sqrt{2}} e^{i a_\sigma / v_\sigma} + \dots \ , \quad (1.84)$$

with the VEV hierarchy $v_\sigma \gg v_{1,2}$. Contrary to what happened in the KSVZ model, here the definition of the axion is non-trivial. The presence of different fields contribute, with their VEV, to the final expression of PQ order parameter v_a. In order to obtain the linear combination which define the axion, let us compute the PQ current:

$$J^{PQ}_\mu = -i \left(\sigma^\dagger \overset{\leftrightarrow}{\partial_\mu} \sigma + \sum_{i=1,2} \chi_i H_i^\dagger \overset{\leftrightarrow}{\partial_\mu} H_i + \dots \right) , \quad (1.85)$$

where χ_i represents the PQ charge of the Higgs doublets and dots stand for the fermionic terms which do not contribute to the axion expression. Therefore, focusing on the a_i and a_σ terms we obtain:

$$J^{PQ}_\mu|_a = \sum_{i=1,2,\sigma} \chi_i v_i \partial_\mu a_i \ . \quad (1.86)$$

On the whole, the physical axion field is defined as [46]:

$$a = \frac{1}{v_a} \sum_{i=1,2,\sigma} \chi_i v_i a_i \ , \quad (1.87)$$

[12] A comprehensive analysis on the phenomenologically preferred values of $g^0_{a\gamma}$ can be found in [45].

in such a way that the definition satisfies the Goldstone theorem and the axion current is $J_\mu^{PQ}|_a = v_a \partial_\mu a$. The explicit expression of the PQ order parameter v_a is obtained requiring the invariance under a PQ transformation[13] and it reads as:

$$v_a^2 = \sum_{i=1,2,\sigma} \chi_i^2 v_i^2 \,. \tag{1.88}$$

The combination of the PQ charges can be found by taking into account two points. First of all the last term in eq. 1.82 must preserve the PQ symmetry, so that under a PQ transformation we get $-\chi_1 + \chi_2 - 2\chi_\sigma = 0$, where $\chi_1 \equiv \chi_{H_1}$ and $\chi_2 \equiv \chi_{H_2}$. Secondly, we want the orthogonality between the axion and Z boson field: in this way we are sure that there is no mixing and this guarantees the possibility to integrate the Z boson away in the effective Lagrangian. This is translated in the requirement that the C coefficient in the expression $C\partial_\mu a Z^\mu$ is equal to zero, which in terms of PQ charge gives $\chi_1 v_1^2 + \chi_2 v_2^2 = 0$. Consequently the PQ charges, up to an overall normalization that we fix by choosing $\chi_\sigma = 1$, reads:

$$\chi_\sigma = 1, \qquad \chi_1 = -2\sin^2\beta, \qquad \chi_2 = 2\cos^2\beta, \tag{1.89}$$

where $\cos\beta = \dfrac{v_1}{v}$ and $\sin\beta = \dfrac{v_2}{v}$, with $v^2 = v_1^2 + v_2^2$ and $v \sim 246\text{GeV}$. In this notations one has $\tan\beta = \dfrac{v_2}{v_1}$. By means of eq. 1.88 we then obtain:

$$v_a^2 = v_\sigma^2 + v^2(\sin 2\beta)^2 \,. \tag{1.90}$$

Notice that v_σ can be arbitrary large because it does not break any SM gauge symmetry, hence if $v \ll v_\sigma$, then $v_a \sim v_\sigma$.

At this point, we focus on the Yukawa Lagrangian which is where the axion couplings with the SM fields come from. In the current basis the Yukawa Lagrangian is:

$$\mathcal{L}_Y = -Y_u \bar{q}_L u_R H_1 + Y_d \bar{q}_L d_R \tilde{H}_2 + Y_E \bar{l}_L e_R \tilde{H}_2 + \text{h.c.} \,. \tag{1.91}$$

One can pass in the mass basis putting the expression in the vacuum and replacing the exponential, through eq. 1.87, $a_1/v_1 \to \chi_1 a/v_a$, $a_2/v_2 \to \chi_2 a/v_a$. The Yukawa Lagrangian becomes:

$$\mathcal{L}_Y = -m_u \bar{u}_L u_R e^{i\chi_1 \frac{a}{v_a}} - m_d \bar{d}_L d_R e^{-i\chi_2 \frac{a}{v_a}} - m_E \bar{e}_L e_R e^{-i\chi_2 \frac{a}{v_a}} + \text{h.c.} \,. \tag{1.92}$$

The interaction of quarks and charged lepton with the axion is now explicit. We next perform an axial rotation (as in eq. 1.80 for the KSVZ model) in order to remove the axion field from the Yukawa Lagrangian:

$$\begin{aligned} u &\to e^{-i\gamma_5\chi_1 \frac{a}{2v_a}} u, \\ d &\to e^{i\gamma_5\chi_2 \frac{a}{2v_a}} d, \\ e &\to e^{i\gamma_5\chi_2 \frac{a}{2v_a}} e, \end{aligned} \tag{1.93}$$

which, in turn, are anomalous under QCD and EM. The anomaly yields the following shift on the axion effective Lagrangian:

[13] A general PQ transformation $a_i \to a_i + \alpha\chi_i v_i = \chi_i v_i (a_i + \alpha\chi_i v_i)$ transforms the axion field as $a \to a + \alpha v_a$, so imposing the invariance we obtain the eq. 1.88.

$$\delta\mathcal{L}_Y = \frac{\alpha_s}{8\pi}\frac{a}{f_a}G\tilde{G} + \frac{\alpha}{8\pi}\left(\frac{E}{N}\right)\frac{a}{f_a}F\tilde{F}, \tag{1.94}$$

where f_a is defined as in eq. 1.71, while N and E are found to be:

$$\begin{aligned} N &= n_g\left(\chi_{q_L} + \frac{1}{2}\chi_{u_R} + \frac{1}{2}\chi_{d_R}\right) = \\ &= n_g\left(\frac{1}{2}\chi_1 - \frac{1}{2}\chi_2\right) = -3, \end{aligned} \tag{1.95}$$

$$E = n_g\left(3\left(\frac{2}{3}\right)^2\chi_1 - 3\left(-\frac{1}{3}\right)^2\chi_2 - (-1)^2\chi_2\right) = -8, \tag{1.96}$$

with $n_g = 3$ the number of SM fermion generation. The above fermionic transformations affect also the kinetic terms which generate the derivative couplings between the axion and the SM fields:

$$\delta(\bar{u}i\partial\!\!\!/u) = \chi_1\frac{\partial_\mu a}{2v_a}\bar{u}\gamma^\mu\gamma_5 u = \left(\frac{1}{3}\sin^2\beta\right)\frac{\partial_\mu a}{2f_a}\bar{u}\gamma^\mu\gamma_5 u, \tag{1.97}$$

$$\delta(\bar{d}i\partial\!\!\!/d) = \chi_2\frac{\partial_\mu a}{2v_a}\bar{d}\gamma^\mu\gamma_5 d = \left(-\frac{1}{3}\cos^2\beta\right)\frac{\partial_\mu a}{2f_a}\bar{d}\gamma^\mu\gamma_5 d, \tag{1.98}$$

$$\delta(\bar{e}i\partial\!\!\!/e) = \chi_2\frac{\partial_\mu a}{2v_a}\bar{e}\gamma^\mu\gamma_5 e = \left(-\frac{1}{3}\cos^2\beta\right)\frac{\partial_\mu a}{2f_a}\bar{e}\gamma^\mu\gamma_5 e, \tag{1.99}$$

from which we can read the effective axion-fermion couplings. In the notation of eq. 1.74 these are given by:

$$c^0_{u,c,t} = \frac{1}{3}\sin^2\beta, \quad c^0_{d,s,b} = -\frac{1}{3}\cos^2\beta, \quad c^0_{e,\mu,\tau} = -\frac{1}{3}\cos^2\beta, \tag{1.100}$$

The value of $\tan\beta$ is constrained by perturbative unitarity limits on the Yukawa couplings of the extended Higgs sector $y^{DFSZ}_{t,b} < \sqrt{16\pi/3}$ (see e.g. [47]). Therefore, taking into account the SM relations $y^{SM}_t = \sqrt{2}m_t/v = y^{DFSZ}_t\cos\beta$ and $y^{SM}_b = \sqrt{2}m_t/v = y^{DFSZ}_t\sin\beta$ and using m_t=173.1 GeV, m_b=4.18 GeV and v=246 GeV, one obtains the perturbativity range:

$$\tan\beta \in [0.0024, 4.0]\ . \tag{1.101}$$

Chapter 2

Axion phenomenology

The possible presence of the light axion field opens the door to a wide range of phenomenological and experimental implications. In the previous chapter we discussed how the axion arises as a possible solution to the strong CP problem, and derived its mass range and some general properties such as the couplings to SM particles. The axion parameter space can be constrained via astrophysical and cosmological considerations, that are important in order to narrow down the most interesting regions for experimental searches. In this chapter we will offer a brief overview of stellar evolution and consider the most relevant astrophysical bounds related to axion physics. Subsequently, we will discuss cosmological implications as well as some experimental setups relevant for axion searches.

2.1 Astrophysical implications

Astrophysics and especially stars are excellent tools to derive axion bounds. The crucial properties of stars, such as the high temperature and density, make these possible sources of axion particles and allow us to probe the axion couplings to SM particles. In particular, if there was a significant production of axions this would give physical effects on the thermal evolution of the star. For this reason it is useful to briefly present the life of a star and discussed some thermal characteristics.

The stellar evolution is usually described in terms of the Hertzsprung-Russel (HR) diagram or Colour Magnitude Diagram (CMD) to discuss the various stages in which a star could be. Fig. 2.1 **(a)** is an example of a HR diagram. In the x-axis the colour index (B-V) is used as an effective temperature measure, instead the y-axis represents a measure of the luminosity through the absolute visual magnitude. Note that the upper diagram in Fig. 2.1 represents the CMD of a globular cluster. This is a convenient choice since all the stars in a globular cluster have approximately the same age. In this way, we are able to discuss how the initial features affect the evolution of the star, in particular it can be seen that the larger is the mass of the star, the faster is its evolution, as to sustain the gravitation collapse a greater nuclear energy must be released. We now discussed why the HR diagram represents a powerful tools to test the theory of stellar evolution.

The life of a star is strongly dependent on its initial mass, hence we can divide stars into two main groups: stars with an initial mass

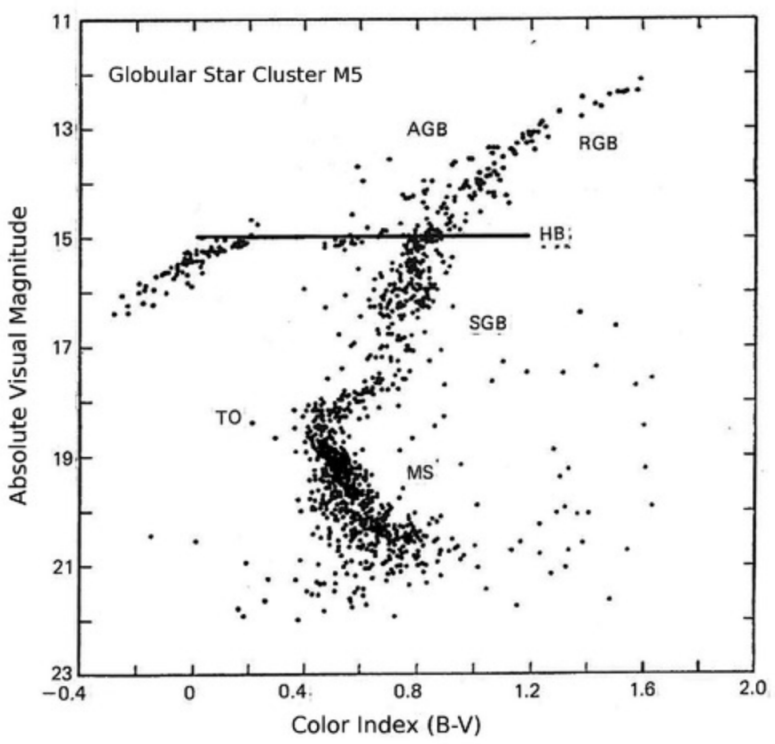

(a) *HR diagram of a globular system.*

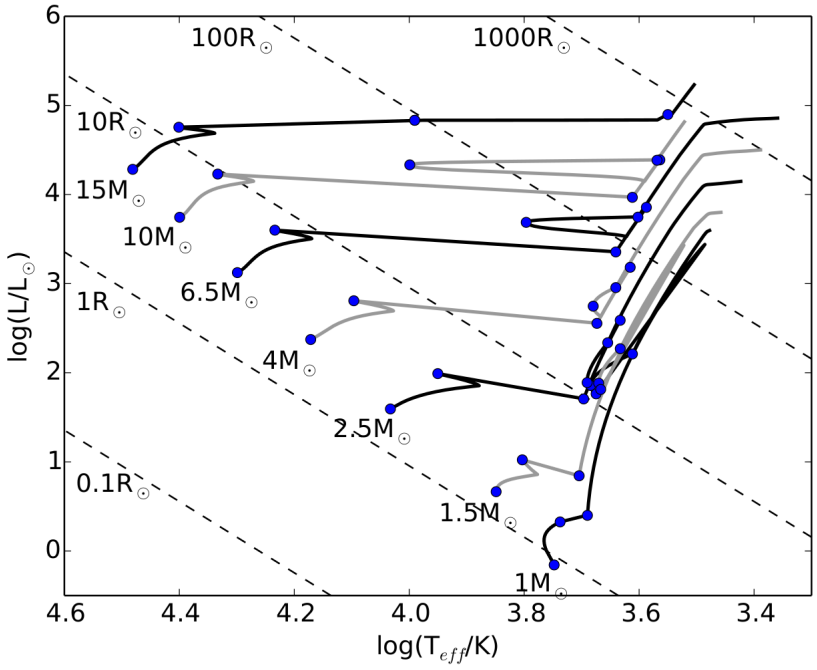

(b) *Theoretical HR diagram shows different stellar evolution.*

Figure 2.1: Figure **(a)** [48]: HR diagram of the Globular Star Cluster M5. The acronyms stand for: MS - Main Sequence, TO - Turn Off, SGB - Sub Giant Branch, HB - Horizontal Branch, RGB - Red Giant Branch, AGB - Asymptotic Giant Branch. Figure **(b)** [49]: HR diagram shows how a different initial star mass has a crucial implication on its evolution. In both figures the hottest star (bluest) are on the left and the temperature decreases towards the right of the diagram.

$M \lesssim 8M_\odot$ and stars with a mass above $8M_\odot$. The main difference is that the lightest stars will become White Dwarfs (WDs), instead the heaviest ones will incur in a supernova core collapse, causing a type II supernova explosion and forming a compact object. In both of the cases, the life of a star begins in the Main Sequence (MS) where it spends most of the time during the burning of the hydrogen. This nuclear reaction gradually forms a helium nucleus and, in stars with a mass close to the solar one, the reaction moves in a thick shell and the star moves in the Sub Giant Branch (SGB). Meanwhile, the He-nucleus starts to shrink to achieve the temperature needed for the helium burning, while the hydrogen shell gradually becomes thinner. Because of the mirror principle, as the nucleus contracts, then the envelopes expand and the star passes into the phase of a Red Giant (RG). Considering stars of $M \lesssim 2M_\odot$, the helium core is degenerate and the ignition of the nuclear reaction causes the so called Helium flash, moving the stars on the Horizontal Branch (HB). On the other hand, stars heavier than the latter regime starts to burn He in thermal equilibrium when they reach sufficiently high temperature and density. Solar-like stars have not enough mass to ignite other elements and they will end as WDs. Proportionally to their initial mass, the star continues to burn until they reach (for stars with $M \gtrsim 8M_\odot$) the production of iron. At this point the burning process is no longer exothermic and the star begins a rapid gravitational collapse. Depending on whether or not this collapse is supported by the pressure of degeneration, neutron stars or black holes will form. Some patterns of evolution of different stars are shown in Fig. 2.1 **(b)**.

In light of all this, one can interpret the HR diagram as a sort of evolutionary map: each star, depending on the phase it is going through, will be placed at a specific point of it. Even though Fig. 2.1 **(b)** is only a theoretical construction, several numerical simulations have confirmed the validity of the HR diagram, confirming that the region with the highest source density in the CMD corresponds to the longest stage of evolution. The compatibility of the theoretical CMD diagram with observations implies strong bounds on new particles which can affect the thermal evolution of a star. The most relevant axions bounds from stellar cooling, depending on the specific axion coupling, are discussed in the following subsections.

2.1.1 Axion production channels in stars

Before discussing astrophysical bounds on axion couplings, we provide here a qualitative description of the main axion production channels in stars.

Primarkoff process

The process describes the creation of an axion particle by a thermal photon. In particular, as it can be seen in the upper-left diagram in Fig. 2.2, the thermal photon interacts with the electrostatic field due to the presence of electrons or ions in the stellar plasma according to the reaction:

$$\gamma + Ze \to a + Ze \,. \tag{2.1}$$

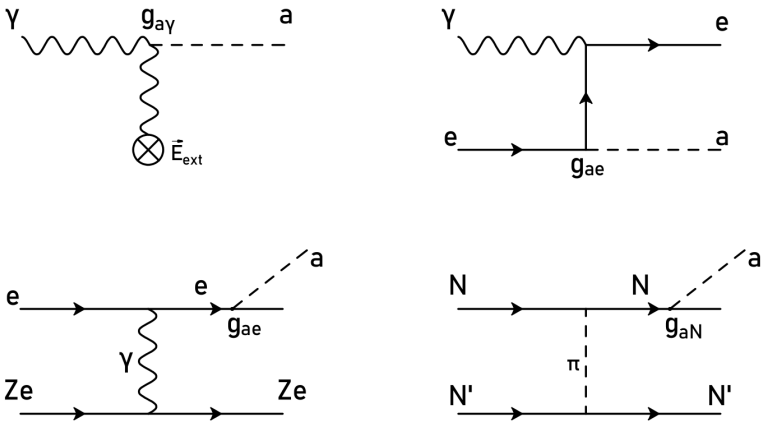

Figure 2.2: Feynman diagrams of different axion production channels. From left to right, from top to bottom: Primarkoff process, Compton process, electron Bremsstrahlung process, nucleon Bremsstrahlung process. In all cases the axion coupling is indicated explicitly.

The transition rate from a photon of a given energy to an axion of the same energy is given by [50]:

$$\Gamma_{\gamma\to a} \simeq \frac{g_{a\gamma}^2 T}{32\pi^2} k_s^2 \,, \tag{2.2}$$

where $g_{a\gamma}$ is defined in eqs. 1.56, 1.57, T is the temperature at which the process takes place and k_s^2 is the so-called Debye-Huckel screening wave number defined by $k_s^2 = \frac{4\pi\alpha}{T}\left(n_e + \sum_{nuclei} Z_j^2 n_j\right)$, with n_e the electron density, n_j the density of the $j-$th ion and the Z_j the charge number of that ion[50]. Moreover, it is possible to define the energy loss rate per unit volume

$$Q \simeq \frac{g_{a\gamma}^2 T^7}{4\pi} \tag{2.3}$$

and the energy loss rate per unit mass, given by [51][1]

$$\epsilon_p \simeq 2.8 \cdot 10^{-31} \left(\frac{g_{a\gamma}}{\mathrm{GeV}^{-1}}\right)^2 \frac{T^7}{\rho} \,\mathrm{erg\,g^{-1}\,s^{-1}} \,, \tag{2.4}$$

where T is defined in K while ρ, which described the density at which the process takes place, is defined in g cm^{-3}. From the last equation, it is clear that the Primarkoff process is strongly dependent on temperature because it controls the number of thermal photons. On the other hand, the Primakoff process turns out to be suppressed in super dense star cores, such as in WDs and RGB.

Compton process

The Compton process is sketched in the upper-right diagram in Fig.2.2 and it is described by:

$$\gamma + e \to a + e \,. \tag{2.5}$$

[1] All the numerical values for the energy loss rate in this section will be taken from this reference, where the authors offer a summary of axion production channels.

In short, as in the Primarkoff process, the scattering of a thermal photon due to an electron creates an axion. However, as it can be seen in the Feynman diagram, this time the coupling corresponds to an axion-electron coupling since the virtual process mediator is an electron. As we have done in the previous case, we can compute the emission rate per unit mass due to the Compton process, it reads

$$\epsilon_c \simeq 2.7 \cdot 10^{-22} g_{ae}^2 \frac{1}{\mu_e} \left(\frac{n_e^{eff}}{n_e} \right) T^6 \, \mathrm{erg\,g^{-1}\,s^{-1}} \, , \tag{2.6}$$

where $\mu_e = (\sum X_j Z_j / A_J)^{-1}$ with X_j the relative mass density of the $j-$th ion while Z_j and A_j the charge and mass number respectively, n_e is the number density of electrons and n_e^{eff} is the effective number density of electrons.

Even in this case, the process is strongly dependent on temperature and, even though it is not explicitly defined, it is inversely proportional to the density. In fact, the value of n_e^{eff} is suppressed at high density since the degeneracy effect reduces the number of the electron targets and this, in turn, reduces the Compton rate. Then, also in this case the Compton process is not efficient in high-density star regions.

Electron Bremsstrahlung process

The Electron Bremsstrahlung, contrary to the above discussed processes, becomes the main channel for the axion-electron coupling in a high density regime. This process is described in the lower-left diagram in Fig. 2.2 and is given the following reaction

$$e + Ze \to e + Ze + a \, . \tag{2.7}$$

In particular, in a matter state where the density is high enough to create degenerate matter, the energy loss rate per unit mass is:

$$\epsilon_{B(el)} \simeq 8.6 \cdot 10^{-7} g_{ae}^2 T^4 \, \mathrm{erg\,g^{-1}\,s^{-1}} \, . \tag{2.8}$$

The conditions which allow for the presence of a degenerate state are in general reached in a star with $\rho \sim 10^6 \mathrm{g\,cm^{-3}}$ and $T \sim 10^7 - 10^8 \mathrm{K}$. Both, the Electron Bremsstrahlung and Compton are processes which involve the production of an axion from an electron coupling. These two processes, combined with the so-called Atomic recombination and de-excitation, are generically called ABC processes.

Nucleon Bremsstrahlung process

The last diagram in Fig. 2.2 is the so-called nucleon Bremsstrahlung process. In axion models with a sizeable axion-nucleon coupling[2] this can be a relevant production channel. Through a nucleon-nucleon collision we can create an axion particle following the reaction

$$N + N' \to N + N' + a \, . \tag{2.9}$$

[2] As we will see in section 3.1.2, it is possible to construct QCD axion models in which the axion-nucleon coupling is suppressed, thus relaxing some strong astrophysical bounds.

This process is suppressed in systems with a temperature $T \lesssim 10$ MeV. Hence, it becomes the dominant process in the SN and NS where it is possible to reach such high temperatures. Indeed, as long as the temperature is too low the process is suppressed by the pion mass in the propagator (see Fig. 2.2) and only when the temperature becomes comparable with the moment exchanged by the nucleon the process becomes relevant. The energy loss rate per unit mass is different if the star is degenerate and if it is not, thus the two expressions are respectively:

$$\epsilon^{D}_{B(nucl)} \sim 4.7 \cdot 10^{39} g^2_{aN} \rho_{14}^{-2/3} T^6_{30} \,\mathrm{erg\,g^{-1}\,s^{-1}}\,, \tag{2.10}$$

$$\epsilon^{ND}_{B(nucl)} \sim 2.0 \cdot 10^{38} g^2_{aN} \rho_{14} T^{7/2}_{30} \,\mathrm{erg\,g^{-1}\,s^{-1}}\,, \tag{2.11}$$

where $T_{30} \equiv \dfrac{T}{(30\mathrm{MeV})}$ and $\rho_{14} \equiv \dfrac{\rho}{10^{14}\mathrm{g\,cm^{-3}}}$.

2.1.2 Solar Axions

Historically the Sun has often provided a natural laboratory for the study of new light particles interactions. The low density of our star allowed the study of both the Primarkoff effect and therefore interaction between photons and axions, as well as the Compton process based on the axion-electron coupling. The Sun is also one of the main sources of axions which are searched on Earth via the so-called helioscopes.

To understand how the axion could interact with matter in the Sun, we derive the mean free path (MFP) λ_a of a hypothetical axion in the core of the star. Considering the interaction with photons and thus the Primarkoff effect, the MFP goes as the inverse of the transition rate, namely

$$\lambda_a = \frac{1}{\Gamma_{\gamma\to a}} \sim \left(\frac{g_{a\gamma}}{10^{-10}\mathrm{GeV}^{-1}}\right)^2 6 \cdot 10^{24}\mathrm{cm} = \left(\frac{g_{a\gamma}}{10^{-10}\mathrm{GeV}^{-1}}\right)^2 8 \cdot 10^{13} R_\odot\,, \tag{2.12}$$

where we have considered $T \sim 1.3$KeV and $k_s \sim 9$KeV. As discussed in [50] and [52], even in the extreme case where the axion is trapped in the core and the axion-photon coupling is large, namely $g_{a\gamma} \geq 10^{-3}\mathrm{GeV}^{-1}$, the MFP should be smaller than the photon one in order to avoid dramatic consequences in the solar structure. Indeed, in the extreme case, axions could carry most of the bulk of energy otherwise carried by photons. Thus, unless axion-photon couplings are large, a case excluded by other bound as we will discuss in a moment, the axion can easily escape from the Sun.

Due to the low density of the Sun, the Compton process is an important axion production channel too. In the left panel of Fig. 2.3, it is possible to see that the axion flux due to the electron coupling is similar to that from the photon coupling. This is an an important point for axion experimental searches based on helioscopes, which are sensitive both to the axion couplings to photons and electrons. On the other hand, what matters for stellar cooling is the absolute luminosity, namely the energy radiated. From the right plot, it is clear that the Primarkoff process is more energetic. The solar axion flux and luminosity can be respectively approximated as [50]:

$$\Phi_a \sim g^2_{10} 3.8 \cdot 10^{11} \mathrm{cm^{-2} s^{-1}}\,, \tag{2.13}$$

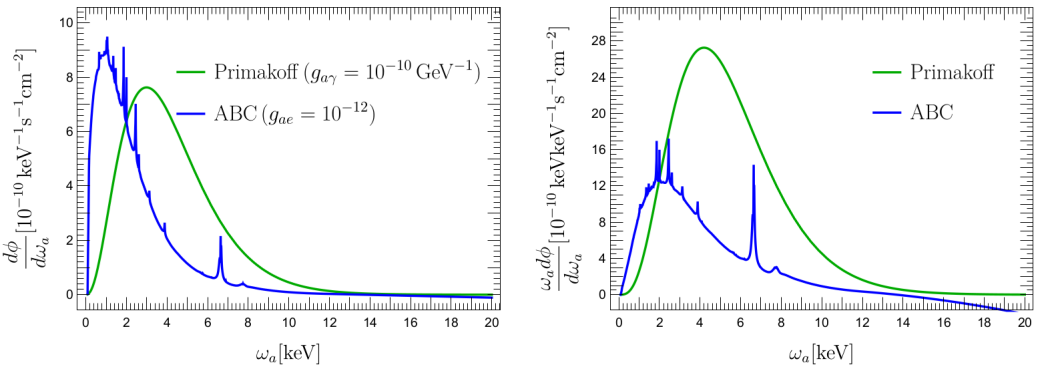

Figure 2.3: The Figure shows the solar axion spectrum as the function of axion energy. In particular, the left diagram shows the axion flux from Primarkoff and ABC process, while the right one shows the energy spectrum for the very same processes. Note that for solar axions the Compton process is the principal production channel involving the axion-electron coupling, namely in ABC processes. Figure from [40]

$$L_a \sim g_{10}^2 1.9 \cdot 10^{-3} L_\odot \,, \tag{2.14}$$

where, as before, $g_{10} \equiv \dfrac{g_{a\gamma}}{(10^{-10}\mathrm{GeV}^{-1})}$. Given the Sun luminosity, it is hence possible to inferred the following constraints:

- the solar age provides a solid bound on the axion-photon coupling. Indeed, an extra energy loss due to axions would increase the rate of energy loss and shorthen the age of the Sun. Imposing $L_a \lesssim L_\odot$, one finds $g_{a\gamma} \lesssim 3 \cdot 10^{-9}\mathrm{GeV}^{-1}$ [53].

- From helioseismology and sound velocity one derives a bound on axion-photon coupling that is $g_{a\gamma} \lesssim 10^{-9}$ [50]. Indeed, the axion energy loss modifies the sound speed profile implying the constraint $L_a \lesssim 0.20 L_\odot$. A stronger bound was presented in [54], yielding $g_{a\gamma} \lesssim 4.1 \cdot 10^{-10}\mathrm{GeV}^{-1}$.

- Due to the axion energy loss, the Sun should compensate for this loss with an increase in nuclear burning and then an increase in temperature. This would also affect the neutrino flux, by increasing it. Hence, from the measurement of the neutrino flux one infers $L_a \lesssim 0.04 L_\odot$, that implies $g_{a\gamma} \lesssim 5 \cdot 10^{-10}\mathrm{GeV}^{-1}$ [50].

2.1.3 Astrophysical axion bounds and hints

White Dwarfs

As already discussed, WDs represent the last stage of a low mass star. They are characterised by a high density in the core and, because of this, the electron Bremsstrahlung is the main axion production channel. The typical values which characterise a WD are $\rho \sim 10^6\mathrm{g\ cm}^{-3}$ and $T \sim 10^6\mathrm{K}$. Moreover, since in this stage the star has run out the nuclear fuel and is characterised by a degenerate core, from that moment on the temperature will decrease. There are two ways to probe the WD cooling, which respectively are associated to two different variables: the WD luminosity function (WDLF) and the oscillation period.

The former represents the WD distribution in terms of WDLF: during the cooling phase, the luminosity decreases following the WDLF shape. The numerical analysis gives a constraint of $g_{ae} \lesssim 2.8 \cdot 10^{-13}$ [40; 55][3]. However, observational results also give a hint of anomalous cooling, which can be fit via the coupling $g_{ae} \simeq 1.4 \cdot 10^{-13}$. The other method regards the period variation. In WDs the period oscillation changes during the century and this is reflected in the cooling rate temperature, namely $\dot{P}/P \propto \dot{T}/T$. If the observation of period changing does not follow the expected shape, then this could be due to the presence of a new energy loss channel. Although the period changes extremely slowly ($\dot{P}/P \sim 10^{-18}$), several data give a bound on the axion-electron coupling that is $g_{ae} \leq 4.1 \cdot^{-13}$, as well as a specific hint of $g_{ae} = 2.9^{+0.6}_{-0.9} \cdot 10^{-13}$ [51].

Tip of Red Giant Branch and Helium burning stars

When a solar-like star runs out the Hydrogen in the core, it shrinks in order to reach the right condition for the Helium burning. As explained above, when the density $\rho \sim 10^6 \mathrm{gr/cm}^3$ and the temperature acquires values around $T \sim 10^8 \mathrm{K}$ then the Helium ignition occurs in a degenerate core. In this phase, even though the surface temperature decrease, the temperature of the core and luminosity increase until the star reaches the Helium flash, yielding a tip in the HR diagram called the tip of the Red Giant Branch. In the presence of extra energy loss channel due to the axion, the star would need more time to reach the temperature needed to burn Helium: this would imply a delay of the Helium flash, which graphically corresponds to a peak shift in the HR diagram. In this way, we can infer a bound on the coupling with the electrons, since in these dense environments the main axion production channel is the electron Bremsstrahlung. The constraints following this idea is $g_{ae} \lesssim 1.5 \cdot 10^{-13} (2\sigma)$ [51].

Besides an increase of luminosity, the presence of an axion would also increase the core mass, since the core accreates a larger mass to start the ignition of Helium. A higher mass would imply a shorter period in the HB. This in turn means a lower number of stars in the HB phase of the HR diagram. To better understand this point we can introduce the R-ratio which is observationally defined as the ratio between the number of the stars in the HB over the number of the stars in the RGB, namely:

$$R \equiv \frac{N_{HB}}{N_{RGB}} \,. \tag{2.15}$$

The axion couplings will affect in some sense this ratio: if we have $g_{ae} \neq 0$ the number of the stars in the horizontal branch decreases, since they evolve faster, meanwhile $g_{a\gamma} \neq 0$ also pulls stars out from the HB due to the Primarkoff process. This observable is an interesting quantity since it is able to correlate two different couplings. Also in this case we can derive some bounds which can be put together in Fig. 2.4, [51]. There, the best fit point suggests a non zero value for both photon and electron couplings, corresponding respectively to $g_{a\gamma} = 0.18 \cdot 10^{-10} \mathrm{GeV}^{-1}$ and

[3] The axion-electron counpling is defined as $g_{ae} = C_{ae} \frac{m_e}{f_a}$ where C_{ae} is defined in eqs. 1.60, 1.61

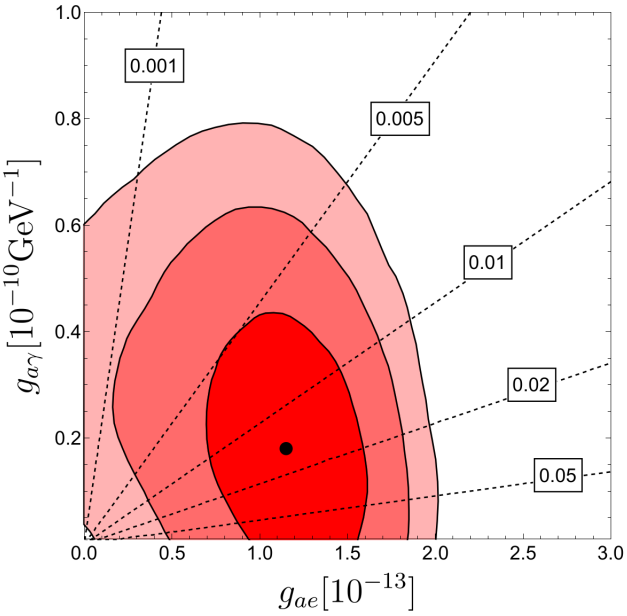

Figure 2.4: Constraints (and hints) from stellar evolution on the axion couplings to electrons and photons. Coloured regions correspond to $1, 2, 3\sigma$ contours, from darker to lighter red. Dashed lines indicate the value of the $C_{ae}/C_{a\gamma}$ ratio. Figure from [51].

$g_{ae} = 1.2 \cdot 10^{-13}$. Moreover, we can already speculate something about the required axion model. Indeed, the dashed lines indicate the ratio between the Wilson adimensional coefficients of electron and photon couplings. From the diagram is clear that a value around 10^-2 is needed and this rules out he KSVZ model which predicts a $C_{ae}/C_{a\gamma}$ ratio of the order of 10^{-4}, since the axion coupling to electrons in only generated radiatively (see eq. 1.61). On the other hand, the DFSZ can easily match the preferred value.

Supernovae and Neutron Stars

Star with a mass $M \gtrsim 8M_\odot$ undergo the core collapse with a typical temperature of $T \sim 30$MeV and density around $\rho \sim 3 \cdot 10^{14}$g cm^{-3}. As discussed above, the nucleon Bremsstrahlung becomes not suppressed when the temperature is above the $\sim$ 10MeV, then SN observations could give a bound on the axion-nucleon coupling. When the core collapse occurs the environment is so dense that matter cannot escape, but for neutrinos which carry away around 99% of the total energy. The energy loss due to neutrinos should be hence compared to an extra energy loss channel due to axions. In 1987 about 20 neutrinos were detected on earth by large underground detectors as Super-Kamiokande, following the SN1987A explosion. Although the data were not so accurate, the observation matched reasonably well with theoretical expectations. If we had an extra cooling channel due to axions, basically we should have expected a reduced number of neutrino events since part of the energy was carried by axions.

A criterium for the axion energy loss of the SN1987A was provided by Raffelt in Ref. [50], based on the results of numerical simulations. That

reads $\epsilon_a \lesssim 1 \cdot 10^{19}$ erg g^{-1} s^{-1}, for typical temperatures and densities as defined above. Given the expression of the energy loss rates due to nucleon Bremsstrahlung (see eqs. 2.10-2.11), it is possible to translate the Raffelt's criterium into a bound on the axion-nucleon coupling, g_{aN}. Most recent analysis of the SN1987A bound find the following constraint on a specific combination of neutron and proton couplings [56]

$$g_{aN}^2 = g_{an}^2 + 0.61 g_{ap}^2 + 0.53 g_{an} g_{ap} \lesssim 8.26 \cdot 10^{-19} \,. \tag{2.16}$$

Approximating $g_{aN} \sim m_N / f_a$, the bound $g_{aN} \lesssim 9.1 \cdot 10^{-10}$ implies in turn $f_a \gtrsim 10^9$GeV.

Also NSs could give a constraint on the axion-neutron coupling. In particular, from observations of the NS in Cassiopeia A, Ref. [57] derived the limit $g_{an} \lesssim 4 \cdot 10^{-10}$. An even stronger bound, $g_{an} \lesssim 2.8 \cdot 10^{-10}$ was presented in [58]. However, these limits are subject to several uncertainties and there is no common consensus at the moment on their reliability.

Finally, black holes (BHs) could give insights into the axion-gravity coupling Gravitational bound states are created by axions around a BH if the axion Compton wavelength is of the order of the BH radius. The superradiance [59] phenomenon describes the increasing of occupation number and this provides a way to extract angular momentum or energy from the BH. From the rate at which the angular momentum is carried out from the BH one can infer the presence and the mass of a possible axion particle. In this case, one is able to give a constraint directly on the axion mass and hence on the axion decay constant. The allow windows for the f_a parameter are [60] $f_a \lesssim 6 \cdot 10^{17}$GeV and $f_a \gtrsim 10^{19}$GeV.

2.2 Cosmological implications

Axion cosmology provides valuable informations on the axion parameter space that are complementary to astrophysical constraints. Since the topic of this thesis is not directly centered on cosomological aspects, we will limit ourselves to a brief description of the main cosmological aspects of axion physics. As already mentioned, axions could be a good DM candidate. From a cosmological point of view, the axion population can be dived into two different classes: thermal axion production which results in dark radiation or hot dark matter (HDM), and non-thermal axion production relevant for cold dark matter (CDM). Both topics are briefly introduced in this section.

2.2.1 Thermal axion

The energy density in relativistic particles at the epoch of matter-radiation equality is described in terms of an effective number of neutrino species N_{eff}^{SM} and it reads:

$$\rho_{rad} = \left[1 + \frac{7}{8}\left(\frac{T_\nu}{T_\gamma}\right)^4 N_{eff}^{SM}\right] \rho_\gamma \,. \tag{2.17}$$

Note that $T_\gamma \equiv T$ represents the temperature of the cosmic bath and, at temperatures below the electron mass, neutrinos are the only relativistic species beyond photons. To exploit this formula it is necessary

to understand the meaning of the $\frac{T_\nu}{T_\gamma}$ ratio. In general a particle is in thermal equilibrium if the interaction rate with the other particles in the thermal bath (Γ) is larger than the rate of expansion of the Universe (H). When $\Gamma \lesssim H$, the particle decouples from the thermal bath. Exploiting this argument, it is possible to find that neutrinos decouple when $T \lesssim 1$ MeV which is of the same order as the photon temperature. However, electron-positron annihilation, which happens at $T \lesssim m_e$, produces more photons which increase the temperature of the thermal bath (photon heating). Using the entropy conservation one finds that

$$\frac{T_\nu}{T_\gamma} = \left(\frac{4}{11}\right)^{1/3} . \tag{2.18}$$

The N_{eff}^{SM} coefficients defined in eq. 2.17 is found to be $N_{eff}^{SM} = 3.046$, in the case of the SM with three active neutrinos. The deviation from 3 is due to the fact that the neutrinos decoupling is not instantaneous and the subsequent electron-positron annihilation produces a residual radiation, as just discussed.

What happens if we insert another relativistic species in eq. 2.17? Let us consider an axion population, then the energy density becomes:

$$\rho_{rad} = \left[1 + \frac{7}{8}\left(\frac{T_\nu}{T_\gamma}\right)^4 N_{eff}^{SM} + \frac{1}{2}\left(\frac{T_a}{T_\gamma}\right)^4\right]\rho_\gamma \, . \tag{2.19}$$

We now define a new N_{eff} which includes both the SM content and an axion population. The deviation from the SM value is described by:

$$\Delta N_{eff} \equiv N_{eff} - N_{eff}^{SM} = \frac{4}{7}\left(\frac{T_a}{T_\nu}\right)^4 . \tag{2.20}$$

This is how the inclusion of another relativistic light particle, namely the axion in our case, changes the value of the N_{eff}^{SM}. In particular, from experimental constraints N_{eff} it is possible to set a limit on the axion mass, since the variation of N_{eff} is proportional to T_a and this is related f_a, which sets the strength of axion interactions with the SM thermal bath. A recent cosmological analysis in Ref. [61] finds the following bound (which applies to the KSVZ model):

$$\begin{aligned} f_a &\gtrsim 2.0 \cdot 10^7 \text{GeV} \, , \\ m_a &\lesssim 0.28 \text{ eV} \, . \end{aligned} \tag{2.21}$$

Although weaker than typical astrophysical bounds, this provides relevant complementary informations on the axion parameter space.

2.2.2 Non-thermal axion

CDM axions are produced via a non-thermal mechanism known as misalignment. To describe this mechanism we need first to discuss the axion potential and mass at finite temperature. Eq. 1.51 represent the chiral axion potential at zero temperature, however in a high-temperature regime when $T \simeq T_C \simeq 160$MeV, QCD deconfines and at even higher temperatures QCD becomes perturbative. This implies that χPT is

no longer a good description and another technique is necessary to describe the axion potential. Using the dilute instanton gas approximation (DIGA) the finite temperature axion potential can be written as:

$$V(a,T)\Big|_{T\gg T_C} = \chi(T)\left[1-\cos\left(\frac{a}{f_a}\right)\right], \tag{2.22}$$

where $\chi(T) = f_a^2 m_a^2(T)$ and the mass is:

$$m_a(T) = \beta m_a(\frac{T_C}{T}), \tag{2.23}$$

with $\gamma \simeq 4$, $\beta \simeq 10^{-2}$ and m_a is defined in eq.1.54. Next, we define the axion angle $\theta(x) = a(x)/f_a$ and we compute the EOM in a Friedmann-Robertson-Walker metric which reads:

$$\ddot{\theta} + 3H(t)\dot{\theta} - \frac{\nabla^2\theta}{R^2} + m_a(t)\sin\theta = 0\,. \tag{2.24}$$

In the following, we concentrate on the zero modes of the field and we neglect the gradient term (this is justified only in the so-called pre-inflationary PQ breaking scenario). Moreover, we work in the harmonic approximation, $\sin\theta \sim \theta$ and assuming a standard cosmological scenario with radiation domination we have $H = 1/2t$. In addition, notice that the initial θ angle can be different depending on the interplay between the scale of inflation and that of PQ breaking. In fact, if the PQ is broken during the inflation and never restored after that (pre-inflationary PQ scenario) the initial value of θ is homogeneous and arbitrary. On the other hand, if PQ is broken after the inflation or restored (post-inflationary PQ breaking scenario), then the initial value of θ should be averaged over different patches of the Universe.

Coming back to eq. 2.24, we can distinguish two regimes. In the very early Universe, when the temperature is large and $m_a \to 0$, we have a decaying solution which after some time corresponds to a constant value of θ. On the other hand, when $m_a(t_1) \sim 3H(t_1)$ the axion field starts to oscillate, describing a harmonic oscillator. The differential equation can be solved analytically in the WKB approximation and it can be shown that the energy density associated to the oscillating axion field

$$\rho_a = f_a^2\left(\frac{1}{2}\dot{\theta}^2 + \frac{1}{2}m_a^2(t)\theta^2\right), \tag{2.25}$$

is such that $\dfrac{\rho_a R^3}{m_a} = const$, where R is the scale factor. The actual energy density today, starting from the onset of oscillations at t_1 is found to be:

$$\rho_a(t_0) \sim \frac{3}{4}\frac{m_a f_a^2}{t_1}\theta_0^2\left(\frac{R_1}{R_0}\right)^3. \tag{2.26}$$

Note that the axion energy density scales as R^{-3}, thus it yields a non-relativistic particle population which, in turn, describes the behaviour of CDM. This is the reason why the misalignment mechanism provides a CDM axion population. The axion relic density can be finally computed using entropy conservation and the temperature dependence of the axion mass, which yields:

$$\Omega_a h^2 \sim 0.12\left(\frac{30\mu\text{eV}}{m_a}\right)^{7/6}\theta_0^2\,. \tag{2.27}$$

Hence, the lighter is the axion the larger is the contribution to the energy density. Axion DM provides an important source of axions for experimental searches based on haloscopes. Finally, we mention for completeness that there are other non-thermal axion DM production mechanisms based on the decay of topological defects following the PQ phase transition (axion strings) and the formation of the QCD axion potential (axion domain walls), which are relevant in the post-inflationary PQ breaking scenario.

2.3 Experimental axion searches

Axion experiments can be classified according to how the axion is produced. There are three conceptually different ways in which an axion flux can be sourced: in the laboratory, from the Sun or via axion DM. Let us discuss the general idea on which they are based on.

- **Light Shining through Wall (LSW)**. This is one of the most important axion laboratory experiments and it exploits the axion coupling to the photon. The idea is to shoot light, produced for example by a laser beam, against a magnetic field transverse to the beam itself. The experiment is based on the possibility that some of these photons interacting with the magnetic field are transformed into axions. At this point, an optical barrier stops photons, allowing the passage of weakly interacting axions. Another magnetic field reconverts back the axion into a photon, making it detectable. The energy range scanned with LSW is around $m_a \lesssim 0.1\text{meV}$ and the principal experiments are ALPS I [62] together with ALPS II[63] and OSQAR [64]. The latter sets the most stringent bound using LSW which is $g_{a\gamma} < 3.5 \times 10^{-8}\text{GeV}^{-1}$.

- **Helioscopes**. In these experiment, we search for axions produced by the Sun leading to a solar axion flux. We try to detect them on the Earth with telescopes which follow the Sun: the solar axion flux coming from our Sun is converted through a magnetic field into X-rays photons which are now detectable. The main experiment with this approach is CERN Solar Axion Experiment (CAST) [65], or the planned Internationa AXion Observatory (IAXO) [66].

- **Haloscopes**. Experiments exploiting the possibility that axions comprise the CDM are known as haloscopes. The basic idea is to use some resonant cavity permeated with a strong magnetic field to convert the axion DM into an electromagnetic detectable signal. The best-scanned range in cavity experiments is above the μeV. Current bounds have been set by different experiments, including the Axion Dark Matter eXperiment (ADMX) [67] which works at frequencies around $m_a \sim 3\mu\text{eV}$.

2.3.1 Axion experiments from the axion couplings perspective

We now briefly present axion searches from the point of view of axion couplings. The plots below are taken from [68] where it is possible to find updated axion constraints and experimental sensitivities.

Axion-photon coupling

The addition of a new piece in the QED Lagrangian, as expressed in eq. 1.69, namely the $aF\tilde{F}$ term, leads extra contributions in the Maxwell's equations. In practice, we can think about the axion as a shift in the electron density and electron current. Thus, the charge density defined in the usual Maxwell's equations is modified by the presence of an extra contribution proportional to the gradient of the axion field and an external magnetic field. Similarly, we have an induced axion current proportional via the magnetic field to the axion time derivative and via the electric field to the axion field gradient. In light of this, the idea is to search the axion field as a deviation from the Maxwell's equations and so a modified electrodynamics.

Moreover, the prediction of $g_{a\gamma}$ can be expressed in terms of the adimensional coupling $C_{a\gamma}$ which in turn contains a model-dependent term, namely E/N. For instance, this coefficient was computed in the previous chapter in the case of the KSVZ or DFSZ axion model.

Fig. 2.5 **(a)** represents the axion-photon coupling as a function of the axion mass. The yellow band indicates the theoretical prediction of DFSZ and generalized KSVZ models which depend on the value of E/N. The coloured regions represent the already experimentally tested values including both astrophysical and laboratory constraints. The strongest astrophysical bound is due to the HB constraint which predicts $g_{a\gamma} \lesssim 10^{-10}$ GeV^{-1}. Notice that the HB bound dilutes away when the axion mass is around 100KeV which corresponds to the temperature of stars in the HB. Similarly, the weaker bound from solar axion dilutes away when we reach the temperature of the Sun. At lower masses, the most important laboratory experiment is due to the helioscopes experiment CAST which still constrains $g_{a\gamma}$ to be of the same order discussed above. The vertical lines are related to haloscope experiments, such as ADMX, which assume that the axion constitutes the DM. Basically, they look for a resonant signal scanning the frequency of the electromagnetic cavity which should lead to an enhancement when the frequency of the cavity matched the axion mass. This is the reason why we have vertical spikes in the plot and the reason why it is important to narrow down as much as possible the range in which to look for the axion.

In the next decades several new experiments will search for axions and in Fig. 2.5 **(b)** some possible future sensitivities of these experiments are projected. The shaded regions represent these new experiments which will cover a large portion of the interesting parameter space, exploring in particular the values predicted by the KSVZ and DFSZ models. Even though this is an experimental plot we have to consider some theoretical assumptions. In fact, haloscopes experiments, again represented with a vertical region in the plot, may reveal new particles or narrow the parameter space, but at the same time, they are based on the non-trivial assumption that the axion comprises the totality of the DM.

Axion-electron coupling

More recently, there have been new proposals to search for axions based on other couplings other than photons. One possibility is based on the

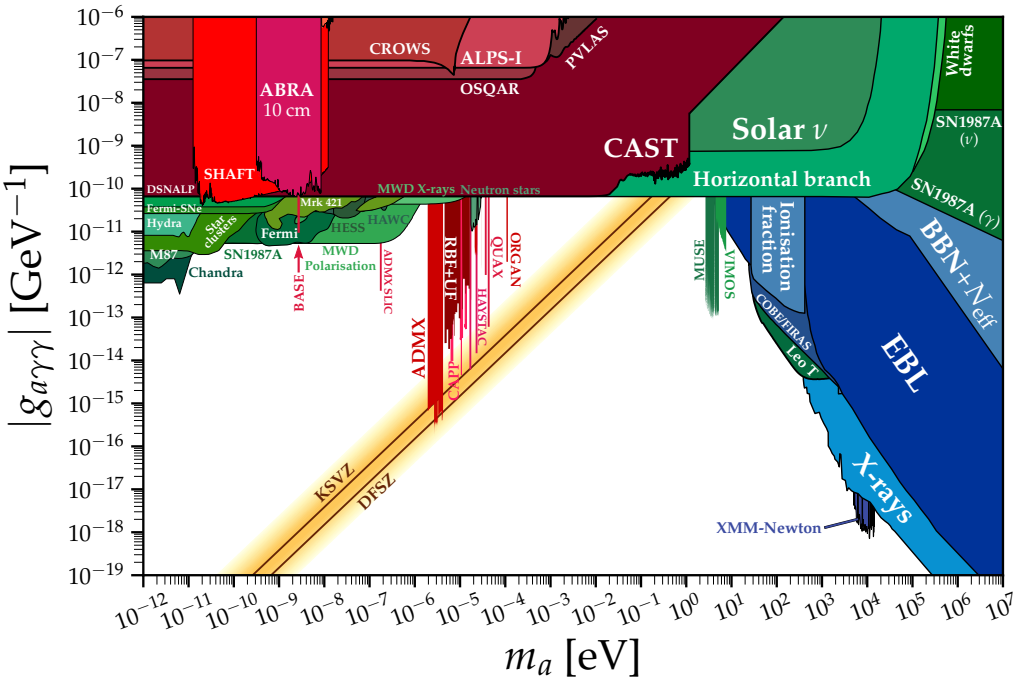

(a) *Axion-photon coupling vs. axion mass (current bounds).*

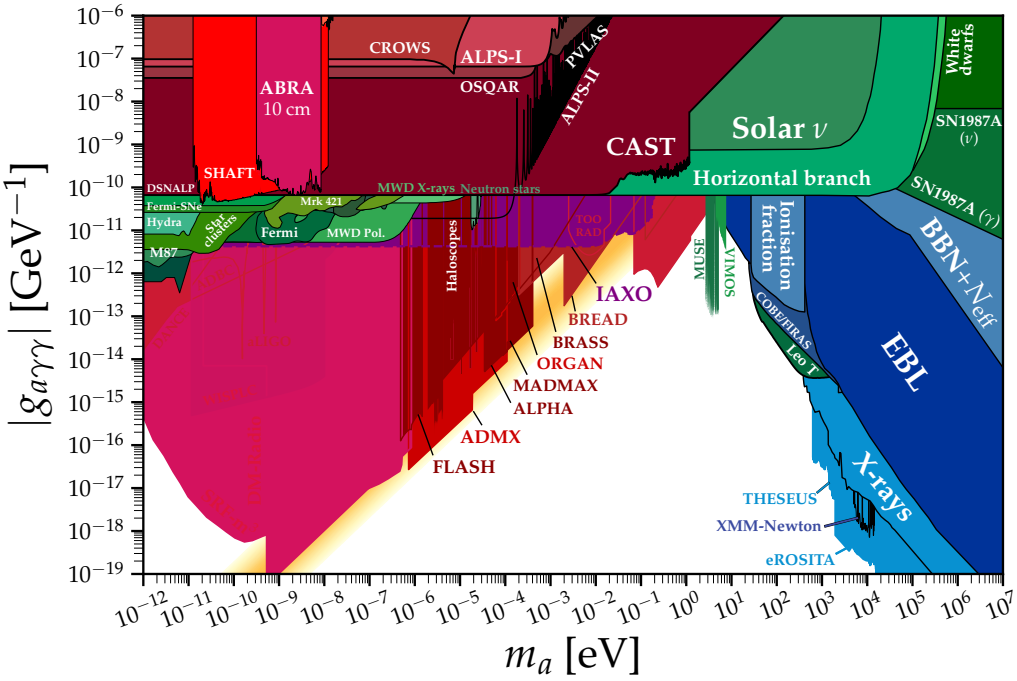

(b) *Axion-photon coupling vs. axion mass (future sensitivities).*

Figure 2.5: Axion-photon coupling parameter space: current bounds **(a)** and future sensitivities **(b)**. The yellow band represents the predicted value of DFSZ and generalized KSVZ models [69; 70]. The coloured regions denote already tested values, while the shadowed one represent future sensitivities. Figure from [68].

axion-electron coupling, described by eq. 1.60. The C_{ae} coefficient depends on the model: it is of the order one in the DFSZ model while it is loop induced in the KSVZ model. The only laboratory experiment which gives some bound exploiting axion-electron coupling is QUaerere AXions experiment [71] (QUAX[4]). The sensitivity of QUAX reaches $g_{ae} \lesssim 10^{-11}$, however astrophysical limits are at the moment more constraining, yielding $g_{ae} \lesssim 10^{-13}$.

Axion-nucleon coupling

Another possibility is to consider the axion coupling to nucleons, which are described by eqs. 1.66 and 1.67. Also in this case astrophysics provides stronger bounds, most notably from SN1987A. Future experiments could test regions covering smaller values of g_{aN}, beyond astrophysical limits, however they are still far from the prediction of DFSZ and KSVZ models. Other promising experimental approaches exploit CP-violating axion couplings to nucleons [72] or to the nucleon EDM [73].

[4]Note that QUAX includes three different experiments also involving other axion couplings.

Chapter 3

Non-universal axion models

In the first chapter of this thesis, we have discussed two standard axion models, namely the KSVZ and DFSZ models. Both of them are universal models, in the sense that the $U(1)_{PQ}$ symmetry does not distinguish different SM fermion generations. On the other hand, *non-universal axion models* are characterised by generation-dependent PQ charges and they were proposed already in 1978 by Bardeen and Tye [74]. In fact, there are no fundamental reasons why every SM fermion generation should carry the same PQ charge and relaxing this hypothesis might actually offer a possible connection between the PQ symmetry and the origin of flavour, as suggested long ago by Wilczek [13].

In this chapter we review the general structure of non-universal axion models, highlighting the modern motivations, their UV completions and the most relevant phenomenological consequences. These include the generation of flavour-violating axion couplings, which open the possibility for new experimental tests of the QCD axion.

3.1 General motivations

There are several motivations behind the construction of non-universal axion model, ranging from theory to astrophysics, as well as experimental considerations. Historically, the possibility of an axion coupled to the SM fermions in a generation dependent way was fuelled by the observation in heavy ion collisions at GSI of a sharp peak at ~ 300keV in the positron spectrum [75]. The data were consistent with the production of a particle of mass ~ 1.7MeV, of probable pseudoscalar character [76], which then decayed into e^+e^-. Although the properties of such a particle were consistent with those of the original WW axion [3; 4], in order to evade a set of stringent experimental constraints one had to break the relation $g_{a\mu}/g_{ae} = m_\mu/m_e$ predicted by universal axion models. Generation dependent axion couplings remained the only way out, and a series of interesting papers analysing this possibility appeared (see e.g. [77; 78]). Later on the GSI anomaly disappeared, but it paved the way for the systematic investigation of non-universal axion models.

More recently, it was pointed out in Ref. [12] that the non-universality of the PQ charges of the SM quarks is a necessary ingredient to allow a simultaneous suppression of the axion coupling both to protons and neutrons, thus opening the possibility to relax the tight astrophysical bounds on the axion decay constant f_a (or equivalently on the axion

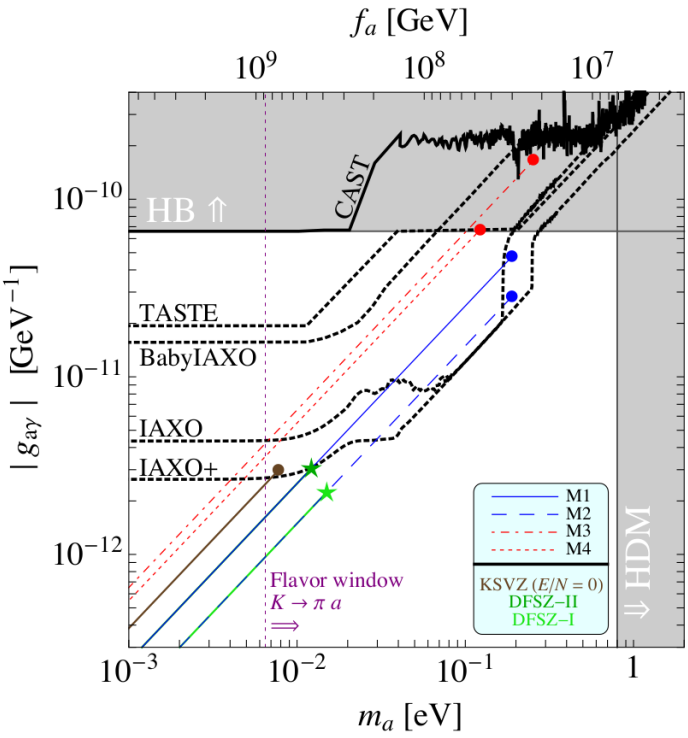

Figure 3.1: Constraints on the $g_{a\gamma}$ vs. m_a plane for different axion models. Blue and red lines are referred to astrophobic non-universal axion models (labelled M1–4), while the green and brown lines to DFSZ and KSVZ respectively. All the predictions for the axion-photon coupling are stopped at the value of m_a set by the astrophysical bounds on the axion couplings to nucleons and electrons. Models M1–4 allow for a sizeable relaxation of astrophysical bounds compared to standard DFSZ/KSVZ models. Figure from [12].

mass m_a) from SN 1987A (see section 2.1.3). In fact, while it is relatively simple to conceive axion models in which the axion coupling to photons or electrons are relatively suppressed (see e.g. [69]), that is not the case for the axion coupling to nucleons. In section 3.1.2 we will review the argument why universal axion models such as the DFSZ do not allow for a simultaneous suppression of axion couplings to nucleons, and illustrate how this conclusion can be avoided in the non-universal case.

The possibility of suppressing the axion couplings to nucleons (relevant for SN 1987A) and electrons (relevant for WDs/RGB) within non-universal axion models leads to the so-called *astrophobic axion* scenario [12], in which the most relevant astrophysical limits from SN 1987A, WDs and RGB can be considerably relaxed (see section 2.1.3 for a collection of astrophysical bounds). This allows in turn to reopen the heavy axion window up to $m_a \sim 0.1$ eV, which will be probed by future helioscopes sensitive to the axion-photon coupling (see Fig. 3.1).

Finally, a remarkable consequence of non-universal axion models, that will be reviewed in section 3.1.1, is that they imply flavour violation effects since the PQ charge matrix is non-diagonal. This opens up the possibility of probing the QCD axion in flavour processes such as $K \to \pi a$, which are complementary to standard axion searches.

Summarizing, non-universal axion models are interesting in several respects: they generalize the universal DFSZ model (discussed in section 1.4.3) allowing for a more general structure of axion couplings. This includes the possibility of suppressing simultaneously the axion coupling to protons and nucleons, as well as the generation of flavour off-diagonal axion couplings, as reviewed in the following.

3.1.1 On the origin of flavour-violating axion couplings

Relaxing the hypothesis of the universality of the PQ current in DFSZ-like constructions leads to flavour-violating axion couplings to quarks and leptons. Here, we preliminary show how such couplings arise in a generalised DFSZ setup with non-universal PQ charges. Let us assume that quarks with the same EM charge but of different generations couple to different Higgs doublets, for definiteness H_1 or H_2, to which we assign the same hypercharge $Y_{H_1} = Y_{H_2} = -\frac{1}{2}$ but different PQ charges $\chi_1 \neq \chi_2$. Let us start by considering the following Yukawa terms for the up-type quarks

$$\mathcal{L}_{Y_u} = -(Y_u)_{11}\bar{q}_{1L}u_{1R}H_1 - (Y_u)_{22}\bar{q}_{2L}u_{2R}H_2 - (Y_u)_{12}\bar{q}_{1L}u_{2R}H_1 + \dots \,, \tag{3.1}$$

where we have made explicit the generation indices and neglected for simplicity the third generation. The quark bilinear $\bar{q}_{1L}u_{2R}$ in the last term is needed to generate the CKM mixing, and for the present discussion it is irrelevant whether it couples to H_1 or H_2. Note, also, that from PQ charge consistency $\chi(\bar{q}_{2L}u_{1R}) = \chi(\bar{q}_{2L}u_{2R}) - \chi(\bar{q}_{1L}u_{2R}) + \chi(\bar{q}_{1L}u_{1R}) = -\chi_2$ it follows that the term $\bar{q}_{2L}u_{1R}H_2$ is also allowed. However, being its structure determined by the first three terms we do not need to consider it explicitly. Projecting out from the Higgs doublets the neutral Goldstone bosons, eq. 1.84, and identifying the axion field precisely as done for the standard DFSZ case in section 1.4.3, we obtain

$$\begin{aligned}\mathcal{L}_{m_u} = &-(m_u)_{11}\bar{u}_{1L}u_{1R}e^{i\chi_1\frac{a}{v_a}} - (m_u)_{22}\bar{u}_{2L}u_{2R}e^{i\chi_2\frac{a}{v_a}} + \\ &-(m_u)_{12}\bar{u}_{1L}u_{2R}e^{i\chi_1\frac{a}{v_a}} + \dots \,.\end{aligned} \tag{3.2}$$

Differently from the case of the standard DFSZ, a purely axial field redefinition as $u \to e^{-i\gamma_5\chi\frac{a}{v_a}}u$ is not sufficient to remove the axion from the mass terms because of the presence of a mixing term. In such a case, it is necessary to add a vectorial part in order to remove the axion and the field redefinitions (distinguishing u_1 and u_2) read:

$$\begin{aligned}u_1 &\to e^{-i(\gamma_5\chi_1+\chi_2)\frac{a}{v_a}}u_1 \\ u_2 &\to e^{-i(\gamma_5\chi_2+\chi_1)\frac{a}{v_a}}u_2 \,.\end{aligned} \tag{3.3}$$

By introducing a vector of the two quark flavours $u = (u_1, u_2)^T$ and the two matrices of charges $\chi_{12} = \mathrm{diag}(\chi_1, \chi_2)$ and $\chi_{21} = \mathrm{diag}(\chi_2, \chi_1)$ the variation of the fermion kinetic terms due to the redefinitions above is:

$$\begin{aligned}\delta(\bar{u}i\partial\!\!\!/u) &= \frac{\partial_\mu a}{v_a}(\bar{u}\chi_{12}\gamma_\mu\gamma_5 u + \bar{u}\chi_{12}\gamma_\mu u) = \\ &= \frac{\partial_\mu a}{v_a}(\bar{u}_L\chi_L\gamma_\mu u_L + \bar{u}_R\chi_R\gamma_\mu u_R),\end{aligned} \tag{3.4}$$

where in the second step $\chi_R = (\chi_1 + \chi_2)(^1\ _1)$ and $\chi_L = (\chi_2 - \chi_1)(^1\ _{-1})$. Note that in the case of right handed fields the PQ charge matrix χ_R is proportional to the identity in generation space. Hence, upon going to the mass basis via a unitary transformation, $u_R \to U_R^u u_R$, the axion interactions remain diagonal. On the other hand, χ_L is not proportional to the identity and hence after the rotation to the mass basis, $u_L \to U_L^u u_L$, flavour off-diagonal couplings controlled by the matrix $(\chi_2 - \chi_1)U_L^u\left(^1\ _{-1}\right)U_L^{u\dagger}$ unavoidably appear. In the light of this example, it should be clear that non-universal axion models, which are characterised by a PQ charge matrix not proportional to the identity, imply flavour-violation axion couplings.

3.1.2 Astrophobic axions

As already mentioned, non-universal models provide a possibility to suppressed the g_{aN} coupling (with $N = p, n$). The goal of this section (which follows Refs. [12; 40]) is to show which conditions have to be fulfilled in order to achieve this suppression. As we will see, a necessary condition is that only the light quarks are responsible for the PQ-colour anomaly. Then either the heavier quarks are not charged at all under the PQ symmetry (but this would be problematic from the point of view of reproducing CKM mixing) or their contribution to the PQ-color anomaly need to cancel among each other.

The general expression for the adimensional axion-nucleon coefficients, $C_{ap,n}$, was provided in eqs. 1.67-1.68. Neglecting a small $\mathcal{O}(5\%)$ contribution due to the strange quark, we can combine the previous two equations into

$$C_{ap} - C_{an} = (c_u^0 + c_d^0 - 1)(\Delta u + \Delta d) \tag{3.5}$$

$$C_{ap} + C_{an} = (c_u^0 - c_d^0 - f_{ud})(\Delta u - \Delta d) \tag{3.6}$$

where $f_{ud} = \dfrac{m_d - m_u}{m_d + m_u} \simeq 1/3$, $c_{u,d}^0$ are model-dependent axion couplings to quarks (defined in eq. 1.38), while Δu and Δd are non-perturbative matrix elements. The nucleophobic axion scenario is hence obtained by requiring that both the above expressions are zero[1], which can be cast as a condition on the model-dependent coefficients $c_{u,d}^0$ (independently from the values of Δu and Δd). However, these conditions cannot be realized in universal axion models, since $c_{u,d}^0 = 0$ in KSVZ and $c_u^0 + c_d^0$ in DFSZ are different from zero.

On the other hand, non-universal axion models offer a way out. Considering only the first-generation Yukawa terms, the associated axion coupling are (see eq. 1.74):

$$\bar{q}_{1L} u_{1R} H_1 \qquad \to \qquad c_u^0 = \frac{1}{2N}(\chi_{q_1} - \chi_{u_1}) = \frac{\chi_1}{2N} \tag{3.7}$$

$$\bar{q}_{1L} d_{1R} \tilde{H}_2 \qquad \to \qquad c_d^0 = \frac{1}{2N}(\chi_{q_1} - \chi_{d_1}) = -\frac{\chi_2}{2N}\,. \tag{3.8}$$

[1] It is possible to show that the axion-pion coupling is proportional to $C_{ap} - C_{an}$. Hence, a nucleophobic axion is necessarily also pionphobic.

Instead the PQ-colour anomaly factors due to all quarks and to the first generation quark only are defined respectively by

$$\begin{aligned} 2N &= \sum_{i=1}^{3}(2\chi_{q_i} - \chi_{u_i} - \chi_{d_i}) \\ 2N_l &= 2\chi_{q_1} - \chi_{u_1} - \chi_{d_1} = \chi_1 + \chi_2 \ . \end{aligned} \tag{3.9}$$

Then we can discuss in turn the two conditions required by nucleophobia.

Setting eq. 3.5 to zero implies $c_u^0 + c_d^0 = 1$, that is:

$$\frac{N_l}{N} = 1 \ . \tag{3.10}$$

Assuming that the light quark sector is associated to the first family, $N_l = N_1$, then the above condition is realized if $N_2 = -N_3$, namely the QCD anomaly coefficients of the second and third generation cancel each other. Clearly, this requires a non-universal assignment of PQ charges, and the simplest option is that $N_1 = N_2 = -N_3 = N$, namely the first two generations of quarks carry the same PQ charge, which differs from that of third generation quarks. This structure of PQ charges will be denoted as 2+1.

The second condition for nucleophobia is obtained by setting to zero eq. 3.6, thus we want $c_u^0 - c_d^0 = f_{ud} \simeq \frac{1}{3}$. From the previous derivation of the DFSZ model and in particular from eq. 1.89 we have that $\tan\beta = v_2/v_1$ and $\tan^2\beta = -\chi_1/\chi_2$. Putting together the eqs. 3.7 and 3.8 and considering the second expression in eq. 3.9, we get:

$$c_u^0 - c_d^0 = \frac{1}{N}(\chi_1 - \chi_2) \ . \tag{3.11}$$

Since $N_2 = -N_3$ from the previous condition, then $N_l = N = N_1$ and we obtain:

$$c_u^0 - c_d^0 = s_\beta^2 - c_\beta^2 \ . \tag{3.12}$$

The second nucleophobic condition, $c_u^0 - c_d^0 \simeq 1/3$, then implies $s_\beta^2 \simeq 2/3$ (or equivalently $\tan^2\beta \simeq 2$).

To sum up, the first nucleophobic condition simply follows from the PQ charge assignment, while the second one is obtained by tuning the vacuum angle β so that $\tan\beta \simeq \sqrt{2}$. It should be finally noted that such a value of $\tan\beta$ is fully within the perturbative domain of the Yukawa couplings [40].

The suppression of axion-electron coupling is still needed in order to evade WDs/RGB bounds, and it can be achieved in two ways. The first one consists in the introduction of a third Higgs doublet, H_3, that couples to leptons. The electrophobia condition implemented in a three-Higgs doublet model (3HDM) is explained in [47], here we will summarise the main concepts. With the introduction of H_3, an extra non-hermitian operator is required in the scalar potential. A possibility is to consider

$$H_3^\dagger H_1 \phi^2 + H_3^\dagger H_2 \phi^\dagger . \tag{3.13}$$

As we have done in the DFSZ model with only two doublets, we impose the PQ charge conservation and the orthogonality condition between the PQ and the hypercharge currents. These requirements read

$$-\chi_3 + \chi_1 + \chi_\phi = 0 \ , \tag{3.14}$$

$$\chi_1 v_1^2 + \chi_2 v_2^2 + \chi_3 v_3^2 = 0 \,. \tag{3.15}$$

In order to decouple the axion from electrons we need to take the limit $\chi_3 \to 0$. Setting the normalization $\chi_\phi = 1$, this is obtained for $\tan^2\beta = 2$. It is remarkable that we obtain then the same condition derived in the section 3.1.2, which also ensures nucleophobia.

A second way to implement electrophobia consists in setting to zero the electron-axion coupling with an extra contribution coming from flavour mixing [12].

3.2 Flavour violation: IR vs. UV dynamics

As discussed in section 3.1.1, when the PQ symmetry is generation dependent, some flavour violating signatures arise. Most of the studies on non-universal axion models focus on the flavour-violating effects involving the axion. We will refer to these effects as due to *IR dynamics* since the low-energy axion field is explicitly involved in the flavour-violating process, as for example $K \to \pi a$. On the other hand, in UV complete models there are also heavy radial modes which might be responsible for flavour-violating 4-fermion operators. In contrast to the previous case, we will refer to this kind of flavour violation as due to *UV dynamics*, since it depends on the degrees of freedom on the UV completion.

The main goal of this thesis is to study the interplay between these two sources of flavour violation. While here the discussion will be kept qualitative and general, in chapter 4 we will focus on a specific non-universal axion model, labelled M1, that will be studied in greater detail.

3.2.1 Flavour violation from IR dynamics

Let us start with the Lagrangian in the IR regime. We are interested in the flavour-violating axion coupling terms, keeping in mind that we have a generation-dependent PQ symmetry which yields a PQ charge matrix which is no more proportional to identity. We call χ_{f_L} and χ_{f_R} the PQ charge matrices for left and right fermion respectively, then the Peccei Quinn current in the full generality is

$$J^\mu_{PQ} = \bar{f}_L \chi_{f_L} \gamma^\mu f_L + \bar{f}_R \chi_{f_R} \gamma^\mu f_R \,. \tag{3.16}$$

In order to go to the mass basis we have to rotate the fields $f_{L,R} \to V_{L,R} f_{L,R}$ and we get

$$J^\mu_{PQ} = \bar{f}_L V_L^\dagger \chi_{f_L} V_L \gamma^\mu f_L + \bar{f}_R V_R^\dagger \chi_{f_R} V_R \gamma^\mu f_R \,, \tag{3.17}$$

which reads in terms of vector and axial components

$$J^\mu_{PQ} = \frac{1}{2}\left(\bar{f} V_L^\dagger \chi_{f_L} V_L \gamma^\mu (1-\gamma_5) f + \bar{f} V_R^\dagger \chi_{f_R} V_R \gamma^\mu (1-\gamma_5) f \right) . \tag{3.18}$$

The non-trivial structure of these non-universal models is now clear: in the case of universal models the PQ charge matrices are proportional to the identity and hence the unitary rotation matrices disappear in the mass basis. Whereas, in the case of generation dependent PQ charges, the charge matrix does not commute anymore with the diagonalization

matrices and flavour mixing terms arise. The Lagrangian can be simply derived from eq. 3.18 and it reads

$$\begin{aligned}\mathcal{L} \supset & \frac{\partial_\mu a}{v_a}\bar{f}\Big[(V_L^\dagger \chi_{f_L} V_L + V_R^\dagger \chi_{f_R} V_R) + (U_R^\dagger \chi_{f_R} V_R - V_L^\dagger \chi_{f_L} V_L)\gamma_5\Big]\gamma^\mu f \\ = & \frac{\partial_\mu a}{2f_a}\bar{f}_i(C_{ij}^V + C_{ij}^A\gamma_5)\gamma^\mu f \ .\end{aligned} \tag{3.19}$$

In the step above we have used the eq. 1.71, while the vector and axial current coefficients are defined as:

$$C^V = \frac{1}{2N}(V_R^\dagger \chi_{f_R} V_R + V_L^\dagger \chi_{f_L} V_L) \ , \tag{3.20}$$

$$C^A = \frac{1}{2N}(V_R^\dagger \chi_{f_R} V_R - V_L^\dagger \chi_{f_L} V_L) \ . \tag{3.21}$$

3.2.2 A paradigmatic example: $K \to \pi a$

Given the expression of C^V and C^A we want to constrain them by applying experimental bounds. Indeed, flavour-violating experiments, such as the meson decay into an invisible final state, can be used in order to probe the value of the off-diagonal terms in $C^{V,A}$ matrices. The process leading to the stronger constraint is the kaon decay, namely

$$K^+ \to \pi^+ a \ . \tag{3.22}$$

It is crucial to note, however, that for this process the only relevant part in the quark current is the vector one. The meson particle is a pseudo-scalar particle, then it is odd under parity. At the same time QCD preserves parity, then in a general current term with an axial and a vector part, the entries corresponding to the axial current do not contribute. Namely we have that $\langle k^+| J_\mu^V + J_\mu^A |\pi^+\rangle = \langle k^+| J_\mu^V |\pi^+\rangle$, since the axial current is proportional to γ_5 and $\langle k^+| J_\mu^A |\pi^+\rangle = 0$. In the light of that, $K^+ \to \pi^+ a$ searches will give constraints only on C^V. Moreover, the process is a flavour violating decay since the positively charged kaon is formed by an up and an anti-strange quark, while the pion is composed by an up quark and an anti-down on. The flavour violation is clear in the left Feynman diagram in Fig. 3.2. The constraints on vector current regard only the strange and down sector and in particular the involved entry in the matrix will be C_{sd}^V.

In order to find the constraints, let us consider the transition rate

$$\Gamma(K^+ \to \pi^+ a) \simeq \frac{m_K^3}{16\pi f_a^2}|C_{sd}^V|^2 \ . \tag{3.23}$$

The principal process through which the kaon decays in the SM is $K^+ \to \mu^+\nu$, represented in the right diagram in Fig. 3.2, with transition rate:

$$\Gamma(K^+ \to \mu^+\nu) \simeq \frac{m_K}{8\pi}(G_F f_K m_\mu |V_{us}|)^2 \ . \tag{3.24}$$

In the last equation, we have labelled with f_K the kaon decay constant, with G_F the Fermi constant and with $|V_{us}|$ the CKM matrix element

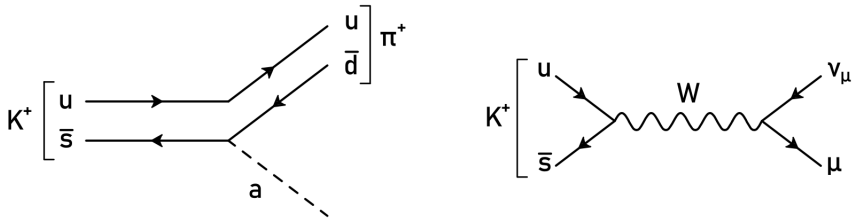

Figure 3.2: Feynman diagrams of different channels of kaon decay. The left diagram represents the kaon decaying into a pion and an axion, while the right one represents the main kaon decay channel into in the SM.

which is relevant for the decay. Approximating $\Gamma_{TOT} \simeq \Gamma(K^+ \to \mu^+\nu)$[2], the branching ratio in $K \to \pi a$ is obtained by taking the ratio between eq. 3.23 and 3.24, that reads:

$$\mathrm{Br}(K^+ \to \pi^+ a) \simeq (G_F f_K m_\mu |V_{us}|)^{-2} \frac{m_K^2}{2f_a^2} |C_{sd}^V|^2 \,. \tag{3.25}$$

From the experiments E949+E787 [79] one infers the experimental bound

$$\mathrm{Br}(K^+ \to \pi^+ a) < 0.73 \cdot 10^{-10} \,, \tag{3.26}$$

which implies

$$|C_{sd}^V| < 2.9 \cdot 10^{-12} f_a(\mathrm{GeV}) \,, \tag{3.27}$$

or equivalently a constraint on the axion mass

$$m_a < 17 \cdot |C_{sd}^V|^{-1} \mu\mathrm{eV}. \tag{3.28}$$

Hence, we conclude that flavour bounds on the axion mass can be even more constraining than astrophysics, depending, of course, on the size of the off-diagonal element C_{sd}^V. We finally observe that it is possible to set constraints also on other elements of $C^{V,A}$ (including axial components) by looking at other flavour-violating processes which involve meson and baryon decays as well as neutral meson oscillations. A collection of bounds can be found for instance in Ref. [80].

3.2.3 Flavour violation from UV dynamics

In UV completions, such as the DFSZ model discussed in section 1.4.3, there are heavy degrees of freedom in the scalar sector which comprise for instance the radial modes of the 2HDM. Beyond the light SM Higgs, h, these results into a CP-even neutral state, H, a CP-odd one, A, and a charged scalar field, $H^\pm$. As it will be shown explicitly in the next chapter, when these states are integrated out in non-universal axion models, they lead to 4-fermion operators which provide new sources of flavour-violation, complementary to the previously discussed flavour-violating processes involving the axion field.

Since the final goal is to constrain the coefficient of four fermion operators arising from the Yukawa sector and in particular the quark

[2] In the SM the branching ratio in $K^+ \to \mu^+\nu$ is around 63.4%.

one, let us restrict the expression of the Lagrangian to the Yukawa terms. We want now to clarify why a non-universal model implies a flavour violating signature from the point of view of the UV degrees of freedom. Making explicit the flavour indices i, j, the Yukawa Lagrangian for the quark sector of the most general 2HDM can be written as

$$\mathcal{L} \supset -\bar{q}_{L,i} u_{R,j} \left[Y^u_{1,ij} H_1 + Y^u_{2,ij} H_2 \right] + \bar{q}_{L,i} d_{R,j} \left[Y^d_{1,ij} \tilde{H}_1 + Y^d_{2,ij} \tilde{H}_2 \right] + \text{h.c.} \,, \tag{3.29}$$

where the $Y^u_{1,2}$ and $Y^d_{1,2}$ are the Yukawa matrices which depend on the specific non-universal model to be considered. Here we will keep the discussion general, while in chapter 4 we will make this structure explicit by referring to a specific non-universal axion model. Then the quark mass matrices are given by:

$$\begin{aligned} M_u &= \frac{v}{\sqrt{2}} c_\beta Y^u_1 + \frac{v}{\sqrt{2}} s_\beta Y^u_2 \,, \\ M_d &= \frac{v}{\sqrt{2}} c_\beta Y^d_1 + \frac{v}{\sqrt{2}} s_\beta Y^d_2 \,, \end{aligned} \tag{3.30}$$

For completeness we also write the Lagrangian for the lepton Yukawas

$$\mathcal{L} \supset \bar{l}_{L,i} e_{R,j} \left[Y^e_{1,ij} \tilde{H}_1 + Y^e_{2,ij} \tilde{H}_2 \right] , \tag{3.31}$$

and the corresponding lepton mass matrix:

$$M_e = \frac{v}{\sqrt{2}} c_\beta Y^e_1 + \frac{v}{\sqrt{2}} s_\beta Y^e_2 \,. \tag{3.32}$$

Again, Y^e_1 and Y^e_2 represent the structure of the lepton Yukawa coupling which will depend on the considered model.

Note that in the case of universal axion models, such as the DFSZ model, H_1 couples only to up-type quarks and H_2 couples only to down-type quarks. In this case one has simply $M_u \propto Y_1$ and $M_d \propto Y_2$, so in the mass basis also the Yukawa interactions of the scalar radial modes contained in $H_{1,2}$ are diagonal and there are no flavour-changing currents. The situation is different instead in the case on non-universal axion models, where both types of Higgses can couple to up-type and down-type quarks. An example of this structure, leading to flavour-violating axion couplings, was given in section 3.1.1 (see eq. 3.1). Then, given the general structure in eq. 3.30, in the basis where quark masses are diagonal, Yukawa interactions are not necessarily diagonal and hence flavour-violating sources mediated by the heavy Higgs radial modes are generated. Upon integrating out the latter, these results in flavour-violating 4-fermion operators.

In the next chapter we will analyse in greater detail a specific UV complete non-universal model, we will diagonalize both the quark and Higgs sectors, and finally derive the flavour-violating 4-fermion operators upon integrating out the heavy radial modes.

Chapter 4

Anatomy of a non-universal axion model

In this chapter we study in more detail an explicit non-universal axion model, labelled *M1 model* and first introduced in Ref. [12], with the final goal of highlighting the interplay between IR and UV sources of flavour violation, due respectively to the axion field and the heavy radial modes of the UV completion. The study of the latter aspect represents the original contribution of this thesis.

4.1 The M1 model

The scalar sector of the M1 model comprises two Higgs doublets $H_{1,2} \sim (1, 2, -1/2)$ and a complex singlet $\sigma \sim (1, 1, 0)$. This is the same field content of the DFSZ model discussed in section 1.4.3, with the only difference that now the Yukawa sector admits for H_1 and H_2 to couple to the same flavours, according to the following Yukawa Lagrangian:

$$\begin{aligned}\mathcal{L}^Y_{M1} = &- y^u_{\alpha\beta}\bar{q}_\alpha u_\beta H_1 - y^u_{33}\bar{q}_3 u_3 H_2 - y^u_{\alpha 3}\bar{q}_\alpha u_3 H_1 - y^u_{3\beta}\bar{q}_3 u_\beta H_2 \\ &+ y^d_{\alpha\beta}\bar{q}_\alpha d_\beta \tilde{H}_2 + y^d_{33}\bar{q}_3 d_3 \tilde{H}_1 + y^d_{\alpha 3}\bar{q}_\alpha d_3 \tilde{H}_2 + y^d_{3\beta}\bar{q}_3 d_\beta \tilde{H}_1 \\ &+ y^l_{\alpha\beta}\bar{l}_\alpha e_\beta \tilde{H}_1 + y^l_{33}\bar{l}_3 e_3 \tilde{H}_2 + y^l_{\alpha 3}\bar{l}_\alpha e_3 \tilde{H}_1 + y^l_{3\beta}\bar{l}_3 e_\beta \tilde{H}_2 \,,\end{aligned} \tag{4.1}$$

where $\alpha, \beta = 1, 2$, denote first two generations. It is crucial to note that the Yukawa terms feature a so-called 2+1 structure, namely with the first two generations always coupling to the same type of Higgs. As we will see in a moment, this implies that first two generations always have the same PQ charge.

The PQ charges of the scalar fields are fixed by imposing two conditions, as already done for the case of the DFSZ model in section 1.4.3. Specifically, we want to impose the PQ invariance and the orthogonality between the PQ and hypercharge currents, namely, we want to ensure that there are no mixing terms between axion and Z boson. If we consider that the singlet σ couples with the two Higgs doublets through the term $H_1 H_2^\dagger \sigma^2$ then the PQ charges for the Higgs doublets can be defined as in the DFSZ case, i.e. $\chi_1 = -2s^2_\beta$ and $\chi_2 = 2c^2_\beta$, where we adopted the normalization $\chi_\sigma = 1$ and defined $\tan\beta = \dfrac{v_2}{v_1}$, which takes values in the perturbative unitarity domain $\tan\beta \in [0.25, 170]$. Eventually, taking into account the PQ invariance of the Yukawa Lagrangian in eq. 4.1,

the PQ charges in the quark sector read:

$$\chi_q = 2(0,0,1), \qquad \chi_u = 2(s_\beta^2, s_\beta^2, s_\beta^2) \qquad \chi_d = 2(c_\beta^2, c_\beta^2, c_\beta^2), \tag{4.2}$$

while for the lepton sector we have:

$$\chi_l = -2(0,0,1), \qquad \chi_e = -2(s_\beta^2, s_\beta^2, s_\beta^2). \tag{4.3}$$

Note that we have simplified the PQ charges by exploiting the invariance of the theory under baryon and lepton number, which have been employed in order to set $\chi_{q_1} = \chi_{q_2} = 0$ and $\chi_{l_1} = \chi_{l_2} = 0$, respectively. Moreover, the M1 model is such that only the LH doublets q and l have non-universal PQ charges, and hence flavour-violating axion couplings will only involve LH fermions (as it can be read from eqs. 3.20-3.21).

To complete the presentation of the M1 model we also specify the scalar potential, which coincides with that of the DFSZ model and reads

$$\begin{aligned} V_{M1} =& - m_{11}^2 (H_1^\dagger H_1) - m_{22}^2 (\tilde{H_2}^\dagger \tilde{H_2}) - m_{33}^2 |\sigma|^2 \\ &+ \lambda_1 (H_1^\dagger H_1)^2 + \lambda_2 (\tilde{H_2}^\dagger \tilde{H_2})^2 + \lambda_3 |\sigma|^2 + \lambda_4 (H_1^\dagger \tilde{H_2})^\dagger (H_1^\dagger \tilde{H_2}) \\ &+ \lambda_{12} (H_1^\dagger H_1)(\tilde{H_2}^\dagger \tilde{H_2}) + \lambda_{13} |\sigma|^2 (H_1^\dagger H_1) + \lambda_{23} |\sigma|^2 (\tilde{H_2}^\dagger \tilde{H_2}) \\ &+ (\lambda_5 \sigma^2 H_2^\dagger H_1 + h.c.). \end{aligned} \tag{4.4}$$

For later purpose we also specify the embedding of the EM charged eigenstates into the scalar representations

$$H_1 = \begin{pmatrix} \frac{v_1 + h_{01} + i\eta_1}{\sqrt{2}} \\ h_1^- \end{pmatrix}, \qquad H_2 = \begin{pmatrix} \frac{v_2 + h_{02} + i\eta_2}{\sqrt{2}} \\ h_2^- \end{pmatrix} \tag{4.5}$$

and

$$\sigma = \frac{v_\sigma + \sigma_0 + i\eta_{0\sigma}}{\sqrt{2}}\,, \tag{4.6}$$

which will be employed for the calculation of the scalar spectrum in section 4.3.1. In the same section we will discussed the tuning mechanism through which we can decouple the electroweak scale, associated to v_1 and v_2 and the f_a scale associated to v_σ. The link between v_σ and f_a is the same discussed in eqs. 1.71 and 1.90.

4.2 Yukawa sector

The goal of this section is to derive the rotation matrices which diagonalise the quark mass matrices, that is

$$M_u^{diag} = V_{uL}^\dagger M_u V_{uR}\,, \qquad M_d^{diag} = V_{dL}^\dagger M_d V_{dR}\,. \tag{4.7}$$

In the case of the M1 model, we can write

$$\begin{aligned} M_u &= \frac{v}{\sqrt{2}} c_\beta Y_1^u + \frac{v}{\sqrt{2}} s_\beta Y_2^u\,, \\ M_d &= \frac{v}{\sqrt{2}} c_\beta Y_1^d + \frac{v}{\sqrt{2}} s_\beta Y_2^d\,, \end{aligned} \tag{4.8}$$

where from eq. 4.1 it follows that

$$Y_1^u = \begin{pmatrix} y_{11}^u & y_{12}^u & y_{13}^u \\ y_{21}^u & y_{22}^u & y_{23}^u \\ 0 & 0 & 0 \end{pmatrix}, \quad Y_2^u = \begin{pmatrix} 0 & 0 & 0 \\ 0 & 0 & 0 \\ y_{31}^u & y_{32}^u & y_{33}^u \end{pmatrix}, \tag{4.9}$$

$$Y_1^d = \begin{pmatrix} 0 & 0 & 0 \\ 0 & 0 & 0 \\ y_{31}^d & y_{32}^d & y_{33}^d \end{pmatrix}, \quad Y_2^d = \begin{pmatrix} y_{11}^d & y_{12}^d & y_{13}^d \\ y_{21}^d & y_{22}^d & y_{23}^d \\ 0 & 0 & 0 \end{pmatrix}, \tag{4.10}$$

Hence, given a Yukawa texture, one can in principle find the diagonalizing matrices by applying the bi-unitary transformations in eq. 4.7. Instead of solving this problem in full generality, we make a simplifying assumption here, namely that rotation matrices are CKM-like. Following Ref. [14], this is obtained via the following ansatz for the Yukawa matrices:

$$Y_1^u = \frac{\sqrt{2}}{v c_\beta} \begin{pmatrix} m_u & 0 & 0 \\ 0 & m_d & 0 \\ 0 & 0 & 0 \end{pmatrix}, \quad Y_2^u = \frac{\sqrt{2}}{v s_\beta} \begin{pmatrix} 0 & 0 & 0 \\ 0 & 0 & 0 \\ 0 & 0 & m_t \end{pmatrix} \tag{4.11}$$

$$Y_1^d = \frac{\sqrt{2}}{v c_\beta} \begin{pmatrix} 0 & 0 & 0 \\ 0 & 0 & 0 \\ 0 & 0 & m_b \end{pmatrix}, \quad Y_2^d = \frac{\sqrt{2}}{v s_\beta} \begin{pmatrix} m_d & \lambda m_s & \rho\lambda^3 m_b \\ 0 & m_s & \lambda^2 m_b \\ 0 & 0 & 0 \end{pmatrix}, \tag{4.12}$$

where $\lambda \simeq 0.23$ and $\rho \simeq 0.12$ are coefficients entering the Wolfenstein parametrization of the CKM matrix [81], that is defined in terms of the LH rotation matrices as

$$V_{CKM} = V_{uL}^\dagger V_{dL} \,. \tag{4.13}$$

Note that the ansatz above corresponds to an already diagonal M_u matrix, hence, $V_{uL} = V_{uR} = \mathbb{1}$ and $V_{CKM} = V_{dL}$, which implies that only mixing in the down-quark sector is physical. Regarding instead axion interactions only the LH matrix V_{dL} appears in eq. 3.20 and 3.21, since PQ charges are universal in the RH sector.

This particular ansatz for the Yukawa matrices might seem quite restrictive. However, it is sufficient for our goal, namely for the comparison between flavour-violation from low- and high-energy dynamics. As discussed in section 3.2.2 the only relevant quantity for the $K \to \pi a$ decay is the vector coefficient C_{sd}^V, which is different from zero with this definition of the Yukawa matrices. On the other hand, if we had for instance considered a diagonal matrix in the down sector, then we would have to consider other processes involving flavour violation in the up-quark sector. A possible follow-up of this work could consist in relaxing the assumptions made previously and define in a very general way the mass

matrices M_u and M_d. For the rest of the thesis, we will limit ourselves to the simpler scenario considering above.

Let us now perform the diagonalization of M_d, in order to show that indeed $V_{dL} \simeq V_{CKM}$. This can be done by working in perturbation theory, i.e. assuming small mixing angles, as reviewed in Appendix A.1. We summarize here the main steps. The general idea is to diagonalize the matrix M_d using a bi-linear transformation, that is:

$$M_d^{diag} = V_{dL}^{\dagger} M_d V_{dR} \,, \tag{4.14}$$

which, in turn, are composed by the product on the rotation matrices (assuming real parameters for simplicity):

$$V_{dL} = V_{12L} \times V_{13L} \times V_{23L} \qquad V_{uR}^{\dagger} = V_{23R} \times V_{13R} \times V_{12R} \,. \tag{4.15}$$

After performing all the steps, see Appendix A.2, the left-handed rotation has, as expected, the following form:

$$V_{CKM} \simeq V_{dL} \simeq \begin{pmatrix} 1 & \lambda & \rho\lambda^3 \\ -\lambda & 1 & \lambda^2 \\ \lambda^3(1-\rho) & -\lambda^2 & 1 \end{pmatrix} \tag{4.16}$$

which reproduce in first approximation the CKM matrix [81].

Note that differently from Ref. [14], here the element "13" in Y_1^d matrix of eq. 4.12 has a dependence from ρ. This is because the authors in that paper wanted to avoid the effects of quark flavour violation. In this sense they set the ρ coefficient equal to unit and, as a result, they got a zero value in an element of the final rotation matrix. Our treatment is more general and matches better the CKM matrix that we want to reproduce.

Considering $\lambda = 0.226$ and $\rho = 0.139$ [81] we obtain the numerical matrix:

$$V_{CKM} \simeq \begin{pmatrix} 1 & 0.226 & 0.0016 \\ 0.226 & 1 & 0.0510 \\ 0.0099 & 0.0510 & 1 \end{pmatrix} \,, \tag{4.17}$$

that is in good agreement with the numerical value of the CKM.

4.3 Higgs sector

Let us discuss now the Higgs sector. Our goal is to compute the mass spectrum of the particles involved in the M1 model scenario. The simpler case of the 2HDM is reviewed in Appendix B. Here, instead, we consider the more involved case including two Higgs doublets and a complex singlet, comprising the M1 model.

4.3.1 The mass spectrum in the M1 model

The potential in the eq. 4.4 represents our starting point. From now on, we will take $\lambda_5^* = \lambda_5$, namely we will consider λ_5 as a real coefficient. This is without loss of generality, since all results will be proportional

to 2 $\mathrm{Re}(\lambda_5)=\lambda_5^* + \lambda_5$ and, moreaover, it is possible to set λ_5 real via a proper re-phasing of the scalar fields.

In order to minimize the potential, we start by imposing the stationary conditions:

$$\frac{\partial V_{M1}}{\partial v_1} = 0, \qquad \frac{\partial V_{M1}}{\partial v_2} = 0, \qquad \frac{\partial V_{M1}}{\partial v_\sigma} = 0,$$

which read:

$$m_{11}^2 = \lambda_1 v_1^2 + \frac{\lambda_{12} v_2^2}{2} + \frac{\lambda_{13} v_\sigma^2}{2} + \frac{\lambda_5 v_2 v_\sigma^2}{2 v_1} \tag{4.18}$$

$$m_{22}^2 = \lambda_2 v_2^2 + \frac{\lambda_{12} v_1^2}{2} + \frac{\lambda_{23} v_\sigma^2}{2} + \frac{\lambda_5 v_1 v_\sigma^2}{2 v_2} \tag{4.19}$$

.

$$m_{33}^2 = \lambda_3 v_\sigma^2 + \frac{\lambda_{13} v_1^2}{2} + \frac{\lambda_{23} v_2^2}{2} + \lambda_5 v_1 v_2 \tag{4.20}$$

Given the embedding of the EM eigenstates in eq. 4.5 and 4.6, the fields can be divided in two charged states (h_1^-, h_2^-), three CP-odd scalars $(\eta_1, \eta_2, \eta_{0\sigma})$ and three CP-even scalars $(h_{01}, h_{02}, \sigma_0)$. The spectrum is computed by taking the second derivatives of V_{M1} with respects fields and by imposing the stationary conditions above. One finds:

- Firstly, the mass matrix M_c associated to the charged fields h_1^- and h_2^- is:

$$M_c^2 = \begin{pmatrix} \frac{\lambda_4 v_2^2}{2} - \frac{\lambda_5 v_2 v_\sigma^2}{2 v_1} & -\frac{\lambda_4 v_1 v_2}{2} + \frac{\lambda_5 v_\sigma^2}{2} \\ -\frac{\lambda_4 v_1 v_2}{2} + \frac{\lambda_5 v_\sigma^2}{2} & \frac{\lambda_4 v_1^2}{2} - \frac{\lambda_5 v_1 v_\sigma^2}{2 v_1} \end{pmatrix} . \tag{4.21}$$

- Secondly, the pseudo scalar mass matrix M_{ps} associated to η_1, η_2 and $\eta_{0\sigma}$ is:

$$M_{ps}^2 = \begin{pmatrix} -\frac{\lambda_5 v_2 v_\sigma^2}{2 v_1} & \frac{\lambda_5 v_\sigma^2}{2} & -\lambda_5 v_2 v_\sigma \\ \frac{\lambda_5 v_\sigma^2}{2} & -\frac{\lambda_5 v_1 v_\sigma^2}{2 v_2} & \lambda_5 v_1 v_\sigma \\ -\lambda_5 v_2 v_\sigma & \lambda_5 v_1 v_\sigma & -2\lambda_5 v_1 v_2 \end{pmatrix} . \tag{4.22}$$

- Finally, the neutral scalar fields, h_{01}, h_{02} and σ_0 correspond to the mass matrix M_{ns}:

$$M_{ns}^2 = \begin{pmatrix} 2\lambda_1 v_1^2 - \frac{\lambda_5 v_2 v_\sigma^2}{2 v_1} & \lambda_{12} v_1 v_2 + \frac{\lambda_5 v_\sigma^2}{2} & \lambda_{13} v_1 v_\sigma + \lambda_5 v_2 v_\sigma \\ \lambda_{12} v_1 v_2 + \frac{\lambda_5 v_\sigma^2}{2} & 2\lambda_2 v_2^2 - \frac{\lambda_5 v_1 v_\sigma^2}{2 v_2} & \lambda_{23} v_2 v_\sigma + \lambda_5 v_1 v_\sigma \\ \lambda_{13} v_1 v_\sigma + \lambda_5 v_2 v_\sigma & \lambda_{23} v_2 v_\sigma + \lambda_5 v_1 v_\sigma & 2\lambda_3 v_\sigma^2 \end{pmatrix} . \tag{4.23}$$

At this point, to determine the mass eigenvalues we can make some physical considerations. The hierarchy between different mass scales should be imposed: the PQ scale is larger than the electroweak scale, which implies $v_1, v_2 \ll v_\sigma$. As a matter of fact, we can require, at least at tree level, that:

$$\lambda_{13} \sim \frac{c_{13}v^2}{v_\sigma^2}, \qquad \lambda_{23} \sim \frac{c_{23}v^2}{v_\sigma^2}, \qquad \lambda_5 \sim \frac{c_5 v^2}{v_\sigma^2} \tag{4.24}$$

where c_{13}, c_{23}, c_5 are *O(1)* coefficients and $v^2 = v_1^2 + v_2^2$. This choice will ensure the decoupling among the heavy neutral scalar scale (PQ scale) and the other lighter scales present in the mass spectrum (Higgs and 2DHM scale). Given this parametrization, we can now compute the mass eigenvalues perturbatively.

In detail, the charged scalar mass matrix 4.21 is of rank 1. This is due, as in the 2HDM case, to the presence of a null eigenvalue corresponding to the would-be Goldstone boson mode associated to the W boson. Instead, the other eigenvalue is:

$$m_{H^\pm}^2 = v^2\lambda_4 + \frac{v_\sigma^4\lambda_5}{v_1 v_2} \xrightarrow{LO} v^2\lambda_4 + \frac{v^4 c_5}{v_1 v_2} \tag{4.25}$$

where the leading order (LO) expression is computed using 4.24. Similarly also the matrix 4.22 is of rank 1. Being of dimension three, this means that it has two zero eigenvalues: the first one is referred to the Goldstone boson absorbed by the Z boson, while the second one corresponds to the axion, namely the Goldstone boson associated to the breaking of $U(1)_{PQ}$. The third non-zero eigenvalue is

$$m_A^2 = \frac{\lambda_5}{v_1 v_2}(v^2 v_\sigma^2 + 4v_1^2 v_2^2) \xrightarrow{LO} \frac{v^4 c_5}{v_1 v_2} \tag{4.26}$$

For what concerns the CP-even scalar section, the mass matrix is of rank 3. Hence, we expect three non-zero eigenvalues related to the m_h, m_H and m_σ. However, due to the same consideration as before, regarding the hierarchy structure of the mass fields, it is convenient to rewrite the mass matrix 4.23 at leading order using 4.24. Therefore, keeping all terms of $O(v^2)$ the matrix turns out to be:

$$\begin{pmatrix} 2\lambda_1 v_1^2 - \dfrac{v^2 v_2 c_5}{2v_1} & \lambda_{12}v_1 v_2 + \dfrac{v^2 c_5}{2} & 0 \\ 2\lambda_{12}v_1 v_2 + \dfrac{v^2 c_5}{2} & \lambda_2 v_2^2 - \dfrac{v^2 v_1 c_5}{2v_2} & 0 \\ 0 & 0 & 2\lambda_3 v_\sigma^2 \end{pmatrix} \tag{4.27}$$

The eigenvalues associated to it are:

$$m_h^2 \sim m_H^2 \sim O(v^2), \tag{4.28}$$

$$m_\sigma^2 \sim 2\lambda_3 v_\sigma^2 \,. \tag{4.29}$$

Hence, once the heavy σ_0 state is decoupled one is left in the EFT with a standard 2HDM, whose scale is assumed to be not far from the electroweak scale. The diagonalization of the 2HDM can be done by following some standard steps which are reviewed in Appendix B.

4.4 Lagrangian in the mass basis

In the previous sections we have diagonalized both the fermion and the scalar sector. Hence, we proceed now with the identification of the Lagrangian in the mass basis, that is the preliminary step in order to integrate out the heavy radial modes of the 2HDM, that is $H, A, H^{\pm}$.

Let us start with eq. 3.29 and focus for simplicity on the dow-quark sector (similar considerations apply to up-type quarks and charged leptons). Thus, let us consider:

$$\mathcal{L} \supset -\bar{q}_{L,i} d_{R,j} \left[Y^d_{1,ij} \tilde{H}_1 + Y^d_{2,ij} \tilde{H}_2 \right] . \tag{4.30}$$

The decomposition of the Higgs fields are given in eq. 4.5. In the case of tilde fields, we report them here for convenience:

$$\tilde{H}_1 = \begin{pmatrix} h_1^+ \\ -\dfrac{v_1 + h_{01} + i\eta_1}{\sqrt{2}} \end{pmatrix} , \qquad \tilde{H}_2 = \begin{pmatrix} h_2^+ \\ -\dfrac{v_2 + h_{02} + i\eta_2}{\sqrt{2}} \end{pmatrix} . \tag{4.31}$$

To obtain the final Lagrangian in the mass basis we have to follow through three different steps:

- decomposition of $SU(2)_L$ space;
- projection on the Higgs mass basis;
- projection on the fermions mass basis.

It is convenience to first rotate the Higgs doublets in a basis where only one of them, say Φ_1, picks up the whole electroweak VEV, that is

$$\begin{pmatrix} \Phi_1 \\ \Phi_2 \end{pmatrix} = \begin{pmatrix} c_\beta & s_\beta \\ -s_\beta & c_\beta \end{pmatrix} \begin{pmatrix} \tilde{H}_1 \\ \tilde{H}_2 \end{pmatrix} . \tag{4.32}$$

Indeed, it can be easily verified that with this definition:

$$\begin{aligned} \langle \Phi_1 \rangle &\sim c_\beta v_1 + s_\beta v_2 = v \\ \langle \Phi_2 \rangle &\sim -s_\beta v_1 + c_\beta v_2 = 0 . \end{aligned} \tag{4.33}$$

Applying the definition in eq. 4.32, one finds:

$$\Phi_1 = \begin{pmatrix} G^+ \\ \dfrac{1}{\sqrt{2}}(-v - c_\beta h_{01} - s_\beta h_{02} + i G^0) \end{pmatrix} \tag{4.34}$$

$$\Phi_2 = \begin{pmatrix} H^+ \\ \dfrac{1}{\sqrt{2}}(s_\beta h_{01} - c_\beta h_{02} + i A) \end{pmatrix} \tag{4.35}$$

where we have used the following definitions:

$$\begin{aligned} G^+ &= c_\beta h_1^+ + s_\beta h_2^+ \\ G^0 &= c_\beta \eta_1 + s_\beta \eta_2 \\ H^+ &= -s_\beta h_1^+ + c_\beta h_2^+ \\ A^0 &= c_\beta \eta_2 - s_\beta \eta_1 , \end{aligned} \tag{4.36}$$

with $G^{+,0}$ denoting the would-be Goldstone bosons eaten by the W and the Z.

At this point, we decompose the $SU(2)_L$ components in eq. 4.30 and focus, for illustrative purposes, on the terms proportional to the H^+ component, which read:

$$\begin{aligned}
\mathcal{L} =& \bar{q}_L Y_1^d \tilde{H}_1 d_R + \bar{q}_L Y_2^d \tilde{H}_2 d_R \\
\supset& \bar{u}_L Y_1^d (s_\beta(-H^+)) d_R + \bar{u}_L Y_2^d (c_\beta(H^+)) d_R \\
=& -\bar{u}_L \left[V_{uL}^\dagger Y_1^d V_{dR} s_\beta - V_{uL}^\dagger Y_2^d V_{dR} c_\beta \right] d_R H^+ \\
=& -\bar{u}_L V_{CKM} \left[(V_{dL}^\dagger Y_1^d V_{dR}) s_\beta + (V_{dL}^\dagger Y_2^d V_{dR}) \frac{s_\beta^2}{c_\beta} - (V_{dL}^\dagger Y_2^d V_{dR}) \frac{1}{c_\beta} \right] d_R H^+ \\
=& -\bar{u}_L V_{CKM} \left[s_\beta \frac{\sqrt{2} m_d}{v c_\beta} - \frac{1}{c_\beta} V_{dL}^\dagger Y_2^d V_{dR} \right] d_R H^+ \\
=& -\bar{u}_L V_{CKM} \left[\frac{\sqrt{2} m_d}{v c_\beta} s_\beta - \frac{1}{c_\beta} \epsilon_d \right] d_R H^+ \, ,
\end{aligned} \tag{4.37}$$

where we have used the diagonal mass matrices defined as:

$$\sqrt{2} m_u = v s_\beta V_{uL}^\dagger Y_2^u V_{uR} + v c_\beta V_{uL}^\dagger Y_1^u V_{uR} \, , \tag{4.38}$$

$$\sqrt{2} m_d = v s_\beta V_{dL}^\dagger Y_2^d V_{dR} + v c_\beta V_{dL}^\dagger Y_1^d V_{dR} \, . \tag{4.39}$$

A similar procedure can be followed in order to compute the terms proportional to A and H. For the latter case, however, one has to perform a final rotation in order to diagonalize the CP-even sector. This is explicitly obtained via the orthogonal transformation

$$\begin{pmatrix} h_{01} \\ h_{02} \end{pmatrix} = \begin{pmatrix} c_\alpha & s_\alpha \\ -s_\alpha & c_\alpha \end{pmatrix} \begin{pmatrix} H \\ h \end{pmatrix} \, , \tag{4.40}$$

where the angle α can be related to the parameters of the scalar potential of the 2HDM (see Appendix B).

Following the same steps, as already done for the H^+ field, also for the A and H components, and including also the up-quark and charged-lepton sectors, we finally arrive at the full interaction Lagrangian in the mass basis, which can be written in a compact way as

$$\begin{aligned}
\mathcal{L}_Y =& -\bar{u}_{Li} h [C_{ij}^{h_u}] u_{Rj} - \bar{d}_{Li} h [C_{ij}^{h_d}] d_{Rj} - \bar{e}_{Li} h [C_{ij}^{h_e}] e_{Rj} + \\
& - \bar{u}_{Li} H [C_{ij}^{H_u}] u_{Rj} - \bar{d}_{Li} H [C_{ij}^{H_d}] d_{Rj} - \bar{e}_{Li} H [C_{ij}^{H_e}] e_{Rj} + \\
& + \bar{u}_{Li} A [C_{ij}^{A_u}] u_{Rj} + \bar{d}_{Li} A [C_{ij}^{A_d}] d_{Rj} + \bar{e}_{Li} A [C_{ij}^{A_e}] e_{Rj} + \\
& - \bar{d}_{Li} H^- V_{ki}^* [C_{kj}^{H_u^-}] u_{Rj} - \bar{u}_{Li} H^+ V_{ik} [C_{kj}^{H_d^+}] d_{Rj} + \\
& - \bar{\nu}_{Li} H^+ U_{ki}^* [C_{kj}^{H_e^+}] e_{Rj} + \text{h.c.} \, ,
\end{aligned} \tag{4.41}$$

where V and U denore respectively the CKM and PMNS mixing matrices. The C_{ij} coefficients, which encode both the diagonalization of the

fermion and scalar sectors, are found to be:

$$
\begin{aligned}
C_{ij}^{h_u} &= \frac{m_{u_i}}{v s_\beta}\delta_{ij}(c_\alpha) + \epsilon_{ij}^u\left(-\frac{c_{\alpha-\beta}}{s_\beta}\right)\\
C_{ij}^{h_d} &= \frac{m_{d_i}}{v c_\beta}\delta_{ij}(-s_\alpha) + \epsilon_{ij}^d\left(\frac{c_{\alpha-\beta}}{c_\beta}\right)\\
C_{ij}^{h_e} &= \frac{m_{e_i}}{v c_\beta}\delta_{ij}(-s_\alpha) + \epsilon_{ij}^e\left(\frac{c_{\alpha-\beta}}{c_\beta}\right)\\
C_{ij}^{H_u} &= \frac{m_{u_i}}{v s_\beta}\delta_{ij}(s_\alpha) + \epsilon_{ij}^u\left(-\frac{s_{\alpha-\beta}}{s_\beta}\right)\\
C_{ij}^{H_d} &= \frac{m_{d_i}}{v c_\beta}\delta_{ij}(c_\alpha) + \epsilon_{ij}^d\left(\frac{s_{\alpha-\beta}}{c_\beta}\right)\\
C_{ij}^{H_e} &= \frac{m_{e_i}}{v c_\beta}\delta_{ij}(c_\alpha) + \epsilon_{ij}^e\left(\frac{s_{\alpha-\beta}}{c_\beta}\right)\\
C_{ij}^{A_u} &= \frac{m_{u_i}}{v s_\beta}\delta_{ij}(-i c_\beta) + \epsilon_{ij}^u\left(\frac{i}{s_\beta}\right)\\
C_{ij}^{A_d} &= \frac{m_{d_i}}{v c_\beta}\delta_{ij}(-i s_\beta) + \epsilon_{ij}^d\left(\frac{i}{c_\beta}\right)\\
C_{ij}^{A_e} &= \frac{m_{e_i}}{v c_\beta}\delta_{ij}(-i c_\beta) + \epsilon_{ij}^e\left(\frac{i}{c_\beta}\right)\\
C_{kj}^{H_u^-} &= \sqrt{2}\frac{m_{u_i}}{v s_\beta}\delta_{kj}c_\beta - \frac{\epsilon_{kj}^u}{s_\beta}\\
C_{kj}^{H_d^+} &= \sqrt{2}\frac{m_{d_i}}{v c_\beta}\delta_{kj}s_\beta - \frac{\epsilon_{kj}^d}{c_\beta}\\
C_{kj}^{H_e^+} &= \sqrt{2}\frac{m_{e_i}}{v c_\beta}\delta_{kj}s_\beta - \frac{\epsilon_{kj}^e}{c_\beta}\ ,
\end{aligned}
\tag{4.42}
$$

where we have introduced the ϵ matrices:

$$\epsilon^u = V_{uL}^\dagger Y_1^u V_{uR} \tag{4.43}$$

$$\epsilon^d = V_{dL}^\dagger Y_2^d V_{dR} \tag{4.44}$$

$$\epsilon^e = V_{eL}^\dagger Y_2^e V_{eR}\ , \tag{4.45}$$

which encode the source of flavour violation due to the radial modes, H, A, H^+, that we want to integrate out in order to obtain the flavour-violating 4-fermion operators.

4.5 4-fermion operators

The goal of this final section is to derive the 4-fermion coefficients, C_{ijkl}, following the integration of the heavy radial modes, H, A, H^+. This will be done, within an EFT approach, by using the classical equation of motion for the heavy fields in the static limit (i.e. neglecting higher-order derivative terms). The latter are then substituted back into the original Lagrangian, thus formally obtaining the associated effective Lagrangian.

4-fermion operators from H

Let us start with H. The Lagrangian associated to this field, which involves up and down quarks and includes also the hermitian conjugate terms, reads:

$$\begin{aligned}\mathcal{L} \supset & - \bar{d}_{Li} H C^{H_d}_{ij} d_{Rj} - \bar{d}_{Rj} (C^{H_d}_{ji})^\dagger H d_{Li} + \\ & - \bar{u}_{Li} H C^{H_u}_{ij} u_{Rj} - \bar{u}_{Rj} H (C^{H_u}_{ji})^\dagger u_{Li} - \frac{1}{2} m_H^2 H^2 \, .\end{aligned} \tag{4.46}$$

We can now integrate out the heavy field, namely H. To achieve this we derive the Lagrangian in H and we obtain the associated equation of motion:

$$\begin{aligned}\frac{\partial \mathcal{L}}{\partial H} = 0 \Rightarrow H = \frac{1}{m_H^2} [& - \bar{d}_{Li} C^{H_d}_{ij} d_{Rj} - \bar{d}_{Rj} (C^{H_d}_{ji})^\dagger d_{Li} + \\ & - \bar{u}_{Li} C^{H_u}_{ij} u_{Rj} - \bar{u}_{Rj} (C^{H_u}_{ji})^\dagger u_{Li}] \, .\end{aligned} \tag{4.47}$$

After substituting back into eq. 4.46, the final result reads:

$$\begin{aligned}\mathcal{L}_{EFT} \supset + \frac{1}{2} \frac{1}{m_H^2} \Big[& \bar{d}_{Li} C^{H_d}_{ij} d_{Rj} + \bar{d}_{Rj} (C^{H_d}_{ji})^\dagger d_{Li} + \\ & + \bar{u}_{Li} C^{H_u}_{ij} u_{Rj} + \bar{u}_{Rj} (C^{H_u}_{ji})^\dagger u_{Li} \Big]^2 \, .\end{aligned} \tag{4.48}$$

4-fermion operators from A

With the same procedure, we find that the effective Lagrangian containing the 4-fermion operators relative to the A is:

$$\begin{aligned}\mathcal{L}_{EFT} \supset + \frac{1}{2} \frac{1}{m_A^2} \Big[& \bar{d}_{Li} (C^{Ad}_{ij}) d_{Rj} + \bar{d}_{Rj} (C^{Ad}_{ji})^+ d_{Li} \\ & + \bar{u}_{Li} C^{A_u}_{ij} u_{Rj} + \bar{u}_{Rj} (C^{A_u}_{ji})^\dagger u_{Li} \Big]^2 \, .\end{aligned} \tag{4.49}$$

4-fermion operators from $H^\pm$

The case of a complex scalar is slightly different, so we report here the intermediate steps explicitly. The starting Lagrangian is:

$$\begin{aligned}\mathcal{L} \supset & - \bar{d}_{Li} H^- V^*_{ki} C^{H_u^-}_{kj} u_{Rj} - \bar{d}_{Rj} (C^{H_d^+}_{jk})^\dagger V^*_{ik} H^- u_{Li} + \\ & - \bar{u}_{Li} H^+ V_{ik} C^{H_d^+}_{kj} d_{Rj} - \bar{u}_{Rj} (C^{H_u^-}_{jk})^\dagger V_{ki} H^+ d_{Li} - m^2_{H^\pm} H^+ H^-\end{aligned} \tag{4.50}$$

The equations of motion associated to each fields are:

$$\frac{\partial \mathcal{L}}{\partial H^-} = 0 \Rightarrow H^+ = - \frac{1}{m^2_{H^\pm}} [\bar{d}_{Li} V^*_{ki} C^{H_u^-}_{kj} u_{Rj} + \bar{d}_{Rj} V^*_{ik} (C^{H_d^+}_{jk})^\dagger u_{Li}] \tag{4.51}$$

$$\frac{\partial \mathcal{L}}{\partial H^+} = 0 \Rightarrow H^- = - \frac{1}{m^2_{H^\pm}} [\bar{u}_{Li} V_{ik} C^{H_d^+}_{kj} d_{Rj} + \bar{u}_{Rj} V_{ki} (C^{H_u^-}_{jk})^\dagger d_{Li}] \tag{4.52}$$

which are one the complex conjugate of the other. Hence, in terms of the quark bi-linear

$$\begin{aligned} B &= [\bar{d}_{Li} V^*_{ki} C^{H_u^-}_{kj} u_{Rj} + \bar{d}_{Rj} V^*_{ik} (C^{H_d^+}_{jk})^\dagger u_{Li}] \\ B^* &= [\bar{u}_{Li} V_{ik} C^{H_d^+}_{kj} d_{Rj} + \bar{u}_{Rj} V_{ki} (C^{H_u^-}_{jk})^\dagger d_{Li}] \ , \end{aligned} \tag{4.53}$$

the final effective Lagrangian reads:

$$\mathcal{L}_{EFT} \supset \frac{BB^*}{m^2_{H^\pm}} \ . \tag{4.54}$$

While we have focussed here just on quark fields, a similar procedure can of course be applied for charged leptons.

4.5.1 Coefficients of 4-fermion operators

We now collect the coefficients of the 4-fermion operators, by performing the square terms in eq. 4.48, 4.49 and 4.54. The most general effective Lagrangian including the possible 4-fermion operators obtained by integrating out the heavy fields of the 2HDM reads:

$$\begin{aligned} \mathcal{L}^{4-fermion}_{EFT} \supset & \left(C^{\bar{q}_L q_R \bar{q}'_L q'_R}_{ijkl} \bar{q}_{Li} q_{Rj} \bar{q}'_{Lk} q'_{Rl} + \text{h.c.} \right) + \\ & + \left(C^{\bar{q}_L q_R \bar{q}'_R q'_L}_{ijkl} \bar{q}_{Li} q_{Rj} \bar{q}'_{Rk} q'_{Ll} + \text{h.c.} \right) + \\ & + \left(C^{\bar{u}_L d_R \bar{d}_L u_R}_{ijkl} \bar{u}_{Li} d_{Rj} \bar{d}_{Lk} u_{Rl} + \text{h.c.} \right) + \\ & + \left(C^{\bar{u}_L d_R \bar{d}_R u_L}_{ijkl} \bar{u}_{Li} d_{Rj} \bar{d}_{Rk} u_{Ll} \right) + \\ & + \left(C^{\bar{d}_L u_R \bar{u}_R d_L}_{ijkl} \bar{d}_{Li} u_{Rj} \bar{u}_{Rk} d_{Ll} \right) \ , \end{aligned} \tag{4.55}$$

where q, q' stand either for u or d quarks.

Finally, the explicit expression for the 4-fermion coefficients is found to be:

$$
\begin{aligned}
C^{\bar{u}_L u_R \bar{u}_L u_R}_{ijkl} &= \frac{1}{2m_H^2} C^{H_u}_{ij} C^{H_u}_{kl} + \frac{1}{2m_A^2} C^{A_u}_{ij} C^{A_u}_{kl} \\
C^{\bar{d}_L d_R \bar{d}_L d_R}_{ijkl} &= \frac{1}{2m_H^2} C^{H_d}_{ij} C^{H_d}_{kl} + \frac{1}{2m_A^2} C^{A_d}_{ij} C^{A_d}_{kl} \\
C^{\bar{u}_R u_L \bar{u}_R u_L}_{jilk} &= \frac{1}{2m_H^2} (C^{H_u}_{ji})^\dagger (C^{H_u}_{lk})^\dagger + \frac{1}{2m_A^2} (C^{A_u}_{ji})^\dagger (C^{A_u}_{lk})^\dagger \\
C^{\bar{d}_R d_L \bar{d}_R d_L}_{jilk} &= \frac{1}{2m_H^2} (C^{H_d}_{ji})^\dagger (C^{H_d}_{lk})^\dagger + \frac{1}{2m_A^2} (C^{A_d}_{ji})^\dagger (C^{A_d}_{lk})^\dagger \\
C^{\bar{u}_L u_R \bar{d}_L d_R}_{ijkl} &= \frac{1}{m_H^2} C^{H_u}_{ij} C^{H_d}_{kl} + \frac{1}{m_A^2} C^{A_u}_{ij} C^{A_d}_{kl} \\
C^{\bar{u}_L u_R \bar{u}_R u_L}_{ijkl} &= \frac{1}{m_H^2} C^{H_u}_{ij} (C^{H_u}_{kl})^\dagger + \frac{1}{m_A^2} C^{A_u}_{ij} (C^{A_u}_{kl})^\dagger \\
C^{\bar{u}_L u_R \bar{d}_R d_L}_{ijkl} &= \frac{1}{m_H^2} C^{H_u}_{ij} (C^{H_d}_{kl})^\dagger + \frac{1}{m_A^2} C^{A_u}_{ij} (C^{A_d}_{kl})^\dagger \\
C^{\bar{d}_L d_R \bar{u}_R u_L}_{ijlk} &= \frac{1}{m_H^2} C^{H_d}_{ij} (C^{H_u}_{lk})^\dagger + \frac{1}{m_A^2} C^{A_d}_{ij} (C^{A_u}_{lk})^\dagger \\
C^{\bar{d}_L d_R \bar{d}_R d_L}_{ijlk} &= \frac{1}{m_H^2} C^{H_d}_{ij} (C^{H_d}_{lk})^\dagger + \frac{1}{m_A^2} C^{A_d}_{ij} (C^{A_d}_{lk})^\dagger \\
C^{\bar{d}_R d_L \bar{u}_R u_L}_{jilk} &= \frac{1}{m_H^2} (C^{H_d}_{ji})^\dagger (C^{H_u}_{lk})^\dagger + \frac{1}{m_A^2} (C^{A_d}_{ji})^\dagger (C^{A_u}_{lk})^\dagger \\
C^{\bar{d}_L u_R \bar{u}_L d_R}_{ijsr} &= \frac{1}{m_H^{\pm 2}} V^*_{ki} V_{sl} C^{H_u^-}_{kj} C^{H_d^+}_{lr} \\
C^{\bar{d}_L u_R \bar{u}_R d_L}_{ijsr} &= \frac{1}{m_H^{\pm 2}} V^*_{ki} V_{ls} C^{H_u^-}_{kj} (C^{H_u^-}_{rl})^\dagger \\
C^{\bar{d}_R u_L \bar{u}_L d_R}_{ijsr} &= \frac{1}{m_H^{\pm 2}} V^*_{ik} V_{sl} (C^{H_d^+}_{jk})^\dagger C^{H_d^+}_{lr} \\
C^{\bar{d}_R u_L \bar{u}_R d_L}_{ijsr} &= \frac{1}{m_H^{\pm 2}} V^*_{ik} V_{ls} (C^{H_d^+}_{jk})^\dagger (C^{H_u^-}_{rl})^\dagger \, .
\end{aligned}
\tag{4.56}
$$

Similar expressions can be obtained for 4-fermion operators involving lepton fields.

4.6 Comparison between low-energy and high-energy sources of CP violation

In the previous sections we have determined the flavour-violating axion couplings to SM fermions (see section 3.2.1) and the flavour-violating 4-fermion operators induced by the heavy radial modes of the 2HDM (see section 4.5.1). Note that these formulae are general, in the sense that they hold in any non-universal axion model and they depend from the flavour rotation matrices V_{u_L}, etc., and in the case of the axion couplings also from the PQ charge matrices as well as the axion decay constant, f_a, and in the case of the 4-fermion operators from the mass scale of the radial modes, $m_{H,A,H^\pm}$. The latter should be regarded as a free parameter which can be anywhere between the electroweak scale and f_a. On the other hand, in order to make some predictions we need to make further assumptions. First of all, we have considered a specific

non-universal axion model, denoted as M1 model and studied in detail in the present chapter. Moreover, we have done some assumptions on the flavour structure of the quark Yukawa matrices (see Appendix A.2), which basically correspond to trivial mixing in the up-quark sector and $V_{d_L} \simeq V_{\rm CKM}$.

We can now proceed to compare these two sources of flavour violation. For simplicity, we will focus on two observables involving $s \to d$ transitions, namely $K \to \pi a$ and K^0-$\bar{K}^0$ oscillations, which provide two of the most stringent constraints on the kind of scenarios considered in this thesis.

4.6.1 Constraints from $K \to \pi a$

As discussed in section 3.2.2, this kaon decay mode provides the strongest constraint on the coupling C^V_{sd}. The general expression of C^V is given in eq. 3.20, while the bound provided by this process is given in eq. 3.27, that we report here for convenience

$$|C^V_{sd}| < 2.9 \cdot 10^{-12} f_a(\text{GeV}) \, . \tag{4.57}$$

Since we have computed the expression of V_{d_R} and V_{d_L} which correspond respectively to the identity matrix and to $V_{d_L} \simeq V_{\rm CKM}$, we are now able to provide an explicit expression for C^V, defined in our model as $C^V = V^\dagger_{dL} \chi_{dL} V_{dL}$, which reads:

$$C^V = \begin{pmatrix} \lambda^6(1-\rho)^2 & -\lambda^5(1-\rho) & \lambda^3(1-\rho) \\ -\lambda^5(1-\rho) & \lambda^4 & -\lambda^2 \\ \lambda^3(1-\rho) & -\lambda^2 & 1 \end{pmatrix} \, . \tag{4.58}$$

The $K \to \pi a$ process corresponds to an $s \to d$ transition, that is proportional to the 12 element of the matrix above, and hence of order λ^5. Using $\lambda = 0.23$, we can translate the general constraint in eq. 4.57 in a bound on the axion decay constant (holding in our model)

$$f_a \gtrsim 10^9 \text{GeV} \, , \tag{4.59}$$

which is of the same order of the limits set by astrophysics (see section 2.1.3).

4.6.2 Constraints from K^0-$\bar{K}^0$ oscillations

K^0-$\bar{K}^0$ oscillations represent another example of a flavour-violating process involving $s \to d$ transitions, which are particularly relevant in the presence of 4-fermion operators. Fig. 4.1 represents the Feynman diagram for the K^0-$\bar{K}^0$ oscillation process within an EFT approach, where the 4-fermion structure is manifest. Following this approach, in order 2to determine the associated 4-fermion Wilson coefficient, mediated for instance by the CP-even field H, we need the numerical expression of the $\epsilon^d = V^\dagger_{dL} Y^d_2 V_{dR}$ matrix, defined by eq. 4.44. Actually, this is fully determined since $V_{dL} \simeq V_{\rm CKM}$, V_{dR} coincides with the product of eqs. A.20, A.24 and A.28, while the expression of Y^d_2 is defined in eq. 4.12. Since the oscillation involves down and strange quarks and, in particular

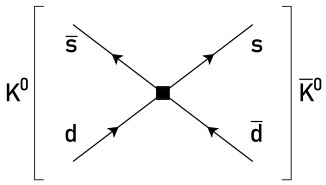

Figure 4.1: The 4-fermion Feynman diagram of K^0-$\bar{K}^0$ oscillations in a EFT approach.

it is described by $\langle K^0|\,\bar{s}d\bar{s}d\,|\bar{K^0}\rangle$, the associated bi-linear operator is (see eq. 4.42):

$$C_{21}^{H_d} = \epsilon_{21}^d \frac{s_{\alpha-\beta}}{c_\beta}\,, \tag{4.60}$$

where $\epsilon_{21}^d \simeq \dfrac{\sqrt{2}m_d\lambda^3}{vs_\beta}$. The Wilson coefficient of the $\bar{s}d\bar{s}d$ 4-fermion operator can be read off the second line in eq. 4.56, where we focus on the H contribution. Hence, we obtain:

$$C_{2121}^{\bar{s}d\bar{s}d} = \left(\frac{m_d}{v}\right)^2 \frac{1}{2m_H^2}\left(\frac{\lambda^3}{s_\beta}\frac{s_{\alpha-\beta}}{c_\beta}\right)^2 \sim \left(\frac{10^{-7}}{m_H}\right)^2\,, \tag{4.61}$$

where we have taken $\mathcal{O}(1)$ trigonometrical functions. Note, however, that in some specific limits the trigonometrical functions might act either as a suppression or enhancement factor. Nevertheless, since our discussion here is somewhat qualitative we will not consider this extra model dependency.

Constraints on the Wilson coefficients, arising from flavour-violating 4-fermion operators, have been derived for instance in Ref. [82]. In the case of K^0-$\bar{K}^0$ oscillations, for the specific operator discussed above, one finds

$$C_{2121}^{\bar{s}d\bar{s}d} \lesssim \left(\frac{1}{10^7\text{GeV}}\right)^2\,, \tag{4.62}$$

which in turn implies

$$m_H \gtrsim 1\text{GeV}\,. \tag{4.63}$$

Strictly speaking this bound is not applicable since the EFT approach implicitly assumes $m_H \gtrsim v$ (which is also phenomenologically required by LHC bounds on the mass scale of the 2HDM). On the other hand, we can conclude that K^0-$\bar{K}^0$ oscillations do not pose an important constraint on the scenario under consideration. Note, however, that this conclusion is strongly dependent on the particular flavour ansatz that we did for the Yukawa matrices, yielding to the suppression factor $(\epsilon^d)^2 \sim (m_d\lambda^3/v)^2$ in the Wilson coefficient of the 4-fermion operator. In more general cases the entries of the rotation matrices can be of $\mathcal{O}(1)$ and hence the constraining power of flavour observables can reach up to $m_H \sim 10^7$ GeV.

Chapter 5

Conclusions

In this thesis, we have studied the interplay between different sources of flavour violation in non-universal axion models, arising both from low-energy (flavour-violating axion couplings) and high-energy dynamics (flavour-violating couplings of the radial modes present in UV complete models). The former type of flavour violation was well studied in the literature, and it is usually approached from an EFT point of view in which one writes the most general effective axion Lagrangian coupling to SM fermions (see eq. 3.19) and sets bounds on the couplings from a series of flavour observables, such as e.g. $K \to \pi a$, involving the axion field. On the other hand, UV completions for flavour-violating axion effective Lagrangians arise in models where the PQ charges are non-universal and, as discussed in this thesis, such constructions can be interesting in several respects. General motivations for non-universal axion models include a potential connection with the SM flavour puzzle, and the possibility of relaxing standard astrophysical axion bounds.

Within a specific class of UV completions, based on the same field content of the standard DFSZ model, but with different types of Higgs doublets coupling to different generations of quarks and leptons (see e.g. eq. 4.1), it turns out that the heavy degrees of freedom of the 2HDM, namely the radial modes $H, A, H^{\pm}$, have in general flavour-violating Yukawa couplings to the SM fermions. Hence, after integrating out these heavy degrees of freedom one generates flavour-violating 4-fermion operators, with a different pattern of flavour violation compared to the axion-induced one.

The main objective of this thesis was to investigate this latter type of flavour violation within a specific non-universal axion model (denoted as M1 model) that was analysed in detail in Chapter 4, which also represents the original contribution of the present thesis. In particular, we have computed the spectrum of the model and diagonalized both the scalar and fermion sector, a preliminary step in order to integrate out the heavy radial modes of the 2HDM and obtain the associated 4-fermion operators.

Not surprisingly, one finds that the two sources of flavour violation discussed above are in general decorrelated, basically for two reasons: first, the axion induced processes scale like $1/f_a$, while the radial modes induced ones scale like $1/m_{H,A,H^{\pm}}$. In general the scale of the 2HDM is a free parameter which is phenomenologically and theoretically bounded to be above the electroweak scale and below f_a. The second reason has to

do with a degeneracy in flavour space, since the rotation angles entering the diagonalizing matrices V_{u_L}, etc., are basically unconstrained (but for the combination which determine the CKM matrix). Hence, it should be clear that extra assumptions need to be made in order to highlight a possible correlation between the two different sources of flavour violation.

To this end, we have further assumed that the structure of the quark Yukawas are such that $V_{u_L} \simeq 1$ and $V_{d_L} \simeq V_{\rm CKM}$, so that the quark flavour coefficients turn out to be all fixed within the M1 model. This flavour ansatz provides a high level of flavour protection and represents the size of minimal flavour violation that is expected in order to reproduce the CKM. Within these flavour assumptions, and taking as an example $s \to d$ transitions which provide very stringent constraints, one finds that axion-mediated flavour violation implies $f_a \gtrsim 10^9$ GeV (still competitive with astrophysical bounds), while flavour violation mediated by the radial modes implies $m_{H,A,H^\pm} \gtrsim 1$ GeV. The latter result (based on a simple estimate) suggests that in the most flavour-protected scenario flavour-violating processes are not competitive with direct searches of the 2HDM at the LHC. However, relaxing the stringent flavour hypothesis $V_{d_L} \simeq V_{\rm CKM}$, and allowing instead for $\mathcal{O}(1)$ mixing angles in the down sector pushes the reach of flavour observables on the scale of the 2HDM up to $m_{H,A,H^\pm} \sim 10^7$ GeV.

To conclude, we remark that this thesis work provides only a first explorative study and it can be extended in several respects. For instance, from a model-independent point of view one should consider a more general class of flavour observables giving constraints an all possible 4-fermion operators (including semi-leptonic and 4-lepton ones). While from a model-dependent point of view other non-universal axion models and flavour ansatz should be considered, in order to classify the patterns of flavour violation which might complementary emerge from an axion discovery in low-energy flavour-violating processes and the correlated signals in other flavour observables, which might help in reconstructing the UV theory.

Appendix A

Perturbative diagonalization of Yukawa matrices

A.1 Bi-unitary transformations for a 3×3 matrix

A general 3×3 matrix can be diagonalized through a bi-unitary transformation. We will follow here the derivation in Ref. [83], in the case of small rotations which can be dealt with in perturbation theory. Let us consider a matrix Y, then we will have $Y_{diag} = U'YU$ where U' and U are two unitary matrices. In particular, we will consider for simplicity the case of real parameters, which corresponds to orthogonal transformations. Let us define the initial matrix Y and the final matrix Y^{diag} respectively as:

$$Y = \begin{pmatrix} y_{11} & y_{12} & y_{13} \\ y_{21} & y_{22} & y_{23} \\ y_{31} & y_{32} & y_{33} \end{pmatrix} \quad , \quad Y^{diag} = \begin{pmatrix} \tilde{\tilde{y}}_{11} & 0 & 0 \\ 0 & \tilde{y}_{22} & 0 \\ 0 & 0 & y_{33} \end{pmatrix} \tag{A.1}$$

We will perform different rotations for each sectors, as indicated by the subscript of the matrix elements. The first rotation is performed in "23" sector, the second one in "13" sector and the last one involves sector "12". The diagonalization reads (note that we keep only the sin since we are working under the assumption of small angles):

$$\begin{aligned} Y^{diag} = & \begin{pmatrix} 1 & -s_{12} & 0 \\ s_{12} & 0 & \\ 0 & 0 & 1 \end{pmatrix} \begin{pmatrix} 1 & 0 & -s_{13} \\ 0 & 1 & 0 \\ s_{13} & 0 & 1 \end{pmatrix} \begin{pmatrix} 1 & 0 & 0 \\ 0 & 1 & -s_{23} \\ 0 & s_{23} & 1 \end{pmatrix} Y \cdot \\ & \cdot \begin{pmatrix} 1 & 0 & 0 \\ 0 & 1 & s'_{23} \\ 0 & -s'_{23} & 1 \end{pmatrix} \begin{pmatrix} 1 & 0 & s'_{13} \\ 0 & 1 & 0 \\ -s'_{13} & 0 & 1 \end{pmatrix} \begin{pmatrix} 1 & s'_{12} & 0 \\ -s'_{12} & 1 & 0 \\ 0 & 0 & 1 \end{pmatrix} \end{aligned} \tag{A.2}$$

The different angles can be found by solving three different systems, one for each rotation, where we constrain the off-diagonal term to be zero. Moreover, after each rotation each element of the matrix will be influenced by the operator that has been applied to it. Note that the one tilde symbol $\tilde{}$ indicates a given element after one rotation, while a double tilde symbol $\tilde{\tilde{}}$ indicates that a given element has been subjected to a double rotation. The following results are truncated at $\mathcal{O}(s^2)$.

Rotation in sector "23"

After the rotation in sector "23" we obtain the following matrix:

$$\begin{pmatrix} y_{11} & y_{12} - s'_{23}y_{13} & s'_{23}y_{12} + y_{13} \\ y_{21} - s_{23}y_{31} & y_{22} - s'_{23}y_{23} - s_{23}y_{32} & s'_{23}y_{22} + y_{23} + s_{23}y_{33} \\ s_{23}y_{21} + y_{31} & s_{23}y_{22} - s'_{23}y_{33} + y_{32} & s_{23}y_{23} + s'_{23}y_{32} + y_{33} \end{pmatrix} + \mathcal{O}(s^2) \ . \tag{A.3}$$

Now we set the off diagonal term in the sector considered to be zero with the following system:

$$\begin{cases} s_{23}y_{22} - s'_{23}y_{33} + y_{32} = 0 \\ s'_{23}y_{22} + y_{23} - s_{23}y_{33} = 0 \end{cases} \ , \tag{A.4}$$

which in turn gives the first rotation angles:

$$s_{23} \simeq \frac{y_{23}}{y_{33}} + \frac{y_{32}y_{22}}{y_{33}^2} \qquad\qquad s'_{23} \simeq \frac{y_{32}}{y_{33}} + \frac{y_{23}y_{22}}{y_{33}^2} \tag{A.5}$$

After this first rotation, the different elements of the matrix become:

$$\tilde{y}_{12} = y_{12} - y_{13}s'_{23} \qquad\qquad \tilde{y}_{21} = y_{21} - y_{31}s_{23} \tag{A.6}$$

$$\tilde{y}_{13} = y_{13} + y_{12}s'_{23} \qquad\qquad \tilde{y}_{31} = y_{31} + y_{21}s_{23} \tag{A.7}$$

$$\tilde{y}_{22} \simeq y_{22} - \frac{2y_{23}y_{32}}{y_{33}} \ . \tag{A.8}$$

Rotation in sector "13"

Now the matrix which we have to rotate in sector "13" is the one obtained from the rotation of the previous sector. In particular, the matrix after this second rotation reads:

$$\begin{pmatrix} y_{11} - \tilde{y}_{13}y_{13}\prime - \tilde{y}_{31}s_{13} & \tilde{y}_{12} & s'_{13}y_{11} + \tilde{y}_{13} - s_{13}y_{33} \\ \tilde{y}_{21} & \tilde{y}_{22} & s'_{13}\tilde{y}_{21} \\ y_{11}s_{13} + \tilde{y}_{31} - s'_{13}y_{33} & \tilde{y}_{12}s_{13} & s_{13}\tilde{y}_{13} + s'_{13}\tilde{y}_{31} + y_{33} \end{pmatrix} + \mathcal{O}(s^2) \ . \tag{A.9}$$

To impose the diagonalization we set

$$\begin{cases} s'_{13}y_{11} + \tilde{y}_{13} - s_{13}y_{33} = 0 \\ y_{11}s_{13} + \tilde{y}_{31} - s'_{13}y_{33} = 0 \end{cases} \tag{A.10}$$

which gives the following rotation angles:

$$s_{13} \simeq \frac{\tilde{y}_{13}}{y_{33}} + \frac{\tilde{y}_{31} y_{11}}{y_{33}^2} \qquad s'_{13} \simeq \frac{\tilde{y}_{31}}{y_{33}} + \frac{\tilde{y}_{13} y_{11}}{y_{33}^2} \tag{A.11}$$

After this rotation the only new relevant term, up to higher orders, is:

$$\tilde{y}_{11} \simeq \tilde{y}_{11} - \frac{2\tilde{y}_{13}\tilde{y}_{31}}{\tilde{y}_{33}} \, . \tag{A.12}$$

Rotation in sector "12"

The final rotation is performed in sector "12" and the matrix is:

$$\begin{pmatrix} y_{11} - s'_{12}\tilde{y}_{12} - s_{12}\tilde{y}_{21} & \tilde{y}_{12} + s'_{12}\tilde{y}_{11} - s_{12}\tilde{y}_{22} & 0 \\ \tilde{y_{11}} s_{12} + \tilde{y}_{12} - s'_{12}\tilde{y}_{22} & s_{12}\tilde{y}_{12} + \tilde{y}_{22} s'_{12}\tilde{y}_{21} & 0 \\ 0 & 0 & y_{33} \end{pmatrix} + \mathcal{O}(s^2) \, . \tag{A.13}$$

Again, imposing the off-diagonal term to be zero we have

$$\begin{cases} \tilde{y}_{12} + s'_{12}\tilde{y}_{11} - s_{12}\tilde{y}_{22} = 0 \\ \tilde{y_{11}} s_{12} + \tilde{y}_{12} - s'_{12}\tilde{y}_{22} = 0 \end{cases} \tag{A.14}$$

which gives:

$$s_{12} \simeq \frac{\tilde{y}_{12}}{\tilde{y}_{22}} + \frac{\tilde{y}_{21}\tilde{y}_{11}}{\tilde{y}_{22}^2} \qquad s'_{12} \simeq \frac{\tilde{y}_{21}}{\tilde{y}_{22}} + \frac{\tilde{y}_{12}\tilde{y}_{11}}{\tilde{y}_{22}^2} \tag{A.15}$$

Finally the only relevant term which change in this rotation is

$$\tilde{\tilde{y}}_{11} \simeq \tilde{y}_{11} - \frac{2\tilde{y}_{12}\tilde{y}_{21}}{y_{22}} \, . \tag{A.16}$$

A.2 Yukawa sector diagonalization

We now apply the previously derived formula to the case relevant for the M1 model discussed in chapter 4, that is for the diagonalization of the matrix

$$M_d = \begin{pmatrix} m_d & \lambda m_s & \rho\lambda^3 m_b \\ 0 & m_s & \lambda^2 m_b \\ 0 & 0 & m_b \end{pmatrix} , \tag{A.17}$$

Let us discuss in turn the perturbative diagonalization in each sector, following the same steps as before. The first rotation in sector "23" is performed by:

$$s_{23} \simeq \lambda^2, \qquad s'_{23} \simeq \lambda^2 \frac{m_s}{m_b} \tag{A.18}$$

which gives the rotation matrices:

$$V_{23L}^{\dagger} = \begin{pmatrix} 1 & 0 & 0 \\ 0 & 1 & -\lambda^2 \\ 0 & \lambda^2 & 1 \end{pmatrix} , \tag{A.19}$$

$$V_{23R} = \begin{pmatrix} 1 & 0 & 0 \\ 0 & 1 & \lambda^2 \dfrac{m_s}{m_b} \\ 0 & -\lambda^2 \dfrac{m_s}{m_b} & 1 \end{pmatrix} . \tag{A.20}$$

After this firs rotation we get:

$$\tilde{M}_d = \begin{pmatrix} m_d & \lambda m_s(1-\lambda^4) & \lambda^3 m_t \left(\rho + \dfrac{m_s^2}{m_b^2}\right) \\ 0 & m_s & 0 \\ 0 & 0 & m_b \end{pmatrix} . \tag{A.21}$$

The second rotation diagonalizes the sector "13" and yields the following angles:

$$s_{13} \simeq \lambda^3 \left(\rho + \frac{m_s^2}{m_b^2}\right), \qquad s'_{13} \simeq \lambda^3 \frac{m_d}{m_b} \left(\rho + \frac{m_s^2}{m_b^2}\right) \tag{A.22}$$

with the associated rotation matrices:

$$V_{13L}^{\dagger} = \begin{pmatrix} 1 & 0 & -\lambda^3 \left(\rho + \dfrac{m_s^2}{m_b^2}\right) \\ 0 & 1 & 0 \\ \lambda^3 \left(\rho + \dfrac{m_s^2}{m_b^2}\right) & 0 & 1 \end{pmatrix} , \tag{A.23}$$

$$V_{13R} = \begin{pmatrix} 1 & 0 & \lambda^3 \dfrac{m_d}{m_b} \left(\rho + \dfrac{m_s^2}{m_b^2}\right) \\ 0 & 1 & 0 \\ -\lambda^3 \dfrac{m_d}{m_b} \left(\rho + \dfrac{m_s^2}{m_b^2}\right) & 0 & 1 \end{pmatrix} . \tag{A.24}$$

The matrix obtained after the second diagonalization reads

$$\tilde{\tilde{M}}_d = \begin{pmatrix} m_d & \lambda_{m_s}(1-\lambda^4) & 0 \\ 0 & m_s & 0 \\ 0 & 0 & m_b \end{pmatrix} . \tag{A.25}$$

The last rotation affects the sector "12" with angles

$$s_{12} \simeq \lambda(1-\rho\lambda^4), \qquad s'_{12} \simeq \lambda \frac{m_d}{m_s} \left(1 - \rho\lambda^4\right) \tag{A.26}$$

and rotation matrices

$$V_{12L}^{\dagger} = \begin{pmatrix} 1 & -\lambda(1-\rho\lambda^4) & 0 \\ \lambda(1-\rho\lambda^4) & 1 & 0 \\ 0 & 0 & 1 \end{pmatrix} , \tag{A.27}$$

$$V_{12R} = \begin{pmatrix} 1 & \lambda\frac{m_d}{m_s}\left(1-\rho\lambda^4\right) & 0 \\ -\lambda\frac{m_d}{m_s}\left(1-\rho\lambda^4\right) & 1 & 0 \\ 0 & 0 & 1 \end{pmatrix} . \tag{A.28}$$

After the combination of all the rotations we obtain the diagonal matrix:

$$M_d = \begin{pmatrix} m_d & 0 & 0 \\ 0 & m_s & 0 \\ 0 & 0 & m_b \end{pmatrix} . \tag{A.29}$$

The final left handed rotation matrix reads

$$V_{CKM} = V_{dL} \simeq \begin{pmatrix} 1 & \lambda & \rho\lambda^3 \\ -\lambda & 1 & \lambda^2 \\ \lambda^3(1-\rho) & -\lambda^2 & 1 \end{pmatrix} , \tag{A.30}$$

matching in a proper way the CKM matrix.

Appendix B

The two Higgs doublet model

The 2HDM model is an extension of the SM based on two Higgs doublets. For a review see e.g. Ref. [84]; we will here focus only on the calculation of the mass spectrum. Let us introduce two $SU(2)_L$ scalar doublets H_1' and H_2', with quantum number $\sim (1, 2, \frac{1}{2})$. We define the fields in the following way:

$$H_1' = \begin{pmatrix} h_1' \\ \dfrac{v_1' + h_{01}' + i\eta_1'}{\sqrt{2}} \end{pmatrix} \qquad H_2' = \begin{pmatrix} h_2' \\ \dfrac{v_2' + h_{02}' + i\eta_2'}{\sqrt{2}} \end{pmatrix}. \tag{B.1}$$

We can now define the most general gauge invariance potential as:

$$\begin{aligned} V_{2HDM} =& m_{11}^2 H_1'^\dagger H_1' + m_{22}^2 H_2'^\dagger H_2' - m_{12}^2 (H_1'^\dagger H_2' + H_2'^\dagger H_1') + \\ &+ \frac{1}{2}\lambda_1 (H_1'^\dagger\ H_1')^2 + \frac{1}{2}\lambda_2 (H_2'^\dagger H_2')^2 + \\ &+ \lambda_3 (H_1'^\dagger H_1')(H_2'^\dagger H_2') + \lambda_4 (H_1'^\dagger H_2')(H_2'^\dagger H_1') + \\ &+ \frac{1}{2}\lambda_5 [(H_1'^\dagger H_2')^2 + (H_2'^\dagger H_1')^2] + \\ &+ \lambda_6 [(H_1'^\dagger H_1')(H_1'^\dagger H_2') + (H_1'^\dagger H_1')(H_2'^\dagger H_1')] + \\ &+ \lambda_7 [(H_2'^\dagger H_2')(H_1'^\dagger H_2') + (H_2'^\dagger H_2')(H_2'^\dagger H_1')] \end{aligned} \tag{B.2}$$

where the minus sign in front of m_{12} is just a convention. Even if some coefficients such as λ_5, λ_6 and λ_7 could be complex, we will assume from now on that they are real. This assumption corresponds to ignore possible effects due to CP-violation [84]. Moreover, if we impose a discrete symmetry $\Phi_1 \to -\Phi_1$ one can get rid of the m_{12} parameter, that is $m_{12} = 0$. In this work, we will consider $m_{12} \neq 0$ to maintain a good level of generality.

The VEVs of these new fields are defined as:

$$\langle H_1' \rangle = \frac{1}{\sqrt{2}} \begin{pmatrix} 0 \\ v_1' \end{pmatrix} \qquad \langle H_2' \rangle = \frac{1}{\sqrt{2}} \begin{pmatrix} 0 \\ v_2' \end{pmatrix}. \tag{B.3}$$

It can be seen that this particular definition of VEVs satifies some constraints. The electric charge matrix Q is defined with the first element different from zero, then, in this way, the only possibility not to break the symmetry is to define the VEV in the second entry. On the other hand, to conserve CP symmetry we have to select v_i to be real. Another approach, in which CP violation is employed, can be found in [85]. In the following, we assume that the vacuum does not break spontaneously electromagnetism and CP.

B.1 Scalar spectrum

In order to derive the stationary conditions, it is convenient to define some quantities as follow:

$$\lambda_{345} \equiv \lambda_3 + \lambda_4 + \lambda_5 \qquad v^2 \equiv v_1'^2 + v_2'^2 \qquad \tan\beta \equiv \frac{v_2'}{v_1'}. \tag{B.4}$$

Note that if v_1' and v_2' are positive, $0 \leq \beta \leq \pi/2$. Moreover, from now on, we will use the shorthand notation $s_\beta \equiv \sin\beta$, $c_\beta \equiv \cos\beta$ etc.

Through the computation of the potential minimum we obtain the following conditions:

$$m_{11}^2 = m_{12}^2 t_\beta - \frac{1}{2}v^2[\lambda_1 c_\beta^2 + 3\lambda_6 c_\beta s_\beta + s_\beta^2(\lambda_{345} + \lambda_7 t_\beta)], \tag{B.5}$$

$$m_{22}^2 = m_{12}^2 cot_\beta - \frac{1}{2}v^2[\lambda_2 s_\beta^2 + 3\lambda_7 c_\beta s_\beta + c_\beta^2(\lambda_{345} + \lambda_6 cot_\beta)]. \tag{B.6}$$

Before going further, it is useful to discuss how the degrees of freedom (dof) are modified after a spontaneous symmetry breaking. The two original complex fields Φ_1 and Φ_2 carry eight real dof. As it happens in the SM, three of them are eaten up by $W^\pm$ and Z gauge bosons. The remaining five dof correspond to a charged Higgs (particle and an antiparticle denoted by $H^\pm$), one CP-odd scalar (denoted by A), two CP-even scalar (denoted by h and H). Notice that h correspond to the SM Higgs boson, as opposed to H which is a heavier companion of the Higgs.

The elements of the different mass matrices can be computed through the second derivative of the potential evaluated on the stationary points. It is possible to define three different mass matrix squared, one for each type of scalar particle present in the theory. In detail, the mass matrix squared corresponding to the charged scalar particles $H^\pm$ is:

$$\begin{pmatrix} m_{12}^2 t_\beta - \frac{1}{2}v^2 s_\beta(c_\beta\lambda_6 + s_\beta(\lambda_4 + \lambda_5 + \lambda_7 t_\beta)) \\ -2m_{12}^2 + \frac{1}{2}v^2(c_\beta s_\beta(\lambda_4 + \lambda_5) + c_\beta^2\lambda_6 + v^2 s_\beta^2\lambda_7) \\ -2m_{12}^2 + \frac{1}{2}v^2(c_\beta s_\beta(\lambda_4 + \lambda_5) + c_\beta^2\lambda_6 + v^2 s_\beta^2\lambda_7)) \\ m_{12}^2 cot_\beta - \frac{1}{2}v^2 c_\beta\lambda_7 s_\beta + (c_\beta(\lambda_4 + \lambda_5 + \lambda_6 cot_\beta)) \end{pmatrix}. \tag{B.7}$$

The mass matrix squared which describes the pseudo-scalar particles η_1 and η_2 is:

$$\begin{pmatrix} m_{12}^2 t_\beta - \frac{1}{2}v^2 s_\beta^2(2\lambda_5 + \lambda_6 cot_\beta + \lambda_7 t_\beta & \\ -m_{12}^2 + \frac{1}{2}v^2(\lambda_5 s_{2\beta} + \lambda_6 c_\beta^2 + \lambda_7 s_\beta^2) & \\ & -m_{12}^2 + \frac{1}{2}v^2(\lambda_5 s_{2\beta} + \lambda_6 c_\beta^2 + \lambda_7 s_\beta^2) \\ & m_{12}^2 cot_\beta - \frac{1}{2}v^2 c_\beta^2(2\lambda_5 + \lambda_6 cot_\beta + \lambda_7 t_\beta) \end{pmatrix}. \quad \text{(B.8)}$$

And finally the neutral scalar particles mass matrix, associated to h_{01} and h_{02} is:

$$\begin{pmatrix} m_{12}^2 t_\beta + \frac{1}{2}v^2 s_\beta^2(2\lambda_1 cot_\beta^2 + 3\lambda_6 cot_\beta - \lambda_7 t_\beta)) & \\ m_{12}^2 + \frac{1}{2}v^2(\lambda_{345} s_{2\beta} + 3\lambda_6 c_\beta^2 + 3\lambda_7 s_\beta^2) & \\ & m_{12}^2 + \frac{1}{2}v^2(\lambda_{345} s_{2\beta} + 3\lambda_6 c_\beta^2 + 3\lambda_7 s_\beta^2) \\ & m_{12}^2 cot_\beta + \frac{1}{2}v^2 c_\beta^2(2\lambda_2 t_\beta^2 + 3\lambda_7 t_\beta - \lambda_6 cot_\beta) \end{pmatrix}. \quad \text{(B.9)}$$

Respectively from B.7 and B.8 we obtain, upon diagonalization, the squared masses for the charged and the neutral CP-odd states:

$$m_{H^\pm}^2 = \frac{m_{12}}{c_\beta s_\beta} - \frac{1}{2}v^2(\lambda_4 + \lambda_5 + \lambda_6 cot_\beta + \lambda_7 t_\beta), \quad \text{(B.10)}$$

$$m_A^2 = \frac{m_{12}}{c_\beta s_\beta} - \frac{1}{2}v^2(2\lambda_5 + \lambda_6 cot_\beta + \lambda_7 t_\beta). \quad \text{(B.11)}$$

Notice that in both matrices one eigenvalue is zero: this is expected since one of the two eigenvalues represent the mass of the would-be Goldstone bosons associated to the W and the Z.

The masses of the CP-even states can be computed from B.9. It is convenient to notice that the neutral mass matrix is define in terms of m_A as:

$$M^2 \equiv m_A^2 \begin{pmatrix} s_\beta^2 & -s_\beta c_\beta \\ -s_\beta c_\beta & c_\beta^2 \end{pmatrix} + B^2 \quad \text{(B.12)}$$

where B^2 is defined as:

$$B^2 \equiv v^2 \begin{pmatrix} \lambda_1 c_\beta^2 + 2\lambda_6 s_\beta c_\beta + \lambda_5 s_\beta^2 & (\lambda_3 + \lambda_4) c_\beta s_\beta + \lambda_6 c_\beta^2 + \lambda_7 s_\beta^2 \\ (\lambda_3 + \lambda_4) c_\beta s_\beta + \lambda_6 c_\beta^2 + \lambda_7 s_\beta^2 & \lambda_2 s_\beta^2 + 2\lambda_7 s_\beta c_\beta + \lambda_5 c_\beta^2 \end{pmatrix} \quad \text{(B.13)}$$

We can diagonalize it using a 2D rotation with of angle α, defined as $m_{diag}^2 = R^{-1} M^2 R$, from which one gets the following CP-even squared mass in terms of the elements of B.12:

$$m_{H,h} = \frac{1}{2}\left(M_{11}^2 + M_{22}^2 \pm \sqrt{(M_{11}^2 - M_{22}^2)^2 + 4(M_{12}^2)^2} \right) \quad \text{(B.14)}$$

Notice that the heaviest eigenvalue corresponds to the mass of H, while the lightest one corresponds to the SM Higgs boson. Finally, the rotation angle, α, is given by

$$\begin{aligned} \sin 2\alpha &= \frac{2M_{12}^2}{\sqrt{(M_{11}^2 - M_{22}^2)^2 + 4(M_{12}^2)^2}} \ , \\ \cos 2\alpha &= \frac{M_{11}^2 - M_{22}^2}{\sqrt{(M_{11}^2 - M_{22}^2)^2 + 4(M_{12}^2)^2}} \ . \end{aligned} \tag{B.15}$$

Bibliography

[1] R. D. Peccei and H. R. Quinn, "CP conservation in the presence of pseudoparticles," *Phys. Rev. Lett.* **38** (Jun, 1977) 1440–1443. https://link.aps.org/doi/10.1103/PhysRevLett.38.1440.

[2] R. D. Peccei and H. R. Quinn, "Constraints imposed by CP conservation in the presence of pseudoparticles," *Phys. Rev. D* **16** (Sep, 1977) 1791–1797. https://link.aps.org/doi/10.1103/PhysRevD.16.1791.

[3] S. Weinberg, "A new light boson?," *Phys. Rev. Lett.* **40** (Jan, 1978) 223–226. https://link.aps.org/doi/10.1103/PhysRevLett.40.223.

[4] F. Wilczek, "Problem of strong p and t invariance in the presence of instantons," *Phys. Rev. Lett.* **40** (Jan, 1978) 279–282. https://link.aps.org/doi/10.1103/PhysRevLett.40.279.

[5] J. Preskill, M. B. Wise, and F. Wilczek, "Cosmology of the Invisible Axion," *Phys. Lett. B* **120** (1983) 127–132.

[6] L. F. Abbott and P. Sikivie, "A Cosmological Bound on the Invisible Axion," *Phys. Lett. B* **120** (1983) 133–136.

[7] M. Dine and W. Fischler, "The Not So Harmless Axion," *Phys. Lett. B* **120** (1983) 137–141.

[8] J. E. Kim, "Weak-interaction singlet and strong CP invariance," *Phys. Rev. Lett.* **43** (Jul, 1979) 103–107. https://link.aps.org/doi/10.1103/PhysRevLett.43.103.

[9] M. Shifman, A. Vainshtein, and V. Zakharov, "Can confinement ensure natural cp invariance of strong interactions?," *Nuclear Physics B* **166** no. 3, (1980) 493–506. https://www.sciencedirect.com/science/article/pii/0550321380902096.

[10] A. R. Zhitnitsky, "On Possible Suppression of the Axion Hadron Interactions. (In Russian)," *Sov. J. Nucl. Phys.* **31** (1980) 260.

[11] M. Dine, W. Fischler, and M. Srednicki, "A simple solution to the strong cp problem with a harmless axion," *Physics Letters B* **104** no. 3, (1981) 199–202. https://www.sciencedirect.com/science/article/pii/0370269381905906.

[12] L. Di Luzio, F. Mescia, E. Nardi, P. Panci, and R. Ziegler, "Astrophobic Axions," *Phys. Rev. Lett.* **120** no. 26, (2018) 261803, arXiv:1712.04940 [hep-ph].

[13] F. Wilczek, "Axions and family symmetry breaking," *Phys. Rev. Lett.* **49** (Nov, 1982) 1549–1552. https://link.aps.org/doi/10.1103/PhysRevLett.49.1549.

[14] M. Badziak, G. G. di Cortona, M. Tabet, and R. Ziegler, "Flavor-violating Higgs decays and stellar cooling anomalies in axion models," *JHEP* **10** (2021) 181, arXiv:2107.09708 [hep-ph].

[15] C. Abel *et al.*, "Measurement of the Permanent Electric Dipole Moment of the Neutron," *Phys. Rev. Lett.* **124** no. 8, (2020) 081803, arXiv:2001.11966 [hep-ex].

[16] J. E. Kim, "Weak Interaction Singlet and Strong CP Invariance," *Phys. Rev. Lett.* **43** (1979) 103.

[17] J. Jaeckel and A. Ringwald, "The Low-Energy Frontier of Particle Physics," *Annual Review of Nuclear and Particle Science* **60** (Nov., 2010) 405–437, arXiv:1002.0329 [hep-ph].

[18] S. Weinberg, "The u(1) problem," *Phys. Rev. D* **11** (Jun, 1975) 3583–3593. https://link.aps.org/doi/10.1103/PhysRevD.11.3583.

[19] S. Weinberg, *The quantum theory of fields. Vol. 2: Modern applications*. Cambridge University Press, 8, 2013.

[20] G. 't Hooft, "How instantons solve the u(1) problem," *Physics Reports* **142** no. 6, (1986) 357–387. https://www.sciencedirect.com/science/article/pii/0370157386901171.

[21] G. 't Hooft, "Symmetry breaking through bell-jackiw anomalies," *Phys. Rev. Lett.* **37** (Jul, 1976) 8–11. https://link.aps.org/doi/10.1103/PhysRevLett.37.8.

[22] E. B. Bogomolny, "Stability of Classical Solutions," *Sov. J. Nucl. Phys.* **24** (1976) 449.

[23] T. Schäfer and E. V. Shuryak, "Instantons in QCD," *Rev. Mod. Phys.* **70** (1998) 323–426, arXiv:hep-ph/9610451.

[24] G. 't Hooft, "Computation of the quantum effects due to a four-dimensional pseudoparticle," *Phys. Rev. D* **14** (Dec, 1976) 3432–3450. https://link.aps.org/doi/10.1103/PhysRevD.14.3432.

[25] C. Callan, R. Dashen, and D. Gross, "The structure of the gauge theory vacuum," *Physics Letters B* **63** no. 3, (1976) 334–340. https://www.sciencedirect.com/science/article/pii/037026937690277X.

[26] A. Belavin, A. Polyakov, A. Schwartz, and Y. Tyupkin, "Pseudoparticle solutions of the yang-mills equations," *Physics Letters B* **59** no. 1, (1975) 85–87. https://www.sciencedirect.com/science/article/pii/037026937590163X.

[27] H. Leutwyler, "Chiral perturbation theory," *Scholarpedia* **7** no. 10, (2012) 8708. revision #138476.

[28] K. Fujikawa, "Path-integral measure for gauge-invariant fermion theories," *Phys. Rev. Lett.* **42** (Apr, 1979) 1195–1198. https://link.aps.org/doi/10.1103/PhysRevLett.42.1195.

[29] C. Vafa and E. Witten, "Parity conservation in quantum chromodynamics," *Phys. Rev. Lett.* **53** (Aug, 1984) 535–536. https://link.aps.org/doi/10.1103/PhysRevLett.53.535.

[30] C. Vafa and E. Witten, "Restrictions on symmetry breaking in vector-like gauge theories," *Nuclear Physics B* **234** no. 1, (1984) 173–188. https://www.sciencedirect.com/science/article/pii/055032138490230X.

[31] A. Hook, "TASI Lectures on the Strong CP Problem and Axions," *PoS* **TASI2018** (2019) 004, arXiv:1812.02669 [hep-ph].

[32] V. Baluni, "CP-nonconserving effects in quantum chromodynamics," *Phys. Rev. D* **19** (Apr, 1979) 2227–2230. https://link.aps.org/doi/10.1103/PhysRevD.19.2227.

[33] M. Pospelov and A. Ritz, "Theta vacua, qcd sum rules, and the neutron electric dipole moment," *Nuclear Physics B* **573** no. 1, (2000) 177–200. https://www.sciencedirect.com/science/article/pii/S0550321399008172.

[34] A. Pich and E. de Rafael, "Strong cp-violation in an effective chiral lagrangian approach," *Nuclear Physics B* **367** no. 2, (1991) 313–333. https://www.sciencedirect.com/science/article/pii/055032139190019T.

[35] I. Khriplovich and A. Vainshtein, "Infinite renormalization of the -term and the jarlskog invariant for cp violation," *Nuclear Physics B* **414** no. 1, (1994) 27–32. https://www.sciencedirect.com/science/article/pii/0550321394904197.

[36] **Particle Data Group** Collaboration, P. A. Zyla *et al.*, "Review of Particle Physics," *PTEP* **2020** no. 8, (2020) 083C01.

[37] A. Nelson, "Naturally weak cp violation," *Physics Letters B* **136** no. 5, (1984) 387–391. https://www.sciencedirect.com/science/article/pii/0370269384920252.

[38] S. Khlebnikov and M. Shaposhnikov, "Extra space-time dimensions: Towards a solution to the strong cp-problem," *Physics Letters B* **203** no. 1, (1988) 121–124. https://www.sciencedirect.com/science/article/pii/0370269388915821.

[39] M. Chaichian and A. B. Kobakhidze, "Extra dimensions and the strong *CP* problem," *Phys. Rev. Lett.* **87** (Oct, 2001) 171601. https://link.aps.org/doi/10.1103/PhysRevLett.87.171601.

[40] L. Di Luzio, M. Giannotti, E. Nardi, and L. Visinelli, "The landscape of QCD axion models," *Phys. Rept.* **870** (2020) 1–117, arXiv:2003.01100 [hep-ph].

[41] P. Di Vecchia and G. Veneziano, "Chiral dynamics in the large n limit," *Nuclear Physics B* **171** (1980) 253–272. https://www.sciencedirect.com/science/article/pii/0550321380903703.

[42] G. Grilli di Cortona, E. Hardy, J. Pardo Vega, and G. Villadoro, "The QCD axion, precisely," *JHEP* **01** (2016) 034, arXiv:1511.02867 [hep-ph].

[43] L. J. Hall and M. B. Wise, "Flavor changing higgs boson couplings," *Nuclear Physics B* **187** no. 3, (1981) 397–408. https://www.sciencedirect.com/science/article/pii/0550321381904697.

[44] F. Wilczek, "Decays of heavy vector mesons into higgs particles," *Phys. Rev. Lett.* **39** (Nov, 1977) 1304–1306. https://link.aps.org/doi/10.1103/PhysRevLett.39.1304.

[45] L. Di Luzio, F. Mescia, and E. Nardi, "Redefining the axion window," *Phys. Rev. Lett.* **118** (Jan, 2017) 031801. https://link.aps.org/doi/10.1103/PhysRevLett.118.031801.

[46] M. Srednicki, "Axion couplings to matter: (i). cp-conserving parts," *Nuclear Physics B* **260** no. 3, (1985) 689–700. https://www.sciencedirect.com/science/article/pii/0550321385900549.

[47] F. Björkeroth, L. Di Luzio, F. Mescia, E. Nardi, P. Panci, and R. Ziegler, "Axion-electron decoupling in nucleophobic axion models," *Phys. Rev. D* **101** no. 3, (2020) 035027, arXiv:1907.06575 [hep-ph].

[48] H. Arp, "The globular cluster m5.," *The Astrophysical Journal* **135** (1962) 311.

[49] S. Toonen, A. Hamers, and S. Portegies Zwart, "The evolution of hierarchical triple star-systems," *Computational Astrophysics and Cosmology* **3** no. 1, (Dec., 2016) 6, arXiv:1612.06172 [astro-ph.SR].

[50] G. G. Raffelt, "Astrophysical axion bounds," *Lect. Notes Phys.* **741** (2008) 51–71, arXiv:hep-ph/0611350.

[51] L. Di Luzio, M. Fedele, M. Giannotti, F. Mescia, and E. Nardi, "Stellar evolution confronts axion models," *JCAP* **02** (2022) 035, arXiv:2109.10368 [hep-ph].

[52] G. G. Raffelt and G. D. Starkman, "Stellar energy transfer by kev-mass scalars," *Phys. Rev. D* **40** (Aug, 1989) 942–947. https://link.aps.org/doi/10.1103/PhysRevD.40.942.

[53] G. G. Raffelt, "Astrophysical axion bounds," in *Lecture Notes in Physics*, pp. 51–71. Springer Berlin Heidelberg. https://doi.org/10.1007%2F978-3-540-73518-2_3.

[54] N. Vinyoles, A. Serenelli, F. L. Villante, S. Basu, J. Redondo, and J. Isern, "New axion and hidden photon constraints from a solar

data global fit," J. Cosmology Astropart. Phys. **2015** no. 10, (Oct., 2015) 015, arXiv:1501.01639 [astro-ph.SR].

[55] A. H. Córsico, L. G. Althaus, M. M. Miller Bertolami, and S. O. Kepler, "Pulsating white dwarfs: new insights," *Astron. Astrophys. Rev.* **27** no. 1, (2019) 7, arXiv:1907.00115 [astro-ph.SR].

[56] P. Carenza, T. Fischer, M. Giannotti, G. Guo, G. Martínez-Pinedo, and A. Mirizzi, "Improved axion emissivity from a supernova via nucleon-nucleon bremsstrahlung," *JCAP* **10** no. 10, (2019) 016, arXiv:1906.11844 [hep-ph]. [Erratum: JCAP 05, E01 (2020)].

[57] L. B. Leinson, "Axion mass limit from observations of the neutron star in Cassiopeia A," *JCAP* **08** (2014) 031, arXiv:1405.6873 [hep-ph].

[58] M. V. Beznogov, E. Rrapaj, D. Page, and S. Reddy, "Constraints on Axion-like Particles and Nucleon Pairing in Dense Matter from the Hot Neutron Star in HESS J1731-347," *Phys. Rev. C* **98** no. 3, (2018) 035802, arXiv:1806.07991 [astro-ph.HE].

[59] R. Penrose, "Gravitational collapse: The role of general relativity," *Riv. Nuovo Cim.* **1** (1969) 252–276.

[60] A. Arvanitaki, M. Baryakhtar, and X. Huang, "Discovering the qcd axion with black holes and gravitational waves," *Phys. Rev. D* **91** (Apr, 2015) 084011. https://link.aps.org/doi/10.1103/PhysRevD.91.084011.

[61] F. D'Eramo, E. Di Valentino, W. Giarè, F. Hajkarim, A. Melchiorri, O. Mena, F. Renzi, and S. Yun, "Cosmological Bound on the QCD Axion Mass, Redux," arXiv:2205.07849 [astro-ph.CO].

[62] **ALPS** Collaboration, K. Ehret *et al.*, "Resonant laser power build-up in ALPS: A 'Light-shining-through-walls' experiment," *Nucl. Instrum. Meth. A* **612** (2009) 83–96, arXiv:0905.4159 [physics.ins-det].

[63] **ALPS** Collaboration, A. Spector, "ALPS II technical overview and status report," in *12th Patras Workshop on Axions, WIMPs and WISPs*, pp. 133–136. 2017. arXiv:1611.05863 [physics.ins-det].

[64] **OSQAR** Collaboration, R. Ballou *et al.*, "New exclusion limits on scalar and pseudoscalar axionlike particles from light shining through a wall," *Phys. Rev. D* **92** no. 9, (2015) 092002, arXiv:1506.08082 [hep-ex].

[65] **CAST** Collaboration, S. Aune *et al.*, "Solar axion search with the CAST experiment," in *34th International Conference on High Energy Physics*. 10, 2008. arXiv:0810.1874 [hep-ex].

[66] **IAXO** Collaboration, I. Irastorza *et al.*, "The International Axion Observatory IAXO. Letter of Intent to the CERN SPS committee,".

[67] **ADMX** Collaboration, S. J. Asztalos *et al.*, "An Improved RF cavity search for halo axions," *Phys. Rev. D* **69** (2004) 011101, arXiv:astro-ph/0310042.

[68] C. O'Hare, "https://github.com/cajohare/AxionLimits,".

[69] L. D. Luzio, F. Mescia, and E. Nardi, "Redefining the axion window," *Physical Review Letters* **118** no. 3, (Jan, 2017) . https://doi.org/10.1103%2Fphysrevlett.118.031801.

[70] L. Di Luzio, F. Mescia, and E. Nardi, "Window for preferred axion models," *Phys. Rev. D* **96** no. 7, (2017) 075003, arXiv:1705.05370 [hep-ph].

[71] R. Barbieri, C. Braggio, G. Carugno, C. S. Gallo, A. Lombardi, A. Ortolan, R. Pengo, G. Ruoso, and C. C. Speake, "Searching for galactic axions through magnetized media: the QUAX proposal," *Phys. Dark Univ.* **15** (2017) 135–141, arXiv:1606.02201 [hep-ph].

[72] A. Arvanitaki and A. A. Geraci, "Resonantly Detecting Axion-Mediated Forces with Nuclear Magnetic Resonance," *Phys. Rev. Lett.* **113** no. 16, (2014) 161801, arXiv:1403.1290 [hep-ph].

[73] D. Budker, P. W. Graham, M. Ledbetter, S. Rajendran, and A. Sushkov, "Proposal for a Cosmic Axion Spin Precession Experiment (CASPEr)," *Phys. Rev. X* **4** no. 2, (2014) 021030, arXiv:1306.6089 [hep-ph].

[74] W. A. Bardeen and S.-H. Tye, "Current algebra applied to properties of the light higgs boson," *Physics Letters B* **74** no. 3, (1978) 229–232. https://www.sciencedirect.com/science/article/pii/0370269378905609.

[75] J. Schweppe *et al.*, "Observation of a peak structure in positron spectra from U + Cm collisions," *Phys. Rev. Lett.* **51** (1983) 2261–2264.

[76] A. Schafer, J. Reinhardt, B. Muller, W. Greiner, and G. Soff, "IS THERE EVIDENCE FOR THE PRODUCTION OF A NEW PARTICLE IN HEAVY ION COLLISIONS?," *J. Phys. G* **11** (1985) L69–L74.

[77] W. A. Bardeen, R. D. Peccei, and T. Yanagida, "CONSTRAINTS ON VARIANT AXION MODELS," *Nucl. Phys. B* **279** (1987) 401–428.

[78] L. M. Krauss and D. J. Nash, "A VIABLE WEAK INTERACTION AXION?," *Phys. Lett. B* **202** (1988) 560–567.

[79] **E949, E787** Collaboration, S. Adler *et al.*, "Measurement of the K+ –> pi+ nu nu branching ratio," *Phys. Rev. D* **77** (2008) 052003, arXiv:0709.1000 [hep-ex].

[80] J. Martin Camalich, M. Pospelov, P. N. H. Vuong, R. Ziegler, and J. Zupan, "Quark Flavor Phenomenology of the QCD Axion," *Phys. Rev. D* **102** no. 1, (2020) 015023, arXiv:2002.04623 [hep-ph].

[81] Z. L. A. Ceccucci and Y. Sakai., "Ckm quark-mixing matrix 12 . ckm quark-mixing matrix,".

[82] **UTfit** Collaboration, M. Bona *et al.*, "Model-independent constraints on $\Delta F = 2$ operators and the scale of new physics," *JHEP* **03** (2008) 049, arXiv:0707.0636 [hep-ph].

[83] L. J. Hall and A. Rasin, "On the generality of certain predictions for quark mixing," *Phys. Lett. B* **315** (1993) 164–169, arXiv:hep-ph/9303303.

[84] J. F. Gunion and H. E. Haber, "Cp-conserving two-higgs-doublet model: The approach to the decoupling limit," *Physical Review D* **67** no. 7, (Apr, 2003) . http://dx.doi.org/10.1103/PhysRevD.67.075019.

[85] L. Lavoura and J. a. P. Silva, "Fundamental cp-violating quantities in an su(2)⊗u(1) model with many higgs doublets," *Phys. Rev. D* **50** (Oct, 1994) 4619–4624. https://link.aps.org/doi/10.1103/PhysRevD.50.4619.